

JOURNAL OF APPLIED MATERIAL SCIENCE



Contents

Volume 1, No. 2, June 2025

Editorial 210135

Aims and scope of the journal, a brief submission guideline, and the list of the editorial board.

Ahmad Allahbakhsh

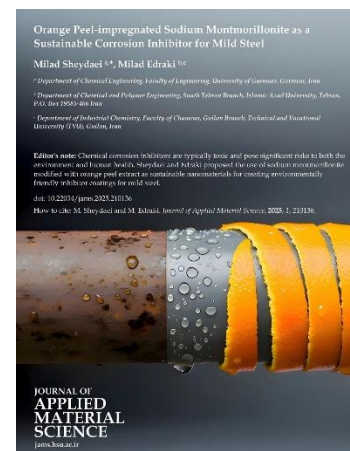
doi: 10.22034/jams.2025.210135

Orange Peel-impregnated Sodium Montmorillonite 210136 as a Sustainable Corrosion Inhibitor for Mild Steel

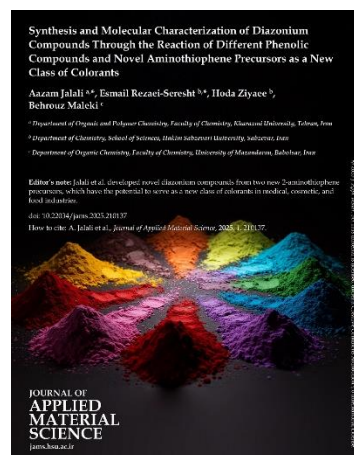
Chemical corrosion inhibitors are typically toxic and pose significant risks to both the environment and human health. Sheydaei and Edraki proposed the use of sodium montmorillonite modified with orange peel extract as sustainable nanomaterials for creating environmentally friendly inhibitor coatings for mild steel

Milad Sheydaei, Milad Edraki

doi: 10.22034/jams.2025.210136



Synthesis and Molecular Characterization of Diazonium Compounds 210137 Through the Reaction of Different Phenolic Compounds and Novel Aminothiophene Precursors as a New Class of Colorants



Jalali et al. developed novel diazonium compounds from two new 2-aminothiophene precursors, which have the potential to serve as a new class of colorants in medical, cosmetic, and food industries.

Aazam Jalali, Esmail Rezaei-Seresht, Hoda Ziyadeh, Behrouz Maleki

doi: 10.22034/jams.2025.210137

Hybrid Ionic Liquid-assisted Biomagnetic Nanocomposite 210138 for Efficient Removal of a Cationic Dye

Conventional methods for dye removal, such as adsorption, have several limitations, including low efficiency, high costs, and the risk of secondary pollution. This has led to significant research interest in developing sustainable and innovative materials for dye absorption. Thati et al. utilized coconut shells as a green resource to create biomagnetic nanocomposites that demonstrate high efficiency in removing cationic dyes.

Mounika Thati, Madhavi Vemula, Santhee Devi Karri

doi: 10.22034/jams.2025.210138



Exploring Corrosion Protection Potential of Sustainable 210139 and Green *Morus alba* 'Pendula' Fruit Extracts



Plant extracts can provide new opportunities for developing next-generation sustainable corrosion protection systems. Shiri utilized Pendula fruit extracts as a novel resource for creating corrosion inhibition systems. The developed system was effective in preventing mild steel corrosion in a salty environment, indicating the potential of this green corrosion protection method for future sustainable applications.

Sara Shiri

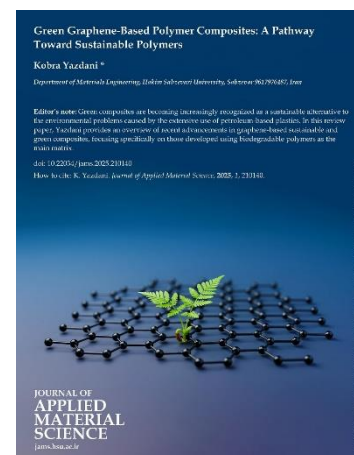
doi: 10.22034/jams.2025.210139

Green Graphene-Based Polymer Composites: A Pathway 210140 Toward Sustainable Polymers

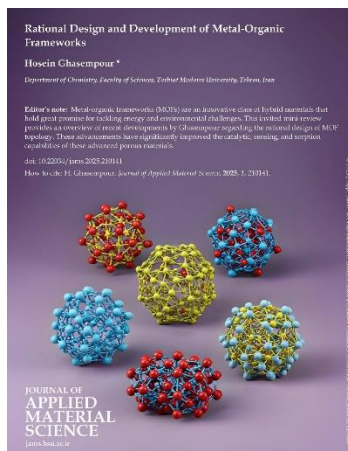
Green composites are becoming increasingly recognized as a sustainable alternative to the environmental problems caused by the extensive use of petroleum-based plastics. In this review paper, Yazdani provides an overview of recent advancements in graphene-based sustainable and green composites, focusing specifically on those developed using biodegradable polymers as the main matrix.

Kobra Yazdani

doi: 10.22034/jams.2025.210140



Rational Design and Development of Metal-Organic Frameworks 210141



Metal-organic frameworks (MOFs) are an innovative class of hybrid materials that hold great promise for tackling energy and environmental challenges. This invited mini-review provides an overview of recent developments by Ghasempour regarding the rational design of MOF topology. These advancements have significantly improved the catalytic, sensing, and sorption capabilities of these advanced porous materials.

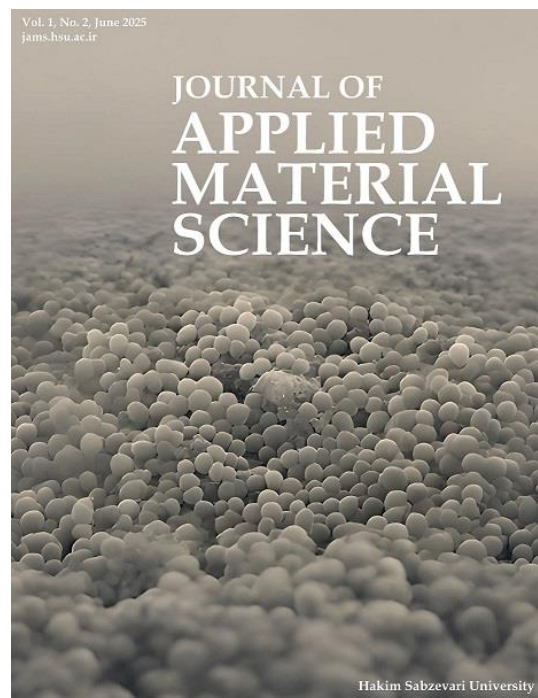
Hosein Ghasempour

doi: 10.22034/jams.2025.210141

ABOUT COVER

Three-dimensional carbon-based materials show great potential for hosting various microorganisms, paving the way for next-generation living materials. The cover features a regenerated image based on a field emission scanning electron microscope (FESEM) image of a graphene-based highly porous aerogel, which was incubated with *Staphylococcus aureus* (*S. aureus*) bacteria for two days.

(Note: The covers of this journal are created in part using artificial intelligence (AI) technologies, with direct human supervision. AI and AI-assisted technologies are permitted only for generating graphical abstract suggestions. If such technologies are used in the manuscript preparation, it must be clearly disclosed in the Acknowledgments section.)



Journal of Applied Material Science:

an *open-access* platform to publish scientific developments in all aspects of material science under the *highest publication standards* and the *fastest peer-review process*

The Journal of Applied Material Science publishes original research in the form of *communications* and *full papers*, as well as *reviews*, invited *mini-reviews*, and invited research news. Publication in this journal is **entirely free of charge**, and all accepted papers will be available online immediately after typesetting. Dr. Ahmad Allahbakhsh, along with an international team of editors, leads the journal to meet the highest publication standards. We are looking forward to receiving your submissions.

Editor-in-Chief: Dr. Ahmad Allahbakhsh (Hakim Sabzevari University)

Director in charge: Prof. Gholamali Farzi (Hakim Sabzevari University)

International Editorial Board Members:

Prof. Ahmad Reza Bahramian (Tarbiat Modares University),
Prof. Mohammadhosein (Momo) Safari (Hasselt University),
Prof. Denis Rodrigue (Laval University),
Prof. Ursula Windberger (Medical University of Vienna),
Prof. Gholamali Farzi (Hakim Sabzevari University),
Prof. Sabu Thomas (Mahatma Gandhi University),
Dr. Hamidreza Oveisi (Hakim Sabzevari University),
Prof. Manoj Balachandran (CHRIST University),
Dr. Rasoul Esmaeely Neisiany (Hakim Sabzevari University),
Dr. Ahmad Allahbakhsh (Hakim Sabzevari University)

Journal of Applied Material Science is an open-access journal, which means that all content is freely available without charge to the users and institutions. Users are allowed to read, download, copy, distribute, print, search, or link to the full texts of the articles, or use them for any other lawful purpose, without asking prior permission from the publisher or the author. This is in accordance with the BOAI definition of open access. Authors are free to deposit a copy of their paper (Published version, Version of Record) in an institutional or other repository of their choice.

To submit a manuscript: Please consult the **aim and scope** of the journal at:
https://jams.hsu.ac.ir/journal/aim_scope

Guide for Authors is available at: <https://jams.hsu.ac.ir/journal/authors.note>

To **submit** your paper, please visit: <https://jams.hsu.ac.ir/author>

Orange Peel-impregnated Sodium Montmorillonite as a Sustainable Corrosion Inhibitor for Mild Steel

Milad Sheydaei ^{a,*}, Milad Edraki ^{b,c}

^a Department of Chemical Engineering, Faculty of Engineering, University of Garmsar, Garmsar, Iran

^b Department of Chemical and Polymer Engineering, South Tehran Branch, Islamic Azad University, Tehran, P.O. Box 19585-466 Iran

^c Department of Industrial Chemistry, Faculty of Chamran, Guilan Branch, Technical and Vocational University (TVU), Guilan, Iran

Editor's note: Chemical corrosion inhibitors are typically toxic and pose significant risks to both the environment and human health. Sheydaei and Edraki proposed the use of sodium montmorillonite modified with orange peel extract as sustainable nanomaterials for creating environmentally friendly inhibitor coatings for mild steel.

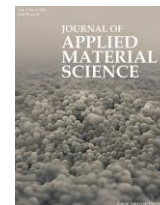
doi: 10.22034/jams.2025.210136

How to cite: M. Sheydaei and M. Edraki. *Journal of Applied Material Science*, 2025, 1, 210136.



JOURNAL OF
**APPLIED
MATERIAL
SCIENCE**

jams.hsu.ac.ir



Original Research

Orange Peel-impregnated Sodium Montmorillonite as a Sustainable Corrosion Inhibitor for Mild Steel

Milad Sheydaei ^{a,*}, Milad Edraki ^{b,c}

^a Department of Chemical Engineering, Faculty of Engineering, University of Garmsar, Garmsar, Iran

^b Department of Chemical and Polymer Engineering, South Tehran Branch, Islamic Azad University, Tehran, P.O. Box 19585-466, Iran

^c Department of Industrial Chemistry, Faculty of Chamran, Guilan Branch, Technical and Vocational University (TVU), Guilan, Iran

Abstract

Metal structures are always exposed to corrosion, and this slow but continuous phenomenon causes a decrease in the strength of metals, ultimately causing their destruction and inflicting financial and human losses. Chemical inhibitors have always been used to prevent the corrosion process, but due to their irreparable harm to the environment, the use of green corrosion inhibitors has received much attention. This study investigates the corrosion inhibition properties of sodium montmorillonite nanoparticles (Na⁺-MMT) with orange peel compounds. The prepared nanoparticles (O-MMT) were evaluated using Fourier transform infrared spectroscopy (FTIR), X-ray diffraction (XRD), and scanning electron microscopy (SEM). The evaluation results showed that the orange peel compounds were successfully added to the host (MMT). Then, the nanoparticles were added to the epoxy (EP) matrix and the effect of improving their anti-corrosion resistance was evaluated using electrochemical impedance spectroscopy (EIS) and polarization methods. The results showed that the inhibition efficiency (IE) for O-MMT is around 94%.

Keywords: Anticorrosion; Green chemistry; Environmental pollution; Sustainable inhibitors.

1. Introduction

Today, many industries use mild steel in various applications, which can be attributed to its formability, acceptable hardness, and relatively low cost [1]. However, its vulnerability to corrosion can be considered a negative factor in contrast to these advantages [2]. Researchers

have been working on various approaches to improve the corrosion resistance of mild steel for decades, but perhaps the most effective approach is the use of corrosion inhibitors [3,4].

There are many definitions of an inhibitor in the literature, but perhaps the simplest definition for an inhibitor is: a substance that, at low concentrations,

* Corresponding author.

Email addresses: md.sheydaei@fmgarmsar.ac.ir, m.sheydaei@yahoo.com (M. Sheydaei)

Received 27 December 2024

Revised 6 February 2025

Accepted 20 February 2025

Available online 25 February 2025

prevents corrosion (or slows its progress) [5]. Although they have many advantages such as fast reaction and high efficiency, many chemical inhibitors are toxic and are extremely harmful to the environment and humans [6-8]. Therefore, researchers have been looking for alternatives for these materials in recent years, using expired drugs, natural gums, bio-polymers, surfactants, food supplements, and plants [9-12]. Among them, plants are of great interest because they are low-cost and environmentally friendly in nature, due to their non-toxic compounds [13,14].

The peel of many fruits is discarded as waste or used in the preparation of fertilizers [15,16]. Orange peel contains bioactive components such as polyphenolic compounds, flavonoids, and carotenoids, which in addition to antibacterial properties have the ability to provide corrosion resistance [17,18]. One simple method for introducing the compounds of an extract into a host is the cation exchange process, in which the cationic compounds of the host are removed and replaced by the cationic compounds of the extract [19-22].

Na⁺-MMT, a type of nanoclay mineral, can expand in its interlayer spaces when immersed in water or ethanol. This swelling alters its chemical structure and allows it to accept other compounds through cation exchange. In this study, compounds derived from orange peel were incorporated into the interlayer space of sodium montmorillonite (Na⁺-MMT). Then, the modified MMT (O-MMT) was added to an epoxy matrix and applied to a mild steel substrate. The anti-corrosion properties of this coating in a saline solution were then examined using Electrochemical Impedance Spectroscopy (EIS) and polarization techniques.

2. Experimental

2.1. Materials

The Na⁺-MMT, orange peel powder, sodium chloride, and mild steel were obtained from Rockwood Company (USA), Giyahkala Company (Iran), Ghatran Shimi Tajhiz Company (Iran), and Iranian Mobarakeh Steel Company, respectively.

2.2. Preparation of O-MMT and coatings

In this study, O-MMT was prepared using a cation exchange process in an aqueous solution, as reported in the literature [19-22]. For the preparation of nanocomposite

coatings, bisphenol A diglycidyl ether (containing nanoparticles) was first added to xylene and methyl ethyl ketone (ratio 1:1) and stirred for 60 min. Next, Jefamine D230 was used as a hardener and added to the mixture in a ratio of 1:2 (relative to resin) and stirred for 5 min. The substrates were covered with the mixture and kept at ambient temperature for 1 day, and finally placed in an oven at 80°C for 24 h. Also, the content of nanoparticles used in the coatings was 1.5 and 3 wt%.

2.3. Measurements

A Tensor II spectrometer was used for FTIR evaluation. SEM VEGA3 was used for images. The dispersion of nanoparticles was investigated by energy dispersive spectroscopy (EDX) coupled with SEM (SEM-EDX) on a Cambridge instrument. An XPert PRO MPD instrument was used for XRD evaluation. A potentiostat-galvanostat instrument (CorrTest CS350) was used to evaluate the corrosion resistance of the samples. For this purpose, two electrolytes (O-MMT in NaCl solution and only 3.5 wt% NaCl solution), three electrodes including a working electrode (MS), a saturated calomel electrode (SCE), and an auxiliary electrode (Pt), were used in the electrochemical cell and the measurements were performed in the open circuit potential (OCP) and the perturbation amplitude of ±10 mV. Also, the polarization test was performed in the solution phase after 24 h of immersing the steel coupon in solutions with a scanning rate of 0.5 mV/s and in the range of ±200 mV of OCP using a similar electrochemical cell device used for the EIS test. The following equation was used to calculate the inhibition efficiency (IE) for the coatings [23]:

$$IE(\%) = \frac{I_{\text{pure coating}} - I_{\text{nanocomposite coating}}}{I_{\text{pure coating}}} \times 100 \quad (1)$$

where, $I_{\text{pure coating}}$ and $I_{\text{nanocomposite coatings}}$ are the corrosion current densities of coatings without and with the nanoparticle, respectively.

3. Results and discussion

Figures 1 and 2 show the FTIR spectra and the XRD patterns of fabricated nanoclays, respectively. Moreover, Table 1 summarizes the peak assignments for spectra presented in these two Figures. The presence of orange peel peaks in the O-MMT spectrum indicates that the cation exchange process has been completed and that the O-MMT contains orange peel compounds. Also, the

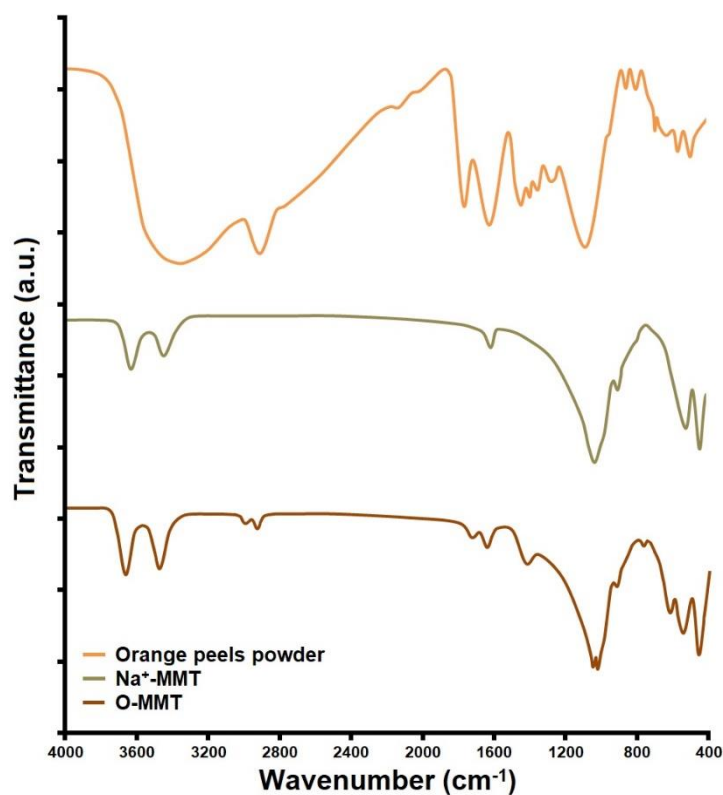


Figure 1. FTIR spectra of orange peel powder, Na⁺-MMT, and O-MMT.

XRD results show a change in 2θ and d -spacing due to the absence of Na⁺ cation and the presence of orange peel compounds in the final product [19-23].

SEM images of the samples in Figure 3 show that the morphology before and after the cation exchange

process did not change significantly, although this behavior has been reported in the literature [19-23].

SEM-EDX mapping images (see Figure 4) clearly show the presence and distribution of O-MMT (the red dots of Si atoms) in the matrix. The excellent distribution

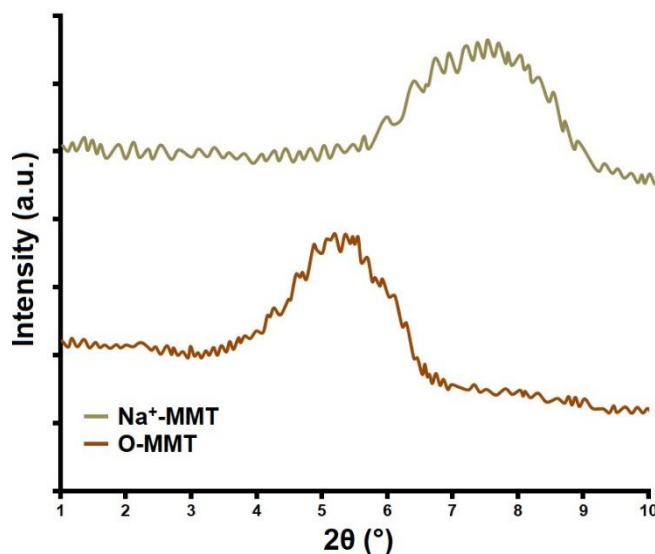
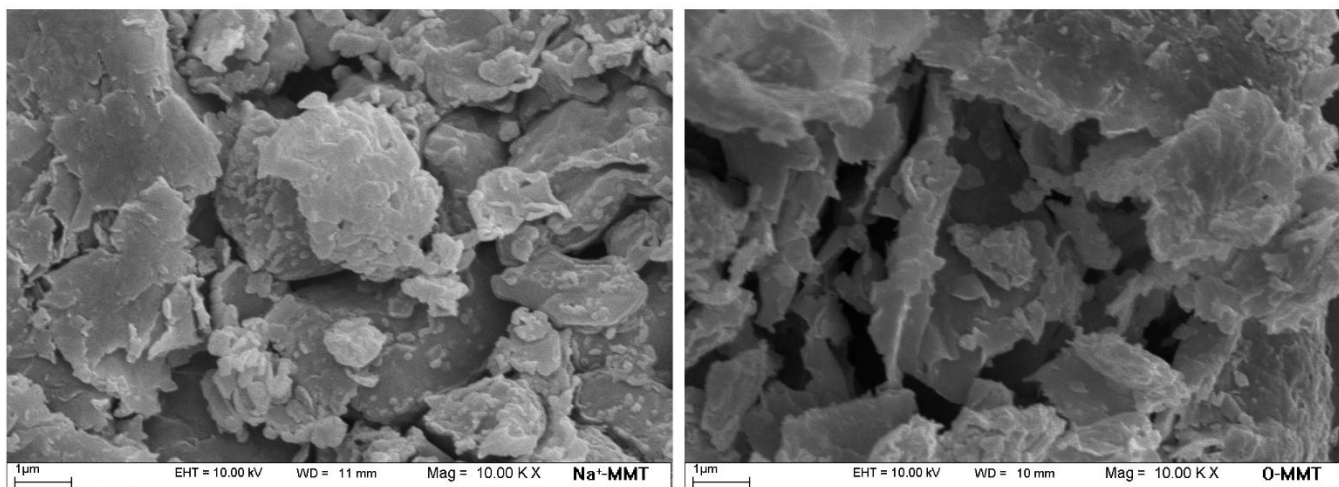


Figure 2. XRD patterns of Na⁺-MMT and O-MMT.

Table 1. FTIR absorption peaks and XRD peaks assignments

Sample	Wavenumber (cm ⁻¹)	Characteristics	Peak 2θ and d-spacing
Na ⁺ -MMT	455 and 1038	Bending and stretching Si-O vibrations	7.4° and 11.22 Å
	534	Si-O-Al vibration and MgO groups	
	916	Al ₂ OH bending groups	
	1616-3405	Scissoring vibrations and symmetric vibrations of OH units	
	3642	Stretching of OH (Si-OH groups)	
Orange peel	3420	OH groups (carbohydrates and lignin groups)	-
	2925	C-H stretching vibration	
	1736	The carbonyl groups (e.g., ester)	
	1617	Aliphatic and/or unsaturated aromatic compounds	
	1428	Aliphatic chains (form the basic structure of lignocellulosic materials)	
O-MMT	1045	C-O-H or C-O-R (alcohols or esters)	5.2° and 17.14 Å
	3680	Stretching of OH (Si-OH groups)	
	3498	Scissoring vibrations and symmetric vibrations of OH units	
	2925 and 3000	C-H stretching vibration	
	1695	The carbonyl groups (like ester)	
	1617	OH units (Na ⁺ -MMT) or Aliphatic and/or unsaturated aromatic compounds (Orange peel)	
	1418	Aliphatic chains (form the basic structure of lignocellulosic materials)	
	1045	C-O-H or C-O-R (alcohols or esters)	
	1038	Bending and stretching Si-O vibrations	
	916	Al ₂ OH bending groups	
	534	Si-O-Al vibration and MgO groups	
	458	Bending and stretching Si-O vibrations	

Notes: References [19-24] were used to assign Na⁺-MMT FTIR peaks, and reference [25] was used to assign orange peel FTIR peaks.

**Figure 3.** SEM images of Na⁺-MMT (left) and O-MMT (right).

in the nanocomposites indicates that the nanoparticles are well-compatible with the matrix and hence do not tend to agglomerate.

The results of the EIS test are reported in Figures 5 and 6 and Table 2. The Nyquist plots in Figure 5 presented that the curve diameter, representing the charge transfer

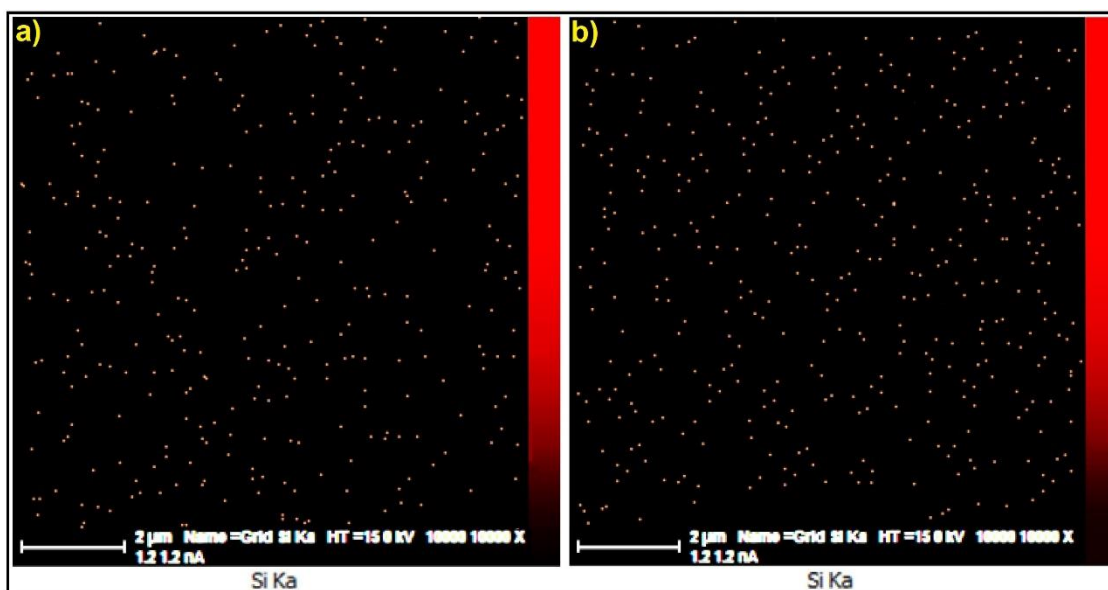


Figure 4. EDX results demonstrate the dispersion of O-MMT in the matrix: (a) EP/1.5% O-MMT and (b) EP/3% O-MMT.

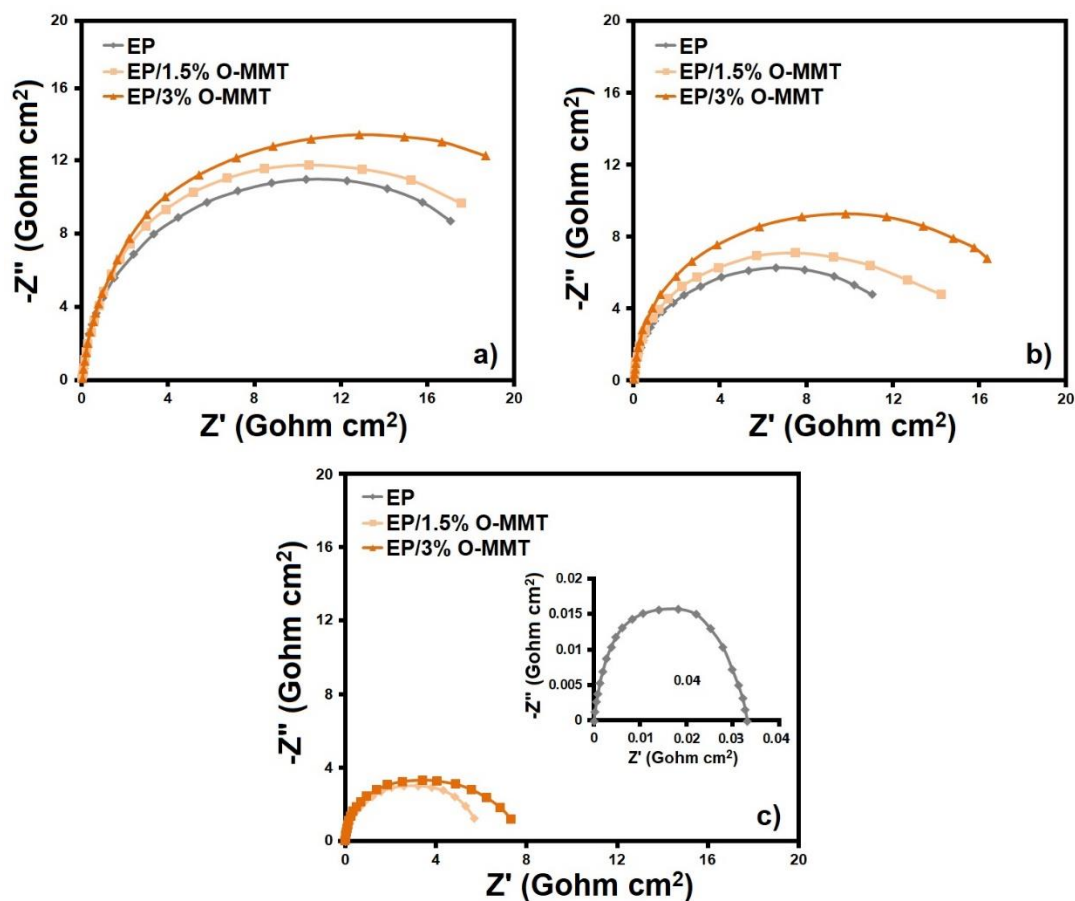


Figure 5. Nyquist diagrams of surfaces coated with EP, EP/1.5%O-MMT, and EP/3%O-MMT after immersion for (a) 9, (b) 16, and (c) 36 days.

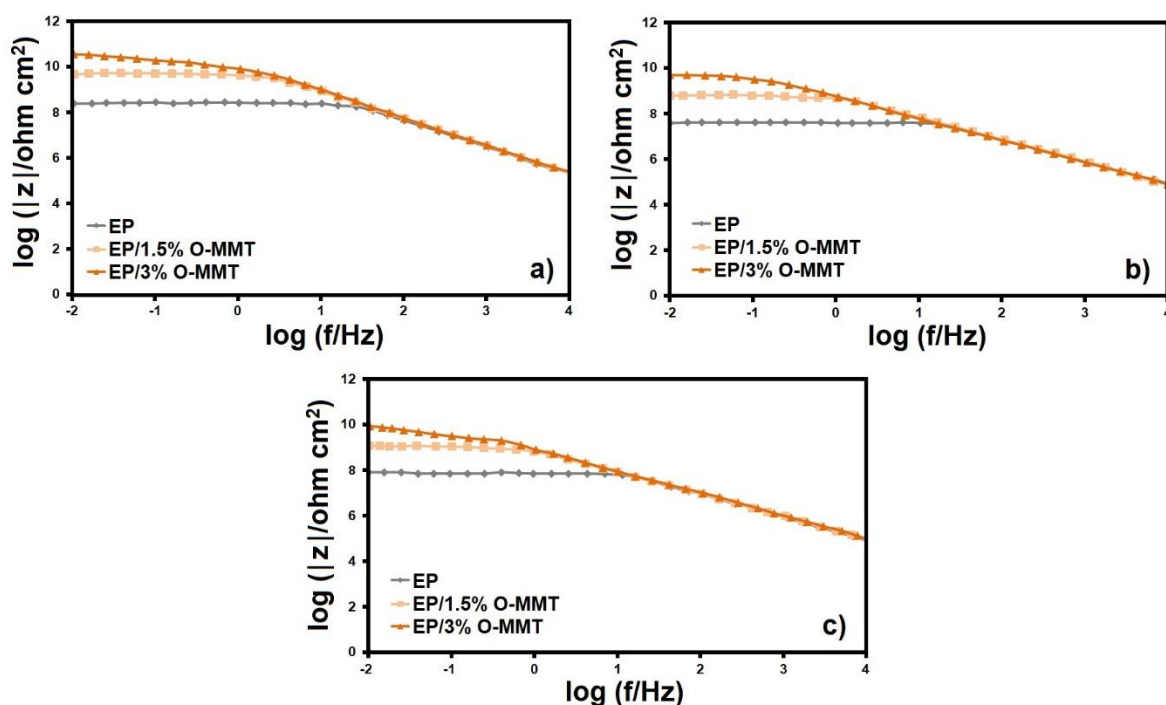


Figure 6. Bode diagrams of the surfaces coated with EP, EP/1.5 % O-MMT, and EP/3 % O-MMT after immersion for (a) 9 days, (b) 18 days, and (c) 36 days.

resistance (R_{ct}), decreases with increasing immersion time. This trend indicates degradation over time, but this degradation occurs much slower for nanocomposites than for pure matrix, indicating that nanoparticles have anti-corrosion properties. In fact, these anti-corrosion properties are related to orange peel compounds because it has been reported in the literature that Na^+ -MMT alone cannot improve anti-corrosion resistance [19].

The results show that the pure matrix is very vulnerable over time and water molecules as well as aggressive ions penetrate it very easily. Figure 6 shows the Bode plots that represent the corrosion resistance and impedance. With the passage of time and increasing immersion time, a large change is seen in the frequency region for the pure matrix, which indicates the capacitive behavior of the pure matrix. The results show that nanocomposite coatings are much more resistant to

Table 2. Electrochemical parameters obtained from EIS results for samples immersed in the 3.5% NaCl solution

Sample	Immersion time (days)	R_{ct} ($\Omega.cm^2$)	R_c ($M\Omega.cm^2$)	CPE _c		Log z ($\Omega.cm^2$)
				$Y_{0,c}$ ($n\Omega^{-1}.cm^2.s^n$)	n_c	
EP	9	17.05×10^9	13151	3.19	0.82	7.87
	18	11.04×10^9	28.9	1.08	0.71	7.50
	36	0.03×10^9	7.3	0.46	0.59	7.04
EP/1.5% O-MMT	9	17.54×10^9	17924	1.39	0.76	9.02
	18	14.25×10^9	6138	1.01	0.68	8.69
	36	5.69×10^9	219	0.10	0.54	8.10
EP/3% O-MMT	9	18.68×10^9	26413	0.42	0.74	9.98
	18	16.36×10^9	10629	0.39	0.72	9.57
	36	7.31×10^9	2388	0.32	0.70	8.85

Notes: R_c : Coating resistance; CPE_c: The constant phase element related to the coating; n_c : The constant related to surface heterogeneity in the coating; $Y_{0,c}$: Admittance of the coating; Log |z|: The impedance module.

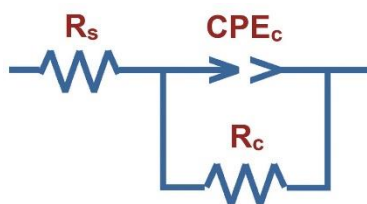


Figure 7. Equivalent circuit for the description of coatings (In this circuit, R_s , R_c , and CPE_c indicate solution resistance, coating resistance, and the constant phase element related to coating, respectively).

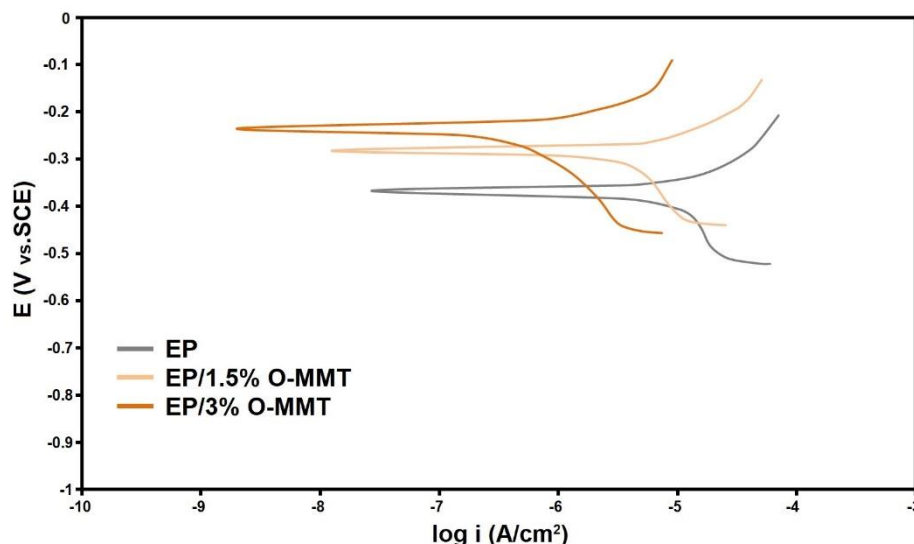


Figure 8. Results of the polarization test after immersing the samples for 24 days.

corrosion, compared to the pure matrix. According to the results of Table 2, it can be said that the use of nanoparticles has caused an increase in the absolute value of the impedance at all immersion times compared to the pure matrix. This indicates better performance and active inhibition of the nanocomposites.

The destruction of pure epoxy can be attributed to the formation of hydroxyl ions at the coating/metal interface in the cathode areas, which causes an increase in pH below the coating surface [19,23]. This increase in pH ultimately causes hydrolysis of the EP interfacial bonds and reduces its adhesion to the substrate surface

[19]. Also, the equivalent circuit that has the maximum compatibility with the impedance results is shown in Figure 7.

The results of the polarization test are reported in Figure 8 and Table 3. According to the results, the corrosion flow has decreased with the addition of nanoparticles and the corrosion potential has shifted to more positive values. Based on the results, it can be said that nanoparticles can be classified as anodic inhibitors. Also, the nanocomposite with a nanoparticle loading content of 3 wt% has the best performance the lowest corrosion current density, and the lowest corrosion rate.

Table 3. Electrochemical parameters obtained from the polarization test on samples immersed in the saline solution

Sample	i_{corr} (A.cm ⁻²)	E_{corr} VS.SCE (mV)	β_a (V.dec)	β_c (V.dec)	IE (%)
EP	1.009×10^{-5}	-367	0.245	0.587	-
EP/1.5% O-MMT	3.27×10^{-6}	-262	0.101	0.346	67.59
EP/3% O-MMT	5.96×10^{-7}	-235	0.114	0.302	94.04

Notes: Corrosion potential: E_{corr} ; Corrosion current density: i_{corr} ; The anodic Tafel slope: β_a ; Cathodic Tafel slope: β_c .

Table 4. Corrosion inhibition performance of some plants in different corrosion media

Plant	Substrate	Corrosive Medium	Maximum IE (%)	Reference
<i>Garcinia cambogia</i>	Mild steel	NaCl	88.85	[4]
<i>Ganoderma Lucidum</i>	Mild steel	NaCl	98.26	[11]
<i>Clitoria ternatea</i>	Mild steel	NaCl	86	[20]
Pine pollen	Mild steel	NaCl	87.16	[23]
<i>Catharanthus roseus</i>	Mild steel	NaCl	84	[26]
Nettle leaves	Mild steel	NaCl	95	[27]
Orange peel	Mild steel	NaCl	94	This study

The improvement of the corrosion resistance of the coatings can be attributed to the synergistic effect of MMT and orange peel. In fact, MMT with its sheet structure can act as a protective shield against aggressive species, and on the other hand, it has the ability to react with hydroxyl ions in the cathodic region and thereby produce insoluble compounds preventing oxygen from reaching this region [23]. Also, orange peel contains compounds such as polyphenols, flavonoids, carotenoids, and vitamin C [18,25]. These compounds contain benzene rings, heteroatoms, and carbonyl groups that can share their free electron pairs with the empty orbitals of the iron atoms on the metal surface [18,20]. They are adsorbed on the surface in this way [5]. Therefore, they block the anodic regions by forming a layer [18,20]. Table 4 presents a comparison between our results and the IE results of several previous studies.

4. Conclusions

In summary, a new corrosion inhibitor was prepared in this study using orange peel powder and Na⁺-MMT. The results showed that this inhibitor can improve corrosion resistance. The highest inhibition efficiency was related to the nanocomposite containing 3 wt% nanoparticles, which was 94%. This inhibitor is environmentally friendly and is obtained from waste resources. The use of plant compounds can be considered a suitable alternative to chemical inhibitors because they are both inexpensive and highly effective.


Conflict of Interest

The authors declare no conflict of interest.

References

1. E.D. Akpan, et al. Coordination compounds as corrosion inhibitors of metals: A review. *Coordination Chemistry Reviews*, **2024**, 499, 215503.
2. K.M. Shwetha, et al. A review on corrosion inhibitors: types, mechanisms, electrochemical analysis, corrosion rate and efficiency of corrosion inhibitors on mild steel in an acidic environment. *Results in Surfaces and Interfaces*, **2024**, 16, 100258.
3. M. Sheydaei and M. Edraki. An Overview of Silane-based Hybrid Sol-gel Coatings for Highly Efficient Metal Corrosion Protection. *Journal of Applied Material Science*, **2025**, 1, 210131.
4. M. Sheydaei and M. Edraki. Anticorrosion, thermal, and mechanical evaluation of epoxy coatings containing *Garcinia cambogia*-modified clay. *Chemical Research and Technology*, **2024**, 1, 108.
5. M. Sheydaei. The Use of Plant Extracts as Green Corrosion Inhibitors: A Review. *Surfaces*, **2024**, 7, 380.
6. O.E. Okon, et al. Experimental investigation and comparative environmental impact analysis of conventional and naturally occurring kinetic hydrate inhibitors in offshore environments using toxicity and bioconcentration tools. *Results in Engineering*, **2024**, 21, 101705.
7. M. Sheydaei. Heavy Metals Contamination in Soil and Rice and their Removal Processes: A Brief Review. *Geomicrobiology Journal*, **2024**, 41, 721.
8. M. Sheydaei. Investigation of Heavy Metals Pollution and Their Removal Methods: A Review. *Geomicrobiology Journal*, **2024**, 41, 213.
9. M. Edraki, et al. A brief review of the performance of azole-type organic corrosion inhibitors. *Chemical Review and Letters*, **2022**, 6, 79.
10. M. Sheydaei, et al. Matcha-modified clay polyurethane coating: improving thermal, mechanical, antimicrobial, and anticorrosion performance. *Iranian Polymer Journal*, **2023**, 32, 1643.

11. M. Sheydaei, et al. *Ganoderma Lucidum*-Modified Clay Epoxy Coating: Investigation of Thermal, Mechanical, Anticorrosion, and Antimicrobial Properties. *Polymer Science, Series B*, **2023**, 65, 991.
12. M. Edraki, et al. The effect of matcha-impregnated sodium montmorillonite on the corrosion mitigation of mild steel in saline medium, *UNEC Journal of Engineering and Applied Sciences*, **2024**, 4, 5.
13. A. Dehghani, et al. Plant extracts: Probable alternatives for traditional inhibitors for controlling alloys corrosion against acidic media—A review. *Biomass Conversion and Biorefinery*, **2024**, 14, 7467.
14. J.R. González-Parra, and F. Di Turo. The Use of Plant Extracts as Sustainable Corrosion Inhibitors for Cultural Heritage Alloys: A Mini-Review. *Sustainability*, **2024**, 16, 1868.
15. N. Khanyile, et al. Preparation of Biofertilizers from Banana Peels: Their Impact on Soil and Crop Enhancement. *Agriculture*, **2024**, 14, 1894.
16. K. Ramamoorthy, et al. Vegetable and fruit wastes: Valuable source for organic fertilizer for effective growth of short-term crops: *Solanum lycopersicum* and *Capsicum annum*. *Environmental Research*, **2024**, 251, 118727.
17. Z.K. Hamze, et al. Corrosion Inhibition Efficiency of Biosynthesized Silver Nanoparticles Using *Citrus aurantium* Peels Extract. *Journal of Bio-and Tribo-Corrosion*, **2024**, 3, 56.
18. D. Özkır. The Consistent Effect of *Citrus aurantium* Fruit Peels Extract as New Type Green Inhibitor on Mild Steel Corrosion in HCl Solution. *Bayburt Üniversitesi Fen Bilimleri Dergisi*, **2022**, 5, 165-172.
19. M. Edraki and M. Sheydaei. Investigation of date seed powder as green corrosion inhibitor for mild steel: a study of solution and coating phases. *Hybrid Advances*, **2024**, 6, 100238.
20. M. Sheydaei, et al. Anticorrosion and Antimicrobial Evaluation of Sol-Gel Hybrid Coatings Containing *Clitoria ternatea* Modified Clay. *Gels*, **2023**, 9, 490.
21. M. Edraki, et al. Protective nanocomposite coating based on ginger modified clay and polyurethane: preparation, characterization and evaluation anti-corrosion and mechanical properties. *Polymer Science, Series B*, **2022**, 64, 756.
22. M. Edraki and M. Sheydaei. Investigation of the Dual Active/Barrier Corrosion Protection, Mechanical and Thermal Properties of a Vinyl Ester Coating Doped with Ginger Modified Clay Nanoparticles. *Russian Journal of Applied Chemistry*, **2022**, 95, 1481.
23. M. Edraki, et al. Enhanced mechanical, anticorrosion and antimicrobial properties of epoxy coating via pine pollen modified clay incorporation. *Iranian Journal of Chemistry and Chemical Engineering*, **2023**, 42, 2775.
24. M. Sheydaei, et al. PVCS/GO nanocomposites: investigation of thermophysical, mechanical and antimicrobial properties. *Journal of Sulfur Chemistry*, **2022**, 43, 376.
25. B. Zapata, et al. Thermo-kinetics study of orange peel in air. *Journal of Thermal Analysis and Calorimetry*, **2009**, 98, 309.
26. N. Palaniappan, et al. Experimental and DFT studies on the ultrasonic energy-assisted extraction of the phytochemicals of *Catharanthus roseus* as green corrosion inhibitors for mild steel in NaCl medium. *RSC Advances*, **2020**, 10, 5399.
27. M. Ramezanzadeh, et al. Highly effective inhibition of mild steel corrosion in 3.5% NaCl solution by green Nettle leaves extract and synergistic effect of eco-friendly cerium nitrate additive: Experimental, MD simulation and QM investigations. *Journal of Molecular Liquids*, **2018**, 256, 67.

© 2025 The Authors. This article is licensed under a Creative Commons Attribution 4.0 BY International License. 

Synthesis and Molecular Characterization of Diazonium Compounds Through the Reaction of Different Phenolic Compounds and Novel Aminothiophene Precursors as a New Class of Colorants

Aazam Jalali ^{a,*}, Esmail Rezaei-Seresht ^{b,*}, Hoda Ziyaee ^b,
Behrouz Maleki ^c

^a Department of Organic and Polymer Chemistry, Faculty of Chemistry, Kharazmi University, Tehran, Iran

^b Department of Chemistry, School of Sciences, Hakim Sabzevari University, Sabzevar, Iran

^c Department of Organic Chemistry, Faculty of Chemistry, University of Mazandaran, Babolsar, Iran

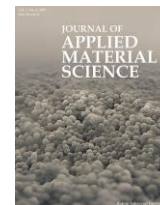
Editor's note: Jalali et al. developed novel diazonium compounds from two new 2-aminothiophene precursors, which have the potential to serve as a new class of colorants in medical, cosmetic, and food industries.

doi: 10.22034/jams.2025.210137

How to cite: A. Jalali et al., *Journal of Applied Material Science*, 2025, 1, 210137.

JOURNAL OF
**APPLIED
MATERIAL
SCIENCE**

jams.hsu.ac.ir



Original Research

Synthesis and Molecular Characterization of Diazonium Compounds Through the Reaction of Different Phenolic Compounds and Novel Aminothiophene Precursors as a New Class of Colorants

Aazam Jalali ^{a,*}, Esmail Rezaei-Seresht ^{b,*}, Hoda Ziyae ^b, Behrouz Maleki ^c

^a Department of Organic and Polymer Chemistry, Faculty of Chemistry, Kharazmi University, Tehran, Iran

^b Department of Chemistry, School of Sciences, Hakim Sabzevari University, Sabzevar, Iran

^c Department of Organic Chemistry, Faculty of Chemistry, University of Mazandaran, Babolsar, Iran

Abstract

Two novel 2-amino thiophene precursors were synthesized from cyclopentanone (or cyclohexanone), sulfur, morpholine, and malononitrile using the Gewald three-component reaction. The synthesis yields of these precursors were 97% and 90%, respectively. The resulting 2-aminothiophenes were then converted into diazonium salts, which reacted in situ with various phenolic compounds, including phenol, resorcinol, and α -naphthol, to produce twelve new azo products. The novel 2-aminothiophene-based azo compounds were synthesized with yields ranging from 58% to 72% for the first set, and 54% to 72% for the second set. Subsequently, the characterization of prepared compounds was performed using ¹H-NMR, FT-IR, UV/Visible spectroscopy, and elemental analysis. UV/Visible spectra confirmed the presence of the azo group (N=N) with absorption in the range of 362–510 nm, which is higher than the previously reported range of 350–370 nm. The increase in λ_{max} can be attributed to the existence of an auxochrome group in the molecular structure of the compounds. Additionally, all of the various analyses performed successfully supported the synthesis of the desired compounds.

Keywords: Synthesis; Azo compounds; 2-aminothiophene; Diazonium salt; Phenolic compounds.

1. Introduction

Azo compounds are chemical compounds that contain the functional group R-N=N-R', where R and R'

can be either aryl or alkyl groups [1]. These compounds have a wide range of applications, including studies in molecular biology. One notable study involved the synthesis of an aryl diazonium compound known as Dz-PEG. Dz-PEG was used for the in-situ conversion of

* Corresponding authors.

Email addresses: aazamjalali@gmail.com (A. Jalali), e.rezaei@hsu.ac.ir (E. Rezaei-Seresht)

Received 24 January 2025

Revised 24 April 2025

Accepted 25 April 2025

Available online 2 May 2025

serotonin into an azo compound. This conversion helps restore biotinylation efficiency by consuming serotonin through an azo-coupling reaction. Our performed proteomics analysis confirmed that biotinylation was inhibited using serotonin and that the inhibiting process was effectively reversed by Dz-PEG. [2].

A recent study presents a sensitive and rapid spectrophotometric procedure for quantifying Ketotifen fumarate in aqueous solutions. The process involves diazotizing 4-amino antipyrine using sodium nitrate in an acidic medium, then coupling it with Ketotifen to produce an orange azo dye. The dye exhibits a peak absorbance at 483 nm and remains stable for over 60 minutes. The method demonstrates high accuracy, with results ranging from 98% to 100.16%, making it practical for pharmaceutical formulations. Compared to existing approaches, it provides notable advantages [3-6], offering superior sensitivity and better solvent suitability [7].

Azo dyes are commonly used as colorants in the textile industry [8, 9]. They are also used as pigments in digital printing [10]. These dyes are utilized in medicine and the cosmetic and food industries [11]. They are valuable in the preparation of advanced materials, too [12]. Some dyes are used in the biomedical field [13], exhibiting antibacterial [14] and Antifungal Activity [15]. From their other applications, we can point to their usage as chiral receptors [16], liquid crystals [17], new glassy materials [18], and chiral switches in photochemistry [19]. They have been applied as semiconductors and optical data storage Equipment [20].

Aminothiophene-based azo dyes are recognized as dyes that exhibit great brightness. They have emerged as a cost-effective alternative to more expensive anthraquinone dyes [8]. The preparation of novel azo derivatives from insoluble amines in aqueous media is crucial as it could lead to technological advancements. In this paper, we report the preparation of several novel azo compounds through a coupling reaction of 2-aminothiophene with phenolic compounds.

2. Experimental

2.1. Materials

Malononitrile, sulfur, cyclohexanone, cyclopentanone, morpholine, HCl (98%), NaOH, resorcinol, catechol, phloroglucinol, phenol, α -naphthol, and β -naphthol were purchased from Merck and were of analytical

grade. All chemicals were used as received without further purification, and solvents were redistilled before use.

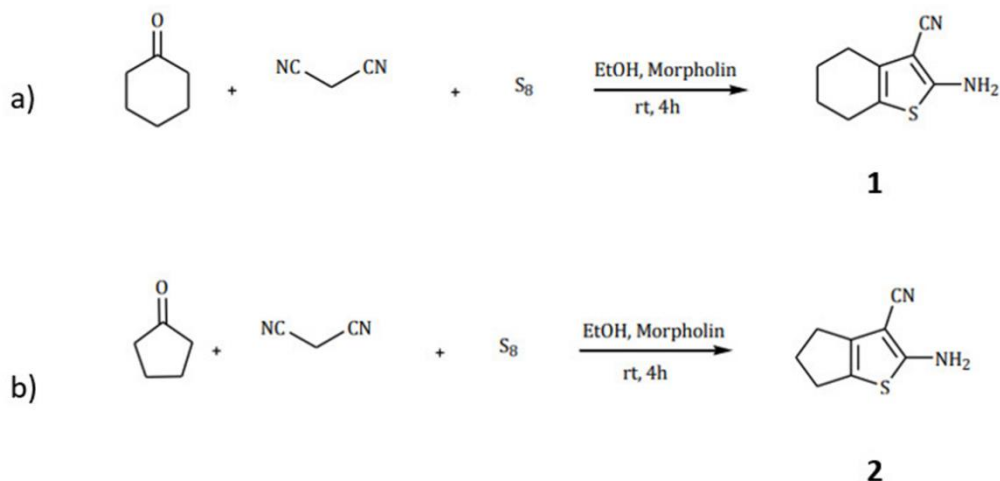
2.2. Synthesis of 2-amino-4,5,6,7-tetrahydro-benzo[b]thiophene-3-carbonitrile

First, 132 grams (2 moles) of malononitrile, 64 grams (2 moles) of sulfur, and 800 mL of ethanol at 20°C, 200 mL (2.3 moles) of morpholine were slowly added to a mixture of 200 grams (2 moles) of cyclohexanone. The mixture was then stirred for four hours, and the formed precipitate was filtered using a Buchner funnel and then washed with distilled water and ethanol, as described in the literature [21]. It was subsequently recrystallized in hot ethanol, resulting in the final compound, which appeared as cream-colored needle crystals with a yield of 97%.

As illustrated in Scheme 1, the first step of this reaction involves the Neunagel-Koop condensation between an active nitrile and a ketone or aldehyde, leading to the production of acrylonitrile. The product of this condensation undergoes sulfurization at the methylene position, followed by a ring addition reaction between the mercaptide and the cyano group. After the alkali catalysis step, the catalyst is removed, resulting in the formation of 2-aminothiophene. The melting point of compound (1) is 145°C, and the distinct TLC spots compared to the starting materials indicate the successful formation of this compound [33]. The IR spectrum data for this compound indicates a peak at 2192 cm⁻¹, associated with the C-N group. Additionally, the peaks observed in the range of 3442-3325 cm⁻¹ are associated with the NH₂ group of the primary amine. A peak at 1618 cm⁻¹ corresponds to the C=C bond, and the peak at 2914 cm⁻¹ is related to the stretching frequency of the aliphatic C-H bond. A similar process was used to synthesize compound 2.

2.3. Synthesis of 2-amino-5,6-dihydro-4H-cyclopenta[b]thiophene-3-carbonitrile

Morpholine (200 mL, 2.3 mol) was slowly added to a mixture of cyclopentanone (200 grams, 2 mol), malononitrile (132 grams, 2 mol), sulfur (64 grams, 2 mol), and 800 mL of ethanol at 20°C. The mixture was stirred for four hours, after which the formed solid was isolated using conventional methods [21]. Then, it was



Scheme 1. Synthesis of amino thiophenes (1 and 2) using the Gewald synthesis method: (a) Reaction with cyclohexanone and (b) Reaction with cyclopentanone.

diluted with water, and the final precipitate was filtered using a Buchner funnel and washed with distilled water and ethanol. The resulting precipitate was recrystallized in hot ethanol, yielding the final compound as brown pellets with a yield of 90%.

The melting point of compound (2) is 142°C. The IR spectrum of this compound indicates the formation of the compound through the following data: the peak of the C-N group (at approximately 2192 cm^{-1}), the NH_2 group (at approximately 3326 and 3421 cm^{-1}), the C=C bond (at approximately 1614 cm^{-1}), and the C-H bond (at approximately 2910 cm^{-1}).

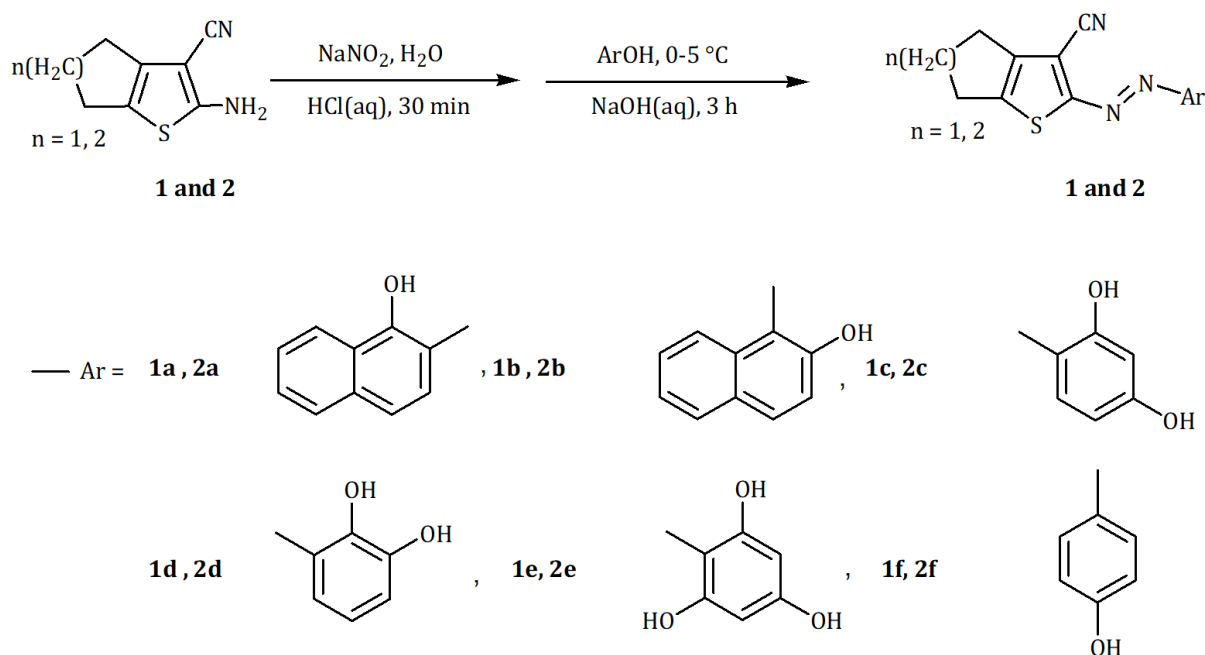
2.4. Measurements

All reactions were monitored using thin-layer chromatography (TLC) on commercially available pre-coated glass plates (silica gel 60 F₂₅₄, Merck), which were visualized under UV light at 254 nm. Melting points were recorded using an uncorrected Electrothermal-9200 melting point apparatus. Fourier-transform infrared (FT-IR) spectra were measured at room temperature with a Shimadzu 8400 FT-IR instrument. Proton nuclear magnetic resonance (^1H NMR) spectra were obtained using a Bruker 300 MHz NMR Spectrometer, with tetramethylsilane (TMS) as the internal reference. Ultraviolet/visible (UV/Vis) spectroscopy analyses were performed using a Shimadzu UV-1601 PC instrument.

3. Results and discussion

The synthesis of the novel azo compounds is illustrated in Scheme 2. The characterization data for the newly prepared azo compounds are summarized in Table 1. The FT-IR data (reported in Table 2) for new azo compounds exhibited characteristic bands corresponding to the coupling agents 1 and 2, the nitrile, hydroxyl, and alkene functional groups. Additionally, the existence of the (N=N) bond was confirmed by a band observed in the range of 1456–1650 cm^{-1} , indicating the success of the synthesis process. Azo compound 1a was selected as a representative example for the ^1H -NMR analysis, and the corresponding spectra are displayed in Figure 1. The ^1H -NMR spectral data for the newly prepared azo compounds are presented in Table 3.

The ^1H -NMR spectrum of compound 1a (Figure 1) indicates that the hydrogen of the O-H group appears at a higher chemical shift than the other prepared derivatives. This phenomenon is likely due to the proximity of the O-H group to the -N=N- double bond, which may result in tautomerism and the replacement of the hydrogen atom in the O-H group (Scheme 3). Based on the ^1H -NMR spectrum of this compound, the peak corresponding to the N-H amino group appears as a singlet at approximately 13.5 ppm. It can be attributed to the formation of an intramolecular hydrogen bond and the highly acidic nature of this hydrogen.



Scheme 2. Synthetic details of twelve novel azo compounds introduced in this work.

The hydrogen attached to carbon number 6, which is in the ortho position relative to the carbonyl group, is observed as a doublet around 7.8 ppm. This doublet results from the electron-withdrawing effect of the C=O group. The hydrogen bonded to carbon atom number 1 appears as a doublet peak in the region of 8.6 ppm. The hydrogens bonded to carbon atoms 2 and 3 appear as two triplet peaks at 7.4 ppm and 7.5 ppm, respectively. Hydrogen 4 is observed as a doublet peak at 7.7 ppm.

Hydrogen 5, which is situated in the meta position relative to the carbonyl group, appears as a doublet peak at 7.2 ppm. The hydrogens attached to carbon atoms 9 and 10, which share the same chemical environment, appear as a singlet peak at 1.8 ppm. Finally, the hydrogens attached to carbon atoms 8 and 11 appear as two singlet peaks at 2.7 ppm and 2.8 ppm, respectively.

The FT-IR spectra (Figure 2) of this compound (1a) include: stretching frequency related to the OH group

Table 1. Characterization results of synthesized azo compounds

Compound	Formula	Molar Mass (g/mol)	Weight Fraction, calc. (%)					Yield (%)	Melting Point (°C)
			C	H	N	S	O		
1	C ₉ H ₁₀ N ₂ S	178.26	53.89	5.65	15.71	17.99	0	97	145
2	C ₈ H ₈ N ₂ S	164.23	58.50	4.9	17.06	15.52	0	90	142
1a	C ₁₉ H ₁₅ N ₃ SO	333.41	68.44	4.53	12.60	9.61	4.79	72	260
1b	C ₁₉ H ₁₅ N ₃ SO	333.41	68.44	4.53	12.60	9.61	4.79	59	220
1c	C ₁₅ H ₁₃ N ₃ SO ₂	299.35	60.18	4.37	14.04	10.71	10.71	81	243
1d	C ₁₅ H ₁₃ N ₃ SO ₂	299.35	60.18	4.37	14.04	10.71	10.71	79	256
1e	C ₁₅ H ₁₃ N ₃ SO ₃	315.35	57.12	4.15	13.32	10.16	15.22	67	278
1f	C ₁₅ H ₁₃ N ₃ SO	283.35	63.57	4.62	14.83	11.31	5.64	58	234
2b	C ₁₈ H ₁₃ N ₃ SO	319.38	67.68	4.10	13.15	10.04	5.00	54	206
2c	C ₁₅ H ₁₃ N ₃ SO ₂	283.35	63.57	4.62	14.83	11.31	11.29	71	236
2d	C ₁₅ H ₁₃ N ₃ SO ₂	283.35	63.57	4.62	14.83	11.31	11.29	68	245
2e	C ₁₅ H ₁₃ N ₃ SO ₃	315.35	57.12	4.15	13.32	10.16	15.22	72	267
2f	C ₁₅ H ₁₃ N ₃ SO	283.35	63.57	4.62	14.83	11.31	5.64	62	228

Table 2. The FT-IR spectral data of newly prepared azo compounds

Compound	Spectral data
1	IR, ν/cm^{-1} : 1247 (C-N), 1417 (C=C), 1456 (N=N), 2214 (C \equiv N), 3064 (CH), 3346 (OH)
2	IR, ν/cm^{-1} : 1303 (C-N), 1523 (C=C), 1566 (N=N), 2223 (C \equiv N), 2927 (CH), 3238 (OH)
1a	IR, ν/cm^{-1} : 1319 (C-N), 1458 (C=C), 1620 (N=N), 2221 (C \equiv N), 3072 (CH), 33303 (OH)
1b	IR, ν/cm^{-1} : 1442 (C-N), 1523 (C=C), 1562 (N=N), 2214 (C \equiv N), 2928 (CH), 3423 (OH)
1c	IR, ν/cm^{-1} : 1427 (C-N), 1521 (C=C), 1639 (N=N), 2225 (C \equiv N), 2935 (CH), 3334 (OH)
1d	IR, ν/cm^{-1} : 1434 (C-N), 1515 (C=C), 1641 (N=N), 2225 (C \equiv N), 2937 (CH), 3400 (OH)
1e	IR, ν/cm^{-1} : 1303 (C-N), 1508 (C=C), 1436 (N=N), 2356 (C \equiv N), 3218 (CH), 3438 (OH)
1f	IR, ν/cm^{-1} : 1334 (C-N), 1515 (C=C), 1569 (N=N), 2206 (C \equiv N), 3421 (CH), 3226 (OH)
2b	IR, ν/cm^{-1} : 1340 (C-N), 1440 (C=C), 1566 (N=N), 2227 (C \equiv N), 3049 (CH), 3232 (OH)
2c	IR, ν/cm^{-1} : 1434 (C-N), 1581 (C=C), 1620 (N=N), 2202 (C \equiv N), 3055 (CH), 3197 (OH)
2d	IR, ν/cm^{-1} : 1407 (C-N), 1521 (C=C), 1631 (N=N), 2202 (C \equiv N), 2920 (CH), 3413 (OH)
2e	IR, ν/cm^{-1} : 1434 (C-N), 1515 (C=C), 1641 (N=N), 2225 (C \equiv N), 2937 (CH), 3400 (OH)
2f	IR, ν/cm^{-1} : 1247 (C-N), 1417 (C=C), 1456 (N=N), 2214 (C \equiv N), 3064 (CH), 3346 (OH)

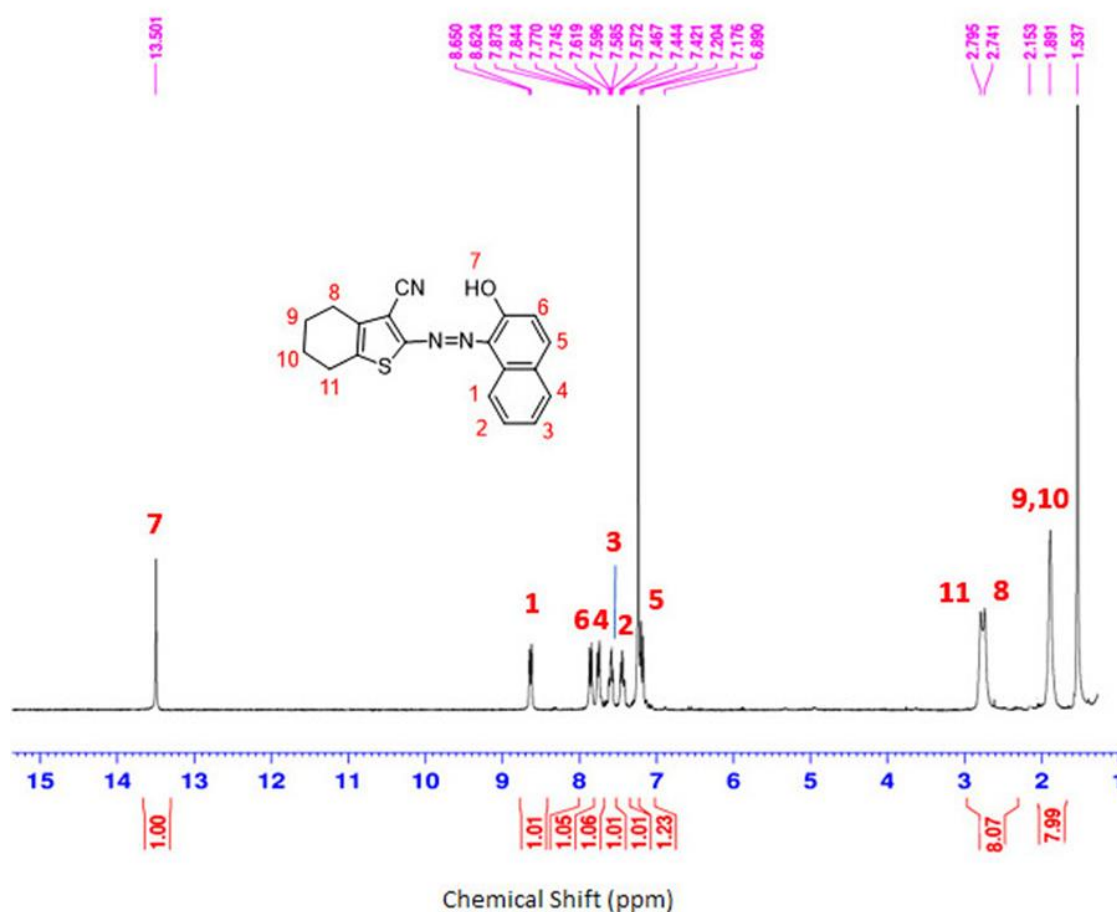
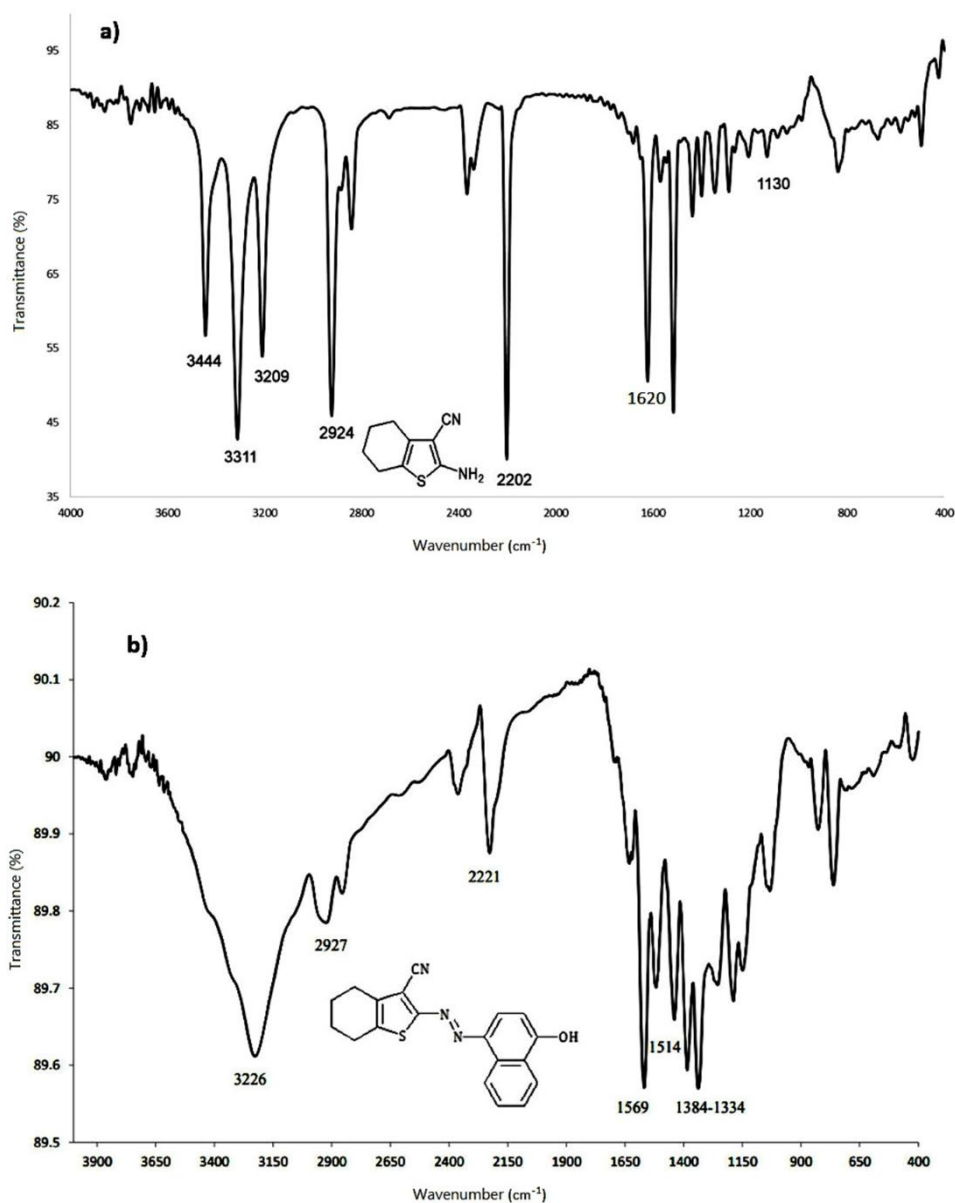
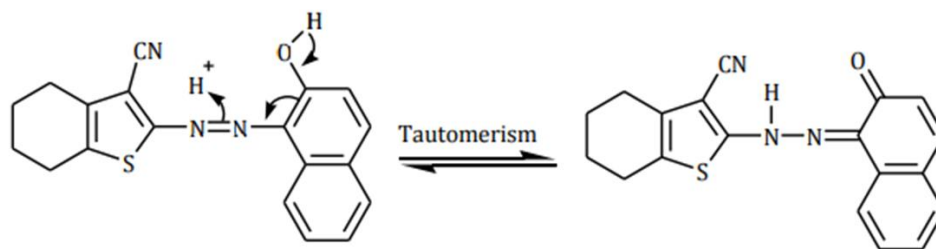
**Figure 1.** ^1H -NMR spectrum of 1a.

Table 3. ^1H -NMR spectral data of newly prepared azo compounds

Compound	Spectral data
1a	^1H NMR (CDCl_3), δ /ppm: 1.8 (s, 4H, CH_2), 2.7 (s, 2H, CH_2), 2.8 (s, 2H, CH_2), 6.8 (d, $J=8.4$ Hz, 2H, ArH), 6.8 (d, $J=8.4$ Hz, 2H, ArH), 7.4 (t, $J=6.9$ Hz, 1H, ArH), 7.5 (t, $J=14.01$ Hz, 1H, ArH), 7.7 (d, $J=7.5$ Hz, 1H, ArH), 7.8 (d, $J=8.7$ Hz, 1H, ArH), 8.6 (d, $J=7.8$ Hz, 1H, ArH), 13.5 (s, 1H, OH).
1b	^1H NMR ($\text{DMSO}-d_6$), δ /ppm: 2.3 (s, 4H, CH_2), 2.7 (s, 2H, CH_2), 2.9 (s, 2H, CH_2), 7.1 (d, $J=7.8$ Hz, 1H, ArH), 7.2 (m, 2H, ArH), 7.9 (d, $J=7.8$ Hz, 1H, ArH), 8.2 (d, $J=7.8$ Hz, 1H, ArH), 8.63 (d, $J=7.8$ Hz, 1H, ArH), 11.63 (s, 1H, OH).
1c	^1H NMR ($\text{DMSO}-d_6$), δ /ppm: 1.8 (s, 4H, CH_2), 2.6 (s, 2H, ArH), 2.7 (s, 2H, ArH), 6.4 (s, 1H, ArH), 6.5 (d, $J=3$ Hz, 1H, ArH), 7.83 (d, $J=1.2$ Hz, 1H, ArH), 10.88 (s, 1H, OH), 11.08 (s, 1H, OH).

Notes: DMSO: dimethyl sulfoxide, J : coupling constant**Figure 2.** FT-IR spectra of: (a) **1** and (b) **1a**.



Scheme 3. The tautomerization in compound 1a.

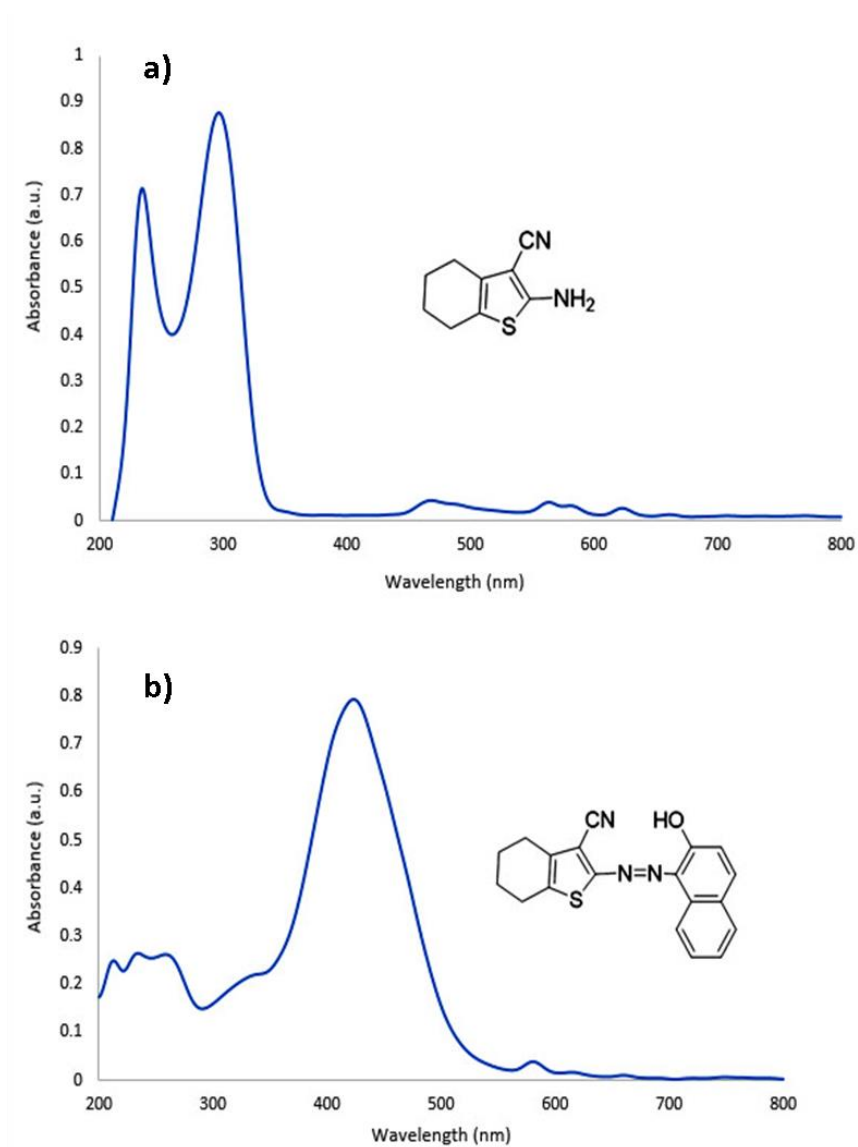
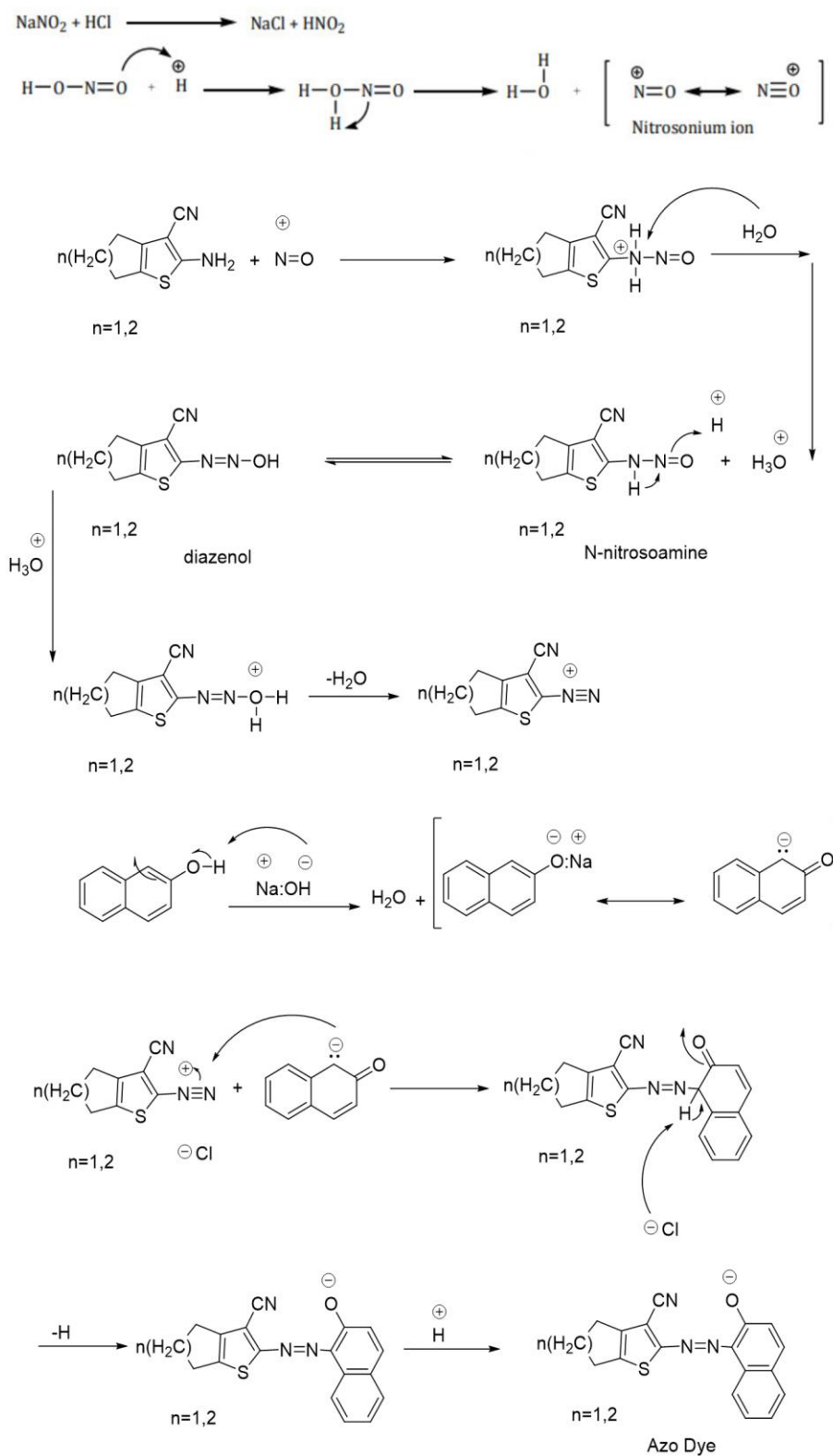


Figure 3. UV-vis spectra of: (a) **1** and (b) **1a**.



Scheme 4. The mechanism of coupling of aminothiophenes (1 and 2) with 2-naphthol.

Table 4. UV-vis spectral data of newly prepared azo compounds

Compound	Spectral data of UV-vis: λ_{\max} (nm)	Color of the compound
1	UV-vis (DMSO): λ_{\max} 510 nm	dark red, almost brown
2	UV-vis (Acetone): λ_{\max} 507 nm	dark red
1a	UV-vis (Acetone): λ_{\max} 470 nm	light brown
1b	UV-vis (Acetone): λ_{\max} 469 nm	brown
1c	UV-vis (Acetone): λ_{\max} 477 nm	light red
1d	UV-vis (Acetone): λ_{\max} 368 nm	brown
1e	UV-vis (DMSO): λ_{\max} 506 nm	dark red
1f	UV-vis (Acetone): λ_{\max} 499 nm	dark red, almost black
2b	UV-vis (Acetone): λ_{\max} 468 nm	dark brown
2c	UV-vis (Acetone): λ_{\max} 467 nm	brown
2d	UV-vis (Acetone): λ_{\max} 475 nm	dark red
2e	UV-vis (Acetone): λ_{\max} 362 nm	dark brown
2f	UV-vis (DMSO): λ_{\max} 510 nm	dark red, almost brown

(due to the formation of an intramolecular hydrogen bond) at around 3346 cm^{-1} , the aromatic peak of C-H is in the area of 3064 cm^{-1} . The peak related to the N=N bond is in the region of 1456 cm^{-1} . A peak of aromatic C=C bond appears at 1417 cm^{-1} . The peaks related to the C≡N bond and C-N bond are observed at 2214 and 1247 cm^{-1} , respectively. As expected, the FT-IR spectra of **1** and **1a** exhibited the same characteristic bands of the coupling agent **1**, namely nitrile and alkene groups. In contrast, the existence of the azo band in 1456 cm^{-1} and hydroxyl group bond in 3346 cm^{-1} [22] in the FT-IR spectrum of **1a**, confirmed that the synthesis is successful. The proposed reaction mechanism appears in Scheme 4.

**Figure 4.** Digital images of samples: (a) **1** and (b) **1a**.

The azo group (N=N) usually gives an absorption in the 350–370 nm range [23]. As expected, the examination of Figure 3 showed that the new azo compounds (**1a**, for example) would exhibit higher λ_{\max} due to the presence of the hydroxyl group in the compounds [24]. The results indicated a positive outcome, revealing a higher absorption wavelength ranging from 362 to 510 nm. The UV/vis data for the azo compounds **1a-f** and **2a-f** are presented in Table 4. Additionally, images of samples **1** and **1a** are shown in Figure 4.

4. Conclusions


In summary, two new 2-aminothiophene compounds were synthesized with excellent yields using the Gewald three-component reaction. Additionally, twelve new azo compounds based on 2-amino-4, 5, 6, 7-tetrahydrobenzo[b]thiophene-3-carbonitrile and 2-amino-5, 6-dihydro-4H-cyclopenta[b]thiophene-3-carbonitrile were successfully synthesized with good yields. These compounds were characterized using ^1H -NMR, FT-IR, UV/Visible spectroscopy, and elemental analysis. All analyses confirmed the successful synthesis of the desired products.

Conflict of Interest

The authors declare no conflict of interest.

References

1. H. Zollinger, *Diazo chemistry I: aromatic and heteroaromatic compounds*. 1994, Germany: VCH Verlagsgesellschaft mbH.
2. Z.C. Chan, et al. Revealing and mitigating the inhibitory effect of serotonin on HRP-mediated protein labelling. *Sci Rep*, **2024**, 14, 32126.
3. I. Ali, et al. Advances in Simple and Chiral-HPLC Methods for Antiallergic Drugs and Chiral Recognition Mechanism. *Analytica*, **2023**, 4, 66.
4. S. Vegesna and C. Prasada Rao. Bio-method development and validation of ketotifen fumarate in rabbit plasma using RP-HPLC. *Journal of Advanced Zoology*, **2024**, 45, 1359.
5. M.A. Salih, D.F. Aziz, and S.I. Ali. Determination of Ketotifen Fumarate in Syrup Dosage Form by High Performance Liquid Chromatography. *Kurdistan Journal of Applied Research*, **2020**, 6, 63.
6. M. Yousuf, et al. Development and validation of HPLC method for simultaneous determination of Ketotifen Fumarate and Salbutamol Sulfate in bulk and tablets dosage forms. *Main Group Chemistry*, **2021**, 21, 1.
7. M.M. Abd, A.D. Hussein, and Y. Aamer. Development of a sensitive spectrophotometric method for the quantification of ketotifen fumarate in aqueous solutions via diazotization of 4-aminoantipyrene. *International Journal of Advanced Chemistry Research*, **2025**, 7, 11.
8. A. Towns. Developments in azo disperse dyes derived from heterocyclic diazo components. *Dyes and Pigments*, **1999**, 42, 3.
9. H.S. Freeman and A.T. Peters, *Colorants for non-textile applications*. 2000, The Netherlands: Elsevier.
10. P. Gregory, *Ink-jet printing*, in *High-Technology Applications of Organic Colorants*. 1991, Springer Science+Business Media: New York. 175.
11. M.I. Velasco, et al. A green alternative to synthesize azo compounds. *Dyes and Pigments*, **2011**, 90, 259.
12. M.S. Yen and J. Wang. Synthesis and absorption spectra of heteroaryl azo dyes derived from coupler 4-aryl-3-cyano-2-aminothiophenes. *Dyes and Pigments*, **2004**, 61, 243.
13. T.S. Jagodzinski. Thioamides as useful synthons in the synthesis of heterocycles. *Chemical reviews*, **2003**, 103, 197.
14. S.M. Al-Mousawi, M.A. El-Asasery, and H.M. Mahmoud. Disperse Dyes Based on Aminothiophenes: Their Dyeing Applications on Polyester Fabrics and Their Antimicrobial Activity. *Molecules*, **2013**, 18, 7081.
15. H. Xu and X. Zeng. Synthesis of diaryl-azo derivatives as potential antifungal agents. *Bioorganic & medicinal chemistry letters*, **2010**, 20, 4193.
16. Y. Kubo, et al. Colorimetric chiral recognition by a molecular sensor. *Nature*, **1996**, 382, 522.
17. B. Bahadur. Ultrasonic velocity and absorption of the nematic liquid crystal HBT. *Journal of Physics C: Solid State Physics*, **1976**, 9, 11.
18. Y. He, et al. Dendritic azo compounds as a new type amorphous molecular material with quick photoinduced surface-relief-grating formation ability. *Optical Materials*, **2008**, 31, 18.
19. S. Pieraccini, et al. A new axially-chiral photochemical switch. *Chemical Communications*, **2003**, 2003, 598.
20. Q.M. Ali, et al. Sudan IV dye based poly (alkyloxymethacrylate) films for optical data storage. *Optics communications*, **2006**, 267, 236.
21. R. Sabnis, D. Rangnekar, and N. Sonawane. 2-Aminothiophenes by the Gewald reaction. *Journal of heterocyclic chemistry*, **1999**, 36, 333.
22. A. Jalali. Synthesis and Characterization of Novel Polyamide-imides Containing Thioether Linkages, Thiazole, and Nitrophenyl Units with High Solubility and Processability for Optical Film Applications. *Journal of Applied Material Science*, **2025**, 1, 210133.
23. H. Allcock, S.D. Wright, and K.M. Kosydar. Poly (organophosphazenes) with chromophores as substituent groups. *Macromolecules*, **1978**, 11, 357.
24. P.S. Singh, et al. Optoelectrochemical Study of Indole-Quinoxaline-Based π -Extended Donor-Acceptor Framework: Dual Blue and Red Fluorescent, n -Type Material. *ChemistrySelect*, **2025**, 10, e202405046.

© 2025 The Authors. This article is licensed under a Creative Commons Attribution 4.0 BY International License. 

Hybrid Ionic Liquid-assisted Biomagnetic Nanocomposite for Efficient Removal of a Cationic Dye

Mounika Thati ^{a,b}, Madhavi Vemula ^{c,*}, Santhee Devi Karri ^{a,*}

^a Department of Environmental Science, GITAM Deemed to be University, Vishakhapatnam, India

^b Department of Environmental Science, BVRIT HYDERABAD College of Engineering for Women, Hyderabad, India

^c Department of Chemistry, BVRIT HYDERABAD College of Engineering for Women, Hyderabad, India

Editor's note: Conventional methods for dye removal, such as adsorption, have several limitations, including low efficiency, high costs, and the risk of secondary pollution. This has led to significant research interest in developing sustainable and innovative materials for dye absorption. Thati et al. utilized coconut shells as a green resource to create biomagnetic nanocomposites that demonstrate high efficiency in removing cationic dyes.

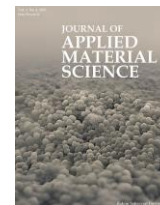
doi: 10.22034/jams.2025.210138

How to cite: M. Thati et al. *Journal of Applied Material Science*, 2025, 1, 210138.



JOURNAL OF
APPLIED
MATERIAL
SCIENCE

jams.hsu.ac.ir



Communication

Hybrid Ionic Liquid-assisted Biomagnetic Nanocomposite for Efficient Removal of a Cationic Dye

Mounika Thati ^{a,b}, Madhavi Vemula ^{c,*}, Santhee Devi Karri ^{a,*}

^a Department of Environmental Science, GITAM Deemed to be University, Vishakhapatnam, India

^b Department of Environmental Science, BVRIT HYDERABAD College of Engineering for Women, Hyderabad, India

^c Department of Chemistry, BVRIT HYDERABAD College of Engineering for Women, Hyderabad, India

Abstract

The presence of organic toxic dyes in the aqueous environment poses a potential threat to the ecosystems. Ionic liquids (ILs), typically considered green solvents, confer diverse benefits and versatility in applications. Magnetite biochar composites and ILs can be combined to form novel hybrid nanocomposites, providing collaborative advantages, preserving features of individual components, and attaining innovative performances. This study aims to fabricate an IL-assisted biomagnetic hybrid nanocomposite material, analyse its physiochemical characteristics, and evaluate its efficiency in the adsorptive removal of toxic rhodamine blue (RhB) dye in aqueous solution. The mean diameter of the IL-assisted biomagnetic nanocomposite material was found to be 45 ± 6 nm. The removal efficiency was optimised using various parameters such as pH, contact time, as well as adsorbent and adsorbate concentrations. The bionanocomposite demonstrated 97.5% of RhB removal percentage and 135 mg/g of adsorption capacity within 45 min and showed remarkable reusability of up to five cycles. The hybrid IL-assisted biomagnetic nanocomposite prepared in this work offers a viable and sustainable approach to removing industrial synthetic dyes in contaminated aquatic ecosystems.

Keywords: Ionic liquids; Biomagnetic nanocomposites; Adsorption; Rhodamine blue dye; Sustainability.

1. Introduction

The indiscriminate release of industrial dyes, such as Rhodamine blue (RhB), into water bodies has become a major environmental concern [1, 2]. RhB dye is not only

aesthetically pleasing but also toxic, carcinogenic, and mutagenic, posing severe threats to aquatic life and human health. Conventional dye removal methods, including adsorption, photocatalysis, and biodegradation, often suffer from limitations such as low efficiency, high cost, and secondary pollution [3-6].

* Corresponding authors.

Email addresses: madhuchem9@gmail.com (M. Vemula), skarri2@gitam.edu (S.D. Karri)

Received 28 April 2025

Revised 9 May 2025

Accepted 11 May 2025

Available online 12 May 2025

<https://doi.org/10.22034/jams.2025.210138>

© 2025 The Authors. This article is licensed under a Creative Commons Attribution 4.0 International License.

210138 (1 of 6)

In recent years, magnetite iron oxide (Fe_3O_4) biochar nanocomposites have emerged as promising adsorbents for dye removal due to their high surface area, magnetic separability, and eco-friendly nature [7-9]. However, their adsorption capacity and selectivity can be further improved by incorporating hybrid ionic liquids (ILs), which can enhance the surface properties and functionality of the nanocomposites [10-13].

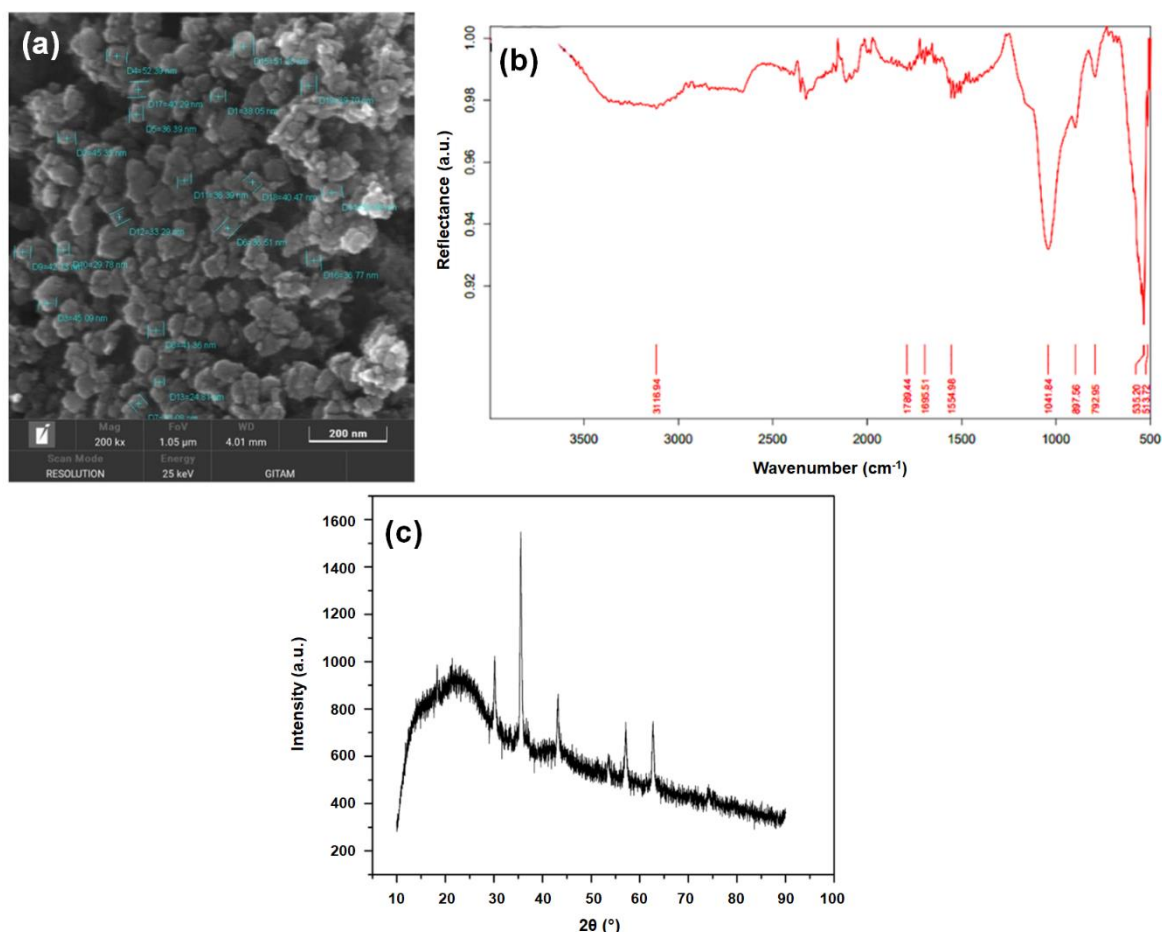
This study focuses on the design and synthesis of hybrid ionic liquid-assisted magnetite biochar nanocomposites for the efficient removal of Rhodamine blue dye from contaminated water.

2. Experimental

Coconut shells were cleaned, ground, oven dried, and calcined to 700°C . The calcined powder was then activated with KOH and neutralised with 0.5M HCl. Ferrous and ferric salts were dissolved in a small volume

of strong and dilute acid, and NaOH was added dropwise with sonication for 2h. The resulting precipitate was magnetically separated, washed, and dried. Magnetite nanoparticles and activated biochar were combined in a 1:2 ratio, followed by the addition of 0.5g of the ionic liquid 1-ethyl-3-methylimidazolium tetrafluoroborate. The mixture was then sonicated in diethyl ether at 50°C for 12 hours. The solid was washed, dried, and labelled as ILMBC.

ILMBC was subjected to different characterization techniques such as FESEM, FTIR, and XRD to assess its morphology, functional groups, and chemical surface character. Batch experiments were performed to investigate the adsorption of RhB dye on ILMBC. In these experiments, 50 mL of RhB dye solutions with concentrations of 50-200 mg/L were treated with ILMBC doses of 0.03 and 0.05 g at pH 8, with contact times ranging from 15-45 minutes. The initial and final concentration of RhB dye was determined using UV-Vis



spectrophotometry at a wavelength of 554 nm. The adsorption efficiency of ILMBC for the removal of RhB dye was calculated using equation (1):

$$\% = \frac{C_0 - C_e}{C_0} \times 100 \quad (1)$$

where C_0 and C_e are the initial and equilibrium concentrations of RHB dye.

3. Results and discussion

FESEM analysis, presented in Figure 1a, revealed a porous surface topology, characterized by spherical particles with an average diameter of 45 nm. Upon high-magnification imaging, the presence of voids and pores within the magnetite biochar structure became evident, suggesting a high surface area. FTIR spectroscopy results in Figure 1b revealed the functional groups present in the IL-based magnetite coconut shell biochar composite. The spectrum showed distinct bands, including hydroxyl (3116 cm^{-1}) and carboxyl (1789 cm^{-1}) groups, C=O stretching vibrations (1695 cm^{-1}), and C=C

stretching vibrations (1554 cm^{-1}). The presence of IL was confirmed by the observed peaks for B-F stretching vibrations (1041 cm^{-1}) and aromatic C-H out-of-plane bending vibrations (792 cm^{-1}). Fe-O stretching vibrations ($535\text{--}513 \text{ cm}^{-1}$) indicated the magnetized nature of the material, confirming the effective immobilization of IL onto the surface of Fe_3O_4 and biochar. The X-ray diffraction (XRD) pattern of the ILMBC hybrid nanocomposite in Figure 1c exhibited a characteristic diffraction peak at a 2θ value of 35.52° corresponding to the (311) planes of magnetite. The absence of sharp IL peaks and iron oxide diffraction peaks indicates the IL's amorphous nature and its effective capping of magnetite, preventing oxidation. The average particle size was approximately 45 nm, as calculated by Debye-Scherrer's equation.

The adsorption efficiency of ILMBC was evaluated using the surface plot in Figure 2a, the contour plot in Figure 2b, and the linear form of the Langmuir adsorption isotherm (equation 2) in Figure 2c.

$$\frac{C_e}{q_e} = \frac{1}{Q_0} C_e + \frac{1}{Q_0 b} \quad (2)$$

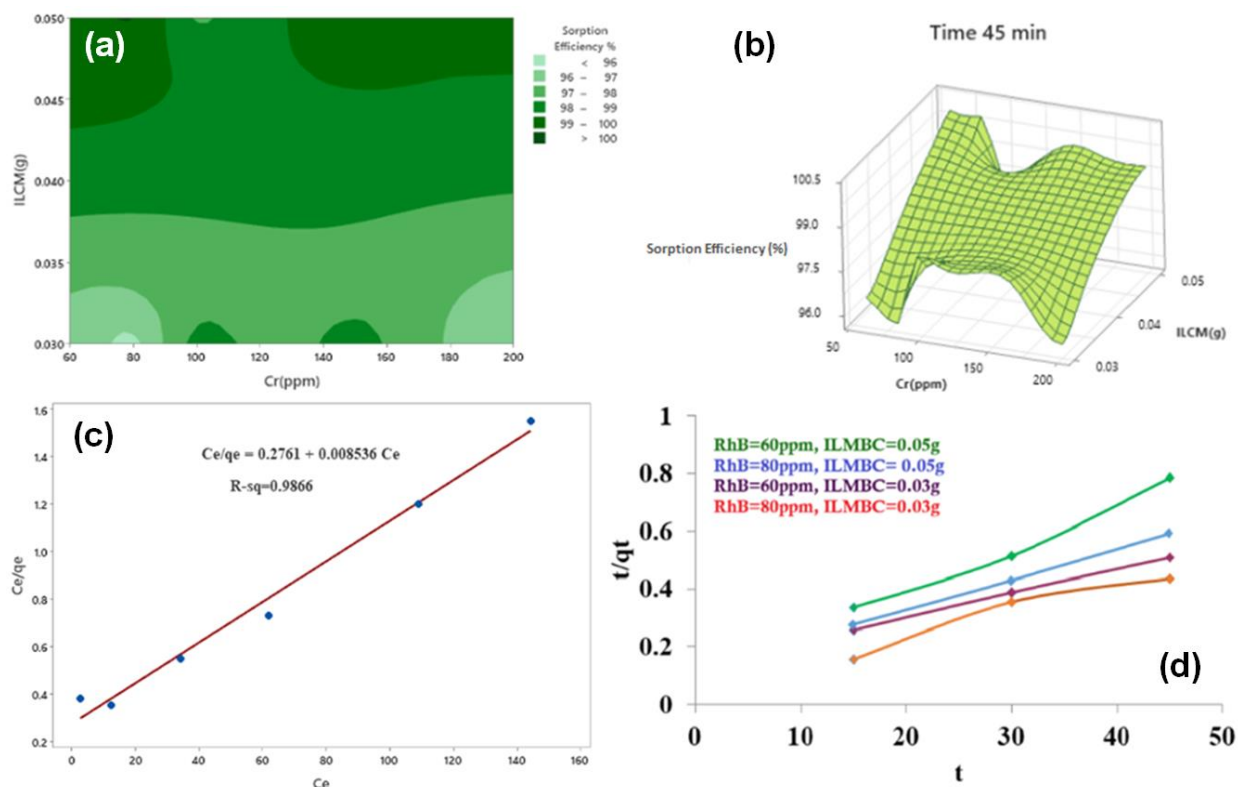


Figure 2. (a) Surface plot and (b) Contour plot of ILMBC for sorption efficiency at 45 min, (c) Langmuir adsorption isotherm, as well as (d) Pseudo second order kinetics results.

Table 1. Comparison of maximum RhB dye adsorption capacities (mg/g) of various adsorbents

Adsorbent	Adsorption capacity (mg/g)	Reference
Furfural residue	37.93	[14]
Coconut coir	14.9	[15]
Sodium montmorillonite	38.27	[16]
Coffee grounds	7.51	[17]
Natural zeolite Clinoptilolite	2.81	[18]
Sulphuric Acid-modified fly ash	36.36	[19]
Casuarina equisetifolia needle	82.34	[20]
Artocarpus heterophyllus	103.92	[21]
ILMBC	135	This study

In this equation, C_e , q_e , Q_0 , and b are the equilibrium concentration (mg/L), adsorption capacity of adsorbent (mg/g), maximum adsorption capacity, and Langmuir adsorption constant (L/mg), respectively. The maximum removal and adsorption capacities of ILMBC were found to be 97.5% and 135 mg/g, respectively.

The adsorption rate was determined by pseudo-second order kinetics to assess the adsorption ability of ILMBC according to equation 3 (Figure 2d). The correlation coefficient was greater than 0.9, suggesting good adsorption fits.

$$\frac{t}{q_t} = \frac{1}{k_2 q_e^2} + \frac{t}{q_e} \quad (3)$$

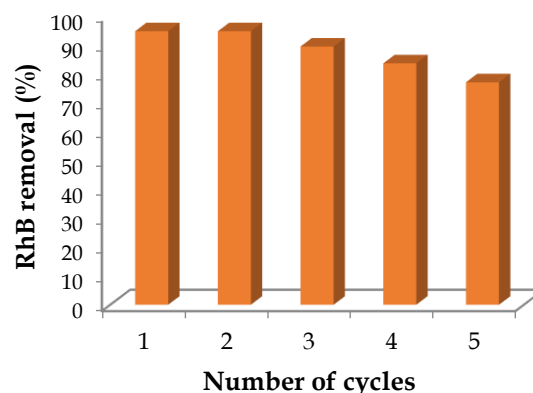
Table 1 provides a comparison between the maximum adsorption capacity (mg/g) of ILMBC nanocomposite in removing RhB dye with different reported adsorbents in the literature. In particular, the ILMBC nanocomposite shows a higher adsorption capacity than most polymeric and bioadsorbents, surpassing natural and synthetic ones.

The magnetic property of ILMBC allows easy regeneration and reusability of the adsorbent. After adsorption, recovery of ILMBC can be easily achieved by employing an external magnet, elution with methanol, and reuse for the next RhB adsorption experiment. Importantly, the adsorbent showed great reusability and retained its performance up to 5 cycles in 50 mL solution containing 100 mg/L RhB solution, as shown in Figure 3

The ILMBC nanocomposite is very promising for the treatment of wastewater because it possesses superior adsorption capability for RhB dye removal. Nonetheless, there are apprehensions about the environmental and biological hazards that the application of ionic liquids

(ILs) and Fe_3O_4 nanoparticles may pose. These include persistence, toxicity, and bioaccumulation in aquatic organisms and microorganisms. In order to combat these risks, future studies will aim to study biodegradability, toxicity, and disposal practices, surface modification, and extensive toxicity testing.

There are various challenges that must be overcome, ranging from technical ones like scaling up synthesis and use, stability, and regeneration of the nanocomposite. There is also the need for regulatory compliance and risk evaluation, as well as economic factors such as cost-effectiveness and industrial scale-up. Through recognition and solution of these challenges, we can ensure safe development and utilization of ILMBC nanocomposite for wastewater treatment and ultimately enhance sustainable use and reduce possible risks.

**Figure 3.** Regeneration efficiency of ILMBC against removal percentage up to 5 cycles.

4. Conclusions

In summary, this research effectively proved the synthesis and application of a new magnetic hybrid nanocomposite, ILMBC, for effective removal of RhB dye from water solutions. The ILMBC showed great adsorption capacity, fast kinetics, and outstanding reusability for several cycles. The magnetic nature of the composite facilitated easy regeneration and separation, and it is a promising candidate for wastewater treatment processes. These results underscore the promise of ILMBC as a cost-effective and environmentally friendly dye removal method and open new avenues for further development and research.

Conflict of Interest

The authors declare no conflict of interest.

References

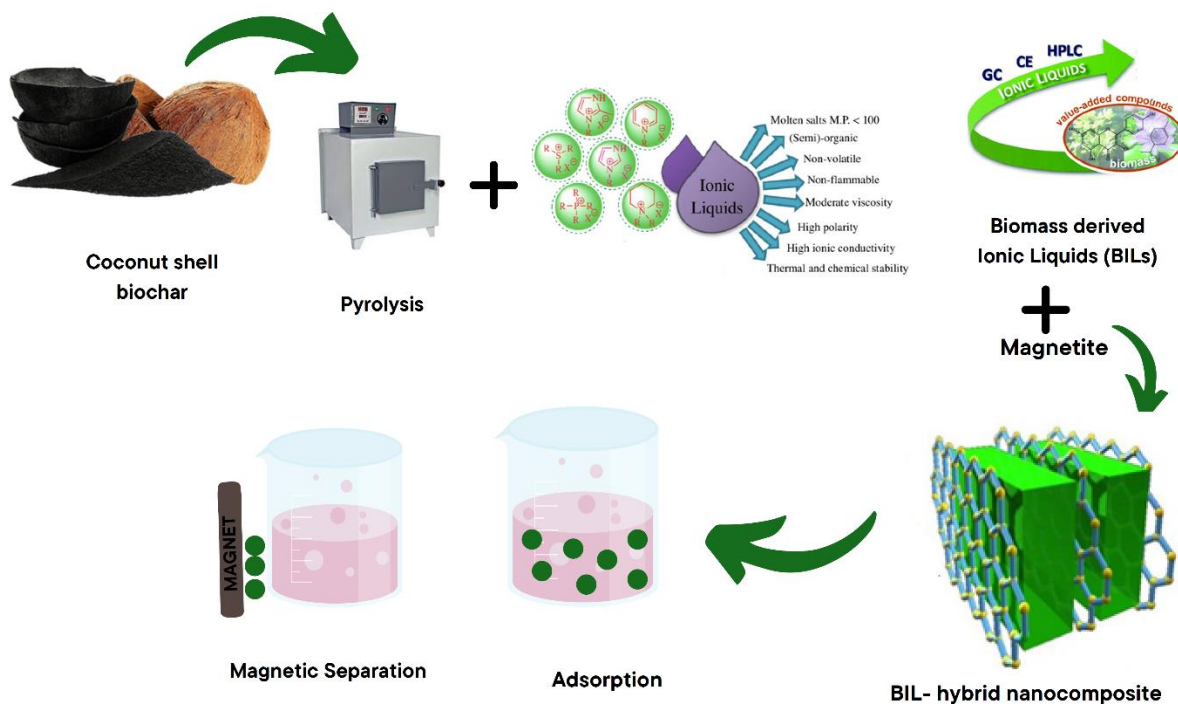
1. R. Kishor, et al. Ecotoxicological and health concerns of persistent coloring pollutants of textile industry wastewater and treatment approaches for environmental safety. *Journal of Environmental Chemical Engineering*, **2021**, 9, 105012.
2. Y. Zhao, et al. Insights into enhanced adsorptive removal of Rhodamine B by different chemically modified garlic peels: Comparison, kinetics, isotherms, thermodynamics and mechanism. *Journal of Molecular Liquids*, **2019**, 293, 111516.
3. A. Ahmad, et al. Recent advances in new generation dye removal technologies: novel search for approaches to reprocess wastewater. *RSC Advances*, **2015**, 5, 30801.
4. M. Biuki, et al. The application of modified walnut shell with magnetite nanoparticles as an adsorbent for the removal of organic dye fuchsin from aqueous solutions. *Separation Science and Technology*, **2025**, 60, 931.
5. İ. Küçük and N. Yıldız Küçük. Composite Formation of Active Biochar from Pomegranate Peel with Magnetite and Alginat Beads for Methylene Blue Adsorption Using Box-Behnken Design. *Applied Sciences*, **2025**, 15, 2085.
6. S.J. Peighambari, et al. Simultaneous elimination of cationic dyes from water media by carboxymethyl cellulose-graft-poly(acrylamide)/magnetic biochar nanocomposite hydrogel adsorbent. *Environmental Research*, **2025**, 273, 121150.
7. P.B. Chouke, et al. Bioinspired metal/metal oxide nanoparticles: A road map to potential applications. *Materials Today Advances*, **2022**, 16, 100314.
8. S. Gitipour, et al. Effective elimination of Pb (II) cations from waste water and polluted water using siderite magnetic biochar. *Scientific Reports*, **2025**, 15, 7912.
9. C. Li, et al. Performance and mechanism of a novel bamboo-based magnetic biochar composite for efficient removal of norfloxacin. *Advanced Composites and Hybrid Materials*, **2025**, 8, 71.
10. F. Karimi, M.A. Zolfigol, and M. Yarie. A novel and reusable ionically tagged nanomagnetic catalyst: Application for the preparation of 2-amino-6-(2-oxo-2H-chromen-3-yl)-4-arylnicotinonitriles via vinylogous anomeric based oxidation. *Molecular Catalysis*, **2019**, 463, 20.
11. Z. Huang, et al. Effect of ionic liquid assisted hydrothermal carbonization on the properties and gasification reactivity of hydrochar derived from eucalyptus. *Journal of Colloid and Interface Science*, **2021**, 586, 423.
12. J. Im, et al. Structural characteristics and thermal properties of regenerated cellulose, hemicellulose and lignin after being dissolved in ionic liquids. *Journal of Industrial and Engineering Chemistry*, **2022**, 107, 365.
13. S.B. Ruvubu and I. Roy. Innovative nanocomposites for pollutant capture: Adsorption of rhodamine B dye using polyaniline-coated chitosan trisodium citrate nanocomposites. *International Journal of Biological Macromolecules*, **2025**, 292, 139293.
14. X. Chen, et al. Effective removal of methyl orange and rhodamine B from aqueous solution using furfural industrial processing waste: Furfural residue as an eco-friendly biosorbent. *Colloids and Surfaces A: Physicochemical and Engineering Aspects*, **2019**, 583, 123976.
15. M.V. Sureshkumar and C. Namasivayam. Adsorption behavior of Direct Red 12B and Rhodamine B from water onto surfactant-modified coconut coir pith. *Colloids and Surfaces A: Physicochemical and Engineering Aspects*, **2008**, 317, 277.
16. P.P. Selvam, et al. Removal of rhodamine B from aqueous solution by adsorption onto sodium montmorillonite. *Journal of Hazardous Materials*, **2008**, 155, 39.
17. T.S. Vo, M.M. Hossain, and K. Kim. Natural bamboo powder and coffee ground as low-cost green adsorbents for the removal of rhodamine B and their recycling performance. *Scientific Reports*, **2023**, 13, 21487.
18. S.F.A. Shah, et al. Modified Clinoptilolite for the Removal of Rhodamine B Dye from Wastewater. *Sustainability*, **2024**, 16, 2267.
19. G.B. Balji, P.S. Kumar, and M.R.R. Kooh. Sulphuric Acid-Modified Coal Fly Ash for the Removal of Rhodamine B Dye from Water Environment: Isotherm, Kinetics, and Thermodynamic Studies. *Adsorption Science & Technology*, **2023**, 2023, 2808794.

20. M.R.R. Kooh, et al. The removal of rhodamine B dye from aqueous solution using *Casuarina equisetifolia* needles as adsorbent. *Cogent Environmental Science*, **2016**, 2, 1140553.
21. S. E. V, B. Mathew, and S. John. Utilization of biomass from *Artocarpus heterophyllus* as a sustainable adsorbent for

cationic dyes from water: mechanistic insights and practical applicability. *Biomass Conversion and Biorefinery*, **2025**, doi: 10.1007/s13399.

© 2025 The Authors. This article is licensed under a Creative Commons Attribution 4.0 BY International License. (cc) (i)

Graphical Abstract



Exploring Corrosion Protection Potential of Sustainable and Green *Morus alba* 'Pendula' Fruit Extracts

Sara Shiri *

^a Department of Chemical Engineering, Faculty of Engineering, University of Garmsar, Garmsar, Iran

Editor's note: Plant extracts can provide new opportunities for developing next-generation sustainable corrosion protection systems. Shiri utilized Pendula fruit extracts as a novel resource for creating corrosion inhibition systems. The developed system was effective in preventing mild steel corrosion in a salty environment, indicating the potential of this green corrosion protection method for future sustainable applications.

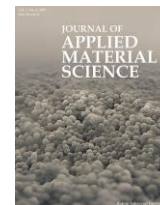
doi: 10.22034/jams.2025.210139

How to cite: S. Shiri. *Journal of Applied Material Science*, 2025, 1, 210139.



JOURNAL OF
APPLIED
MATERIAL
SCIENCE

jams.hsu.ac.ir



Communication

Exploring Corrosion Protection Potential of Sustainable and Green *Morus alba* 'Pendula' Fruit Extracts

Sara Shiri *

Department of Chemical Engineering, Faculty of Engineering, University of Garmsar, Garmsar, Iran

Abstract

With climate change, corrosion is becoming more and more important. This phenomenon reduces the strength of metals and causes both huge damage and environmental pollution. It can be said that among all the methods to prevent corrosion, the use of chemical corrosion inhibitors is very common. But they cause environmental pollution because many of the raw materials used to prepare these inhibitors are toxic. On the other hand, many of them cause the release of heavy metals into the environment. Therefore, today, researchers are evaluating the use of plant extracts as a corrosion inhibitor. These inhibitors are known as green corrosion inhibitors (GCI). In this study, an attempt was made to evaluate the corrosion potential of the ethanolic extract of *Morus alba* 'Pendula' fruit on mild steel (MS) in salt solution. For this purpose, electrochemical impedance spectroscopy (EIS) testing was used. The evaluation results showed that this extract improves corrosion resistance and can be used and evaluated in protective coatings in the future.

Keywords: Green chemistry; Protection of metal; Inhibitory efficiencies.

1. Introduction

Corrosion can be considered a phenomenon that both causes environmental pollution and brings huge economic losses [1, 2]. Researchers consider this phenomenon to be a spontaneous process, although many factors play a role in it, such as temperature, humidity, and chemicals [3-5]. Destruction of metal structures due to corrosion always causes damage to many industries, such as construction and marine [6-8]. To prevent corrosion, chemical corrosion inhibitors have always been the priority, but their use has been very limited due to environmental issues and toxicity [9-11].

In the meantime, researchers have conducted a lot of research on the use of plant extracts to prevent corrosion [12]. Plant extracts are very popular due to their availability, cheapness, and non-toxicity [13-16]. Mulberry is a valuable plant that can be said to be used from almost all parts [17]. In many countries, such as Iran, Türkiye, and Greece, varieties of this plant are cultivated [18]. In traditional medicine, *Morus alba* 'Pendula' is used to treat fever, protect the liver, and reduce blood pressure [19]. Also, *Morus alba* 'Pendula' contains antimicrobial and antioxidant compounds [20]. In this study, the potential of *Morus alba* 'Pendula' fruit extract as a GCI has been evaluated.

* Corresponding author.

Email address: sarashiri.chem.eng@gmail.com (S. Shiri)

Received 09 May 2025

Revised 16 May 2025

Accepted 18 May 2025

Available online 19 May 2025

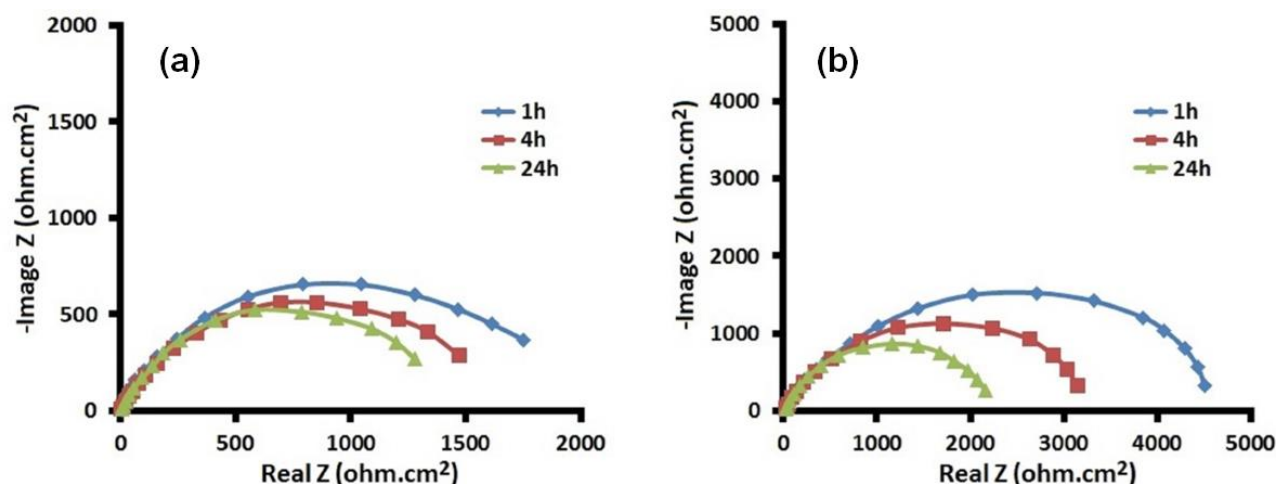


Figure 1. Nyquist plots at different immersion times.

2. Experimental

2.1. Materials

The sodium chloride (NaCl) and MS were obtained from Merck Company (Germany) and Iranian Mobarakeh Steel Company, respectively. Also, *Morus alba* 'Pendula' fruit was obtained from a local market (Ramsar city, a region in northern Iran).

2.2. Preparation of extract, MS substrate, and electrochemical tests

Potentiostat-galvanostat instrument (CorrTest CS350) was used for EIS test. Fruit extract was prepared as reported in the literature [1, 21]. Briefly, fruit extract was extracted with ethanol at 50°C for 20 min. The substrates were prepared as reported in the literature [6, 8]. For the tests, a 1×1 cm² area of the substrate was selected, and the rest of the surface was covered with a mixture of Beeswax melt and colophony resin. 100 ml of the extract

was stirred in 1 liter of NaCl solution (3.5 wt.%) under magnetic stirring, and finally, the substrates were immersed in it. NaCl solution (3.5 wt.%) without extract was used as a reference solution. In this study, inhibition efficiency (η) was obtained using equation 1 [8].

$$\eta(\%) = 100 \left(1 - \frac{R_{ct \text{ Without extract}}}{R_{ct \text{ With extract}}} \right) \quad (1)$$

3. Results and discussion

The results of the EIS test evaluation are reported in Figures 1 and 2 and Table 1. The degradation of MS without extract is observed by changing the diameter of the Nyquist plots in Figure 1a. In fact, the decrease in the diameter of the curves (indicating the charge transfer resistance (R_{ct})) with increasing immersion time indicates the penetration of corrosive species into the MS and its degradation [8]. It can be seen from Figure 1b that the presence of the extract has changed the degradation process of MS, and the R_{ct} value has increased. Typically,

Table 1. Electrochemical parameters obtained from EIS results

Samples	Time (h)	$R_{ct}(a)$ (ohm.cm ²)	R_s (ohm.cm ²)	$\log z $ (ohm.cm ²)	η (%)
Without extract	1	1751.27	7.1	1873.59	-
	4	1472.08	7.9	1493.46	-
	24	1279.19	7.4	1296.63	-
With extract	1	4506.79	15	4465.23	61
	4	3148.86	14	2795.36	47
	24	2158.76	13	1967.78	41

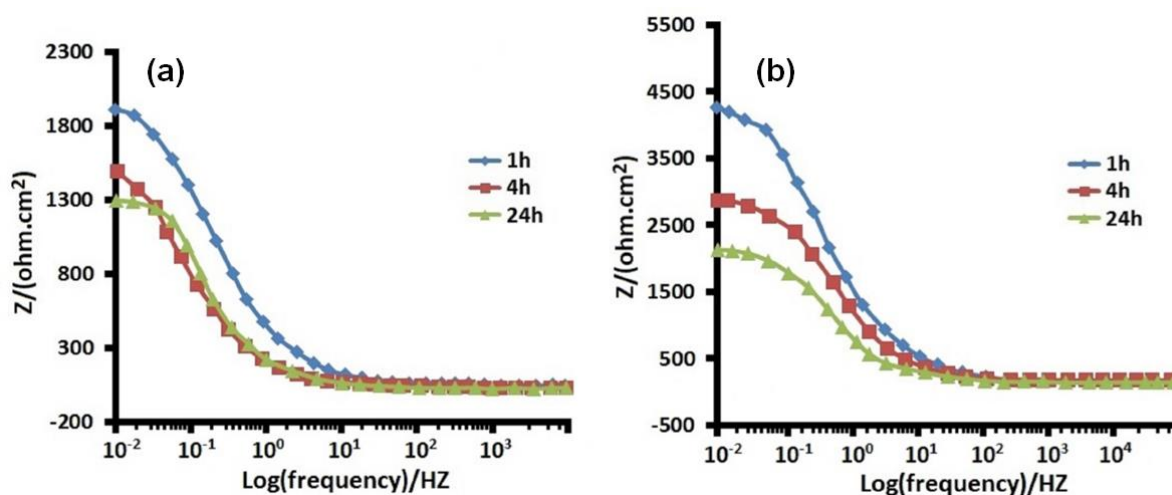


Figure 2. Bode plots at different immersion times.

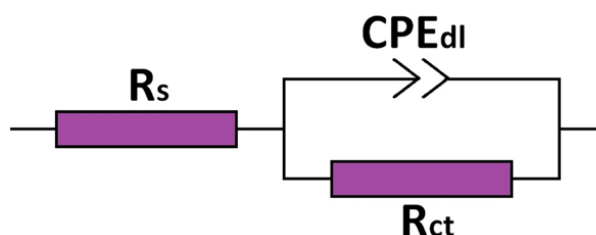


Figure 3. An equivalent circuit to describe the results. Also, R_s represents the solution resistance.

the absolute value of the impedance at low frequencies can be used to compare the inhibition in samples [6, 8]. Considering the R_{ct} value, it can be said that the sample containing the extract has greater resistance after 24h than the sample without the extract after 1h of immersion. The Bode plots (see Figure 2) show that this value decreases with the immersion time for MS without extract, but in the presence of extract, we observe an increase in this value. This behavior is probably related to the interactions between the functional groups in the extract and the MS surface, which cause the surface passivation.

Based on the results, the equivalent circuit that best matched the impedance results was selected (see Figure 3). The results in Table 1 show that the extract compounds were adsorbed on the mild steel surface. The mechanism of inhibition of an extract is directly related to the bioactive compounds present in it. This fruit contains flavonoids, polyphenols, lipids, sterols, and isoquercetin [22]. In the meantime, using a suitable solvent that can extract these compounds is very important. According to the literature, ethanol can extract these compounds [1], which have been used in this study. It can be said that the main compounds of this fruit are adsorbed on

Table 2. Corrosion inhibition performance of some plants

Plant	Substrate	Corrosive Medium	Maximum inhibition efficiency (%)	Reference
Date seed	Mild steel	NaCl	71	[8]
Matcha	Mild steel	NaCl	70	[20]
Zenthoxylum alatum	Mild steel	15% HCl	91	[25]
Argemone mexicana	Mild steel	1 M HCl	92.5	[26]
Ganoderma Lucidum	Mild steel	NaCl	98.26	[27]
Morus alba 'Pendula'	Mild steel	NaCl	61	This study

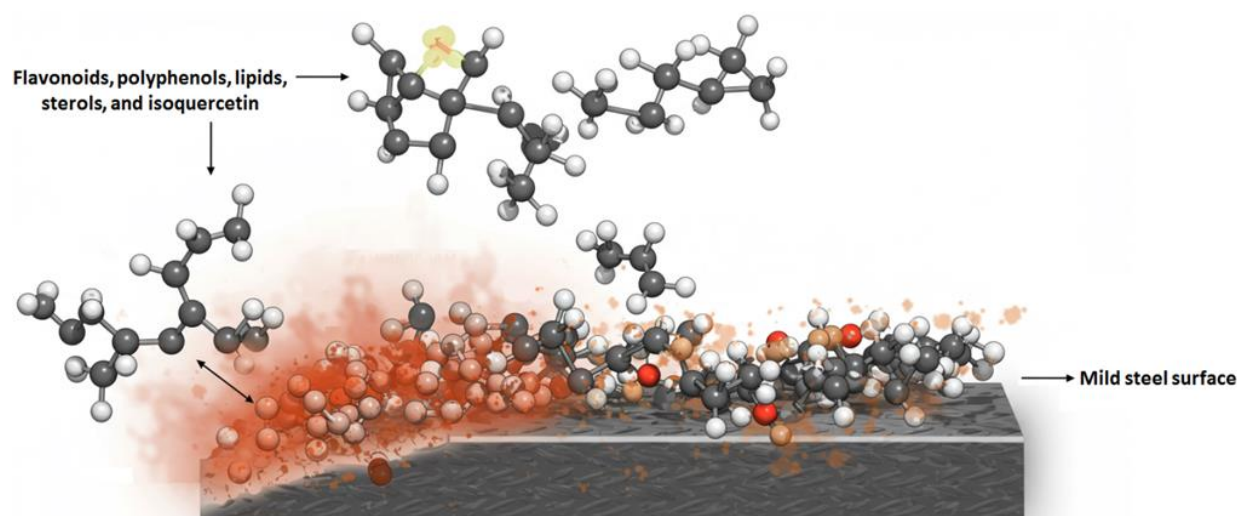


Figure 4. Adsorption of the main components of *Morus alba* 'Pendula' extract on the MS surface.

the MS surface (see Figure 4), which can be attributed to the π -electron transfer between oxygen atoms and aromatic rings of compounds with vacant d -orbitals of the MS surface [23]. In fact, these compounds can interact with the anodic dissolution products and block this region, and can form a protective layer on the surface [23, 24]. Table 2 reports a comparison between the results of this study and the results of several other studies.

4. Conclusions

In summary, a corrosion inhibitor was prepared using *Morus alba* 'Pendula' fruit extract. According to the results, it can be said that this extract can inhibit corrosion. Although the use of environmentally friendly corrosion inhibitors is very attractive, all their aspects, such as their effectiveness over time and temperature changes, should be evaluated in the future. However, it can be said that their non-toxicity and inexpensive encourage researchers to use them. Perhaps in the future, they can be introduced as a suitable alternative to chemical inhibitors.

Conflict of Interest

The authors declare no conflict of interest.

References

1. M. Sheydaei. The Use of Plant Extracts as Green Corrosion Inhibitors: A Review. *Surfaces*, **2024**, 7, 380.
2. M. Lavanya, J. Ghosal, and P. Rao. A comprehensive review of corrosion inhibition of aluminium alloys by green inhibitors. *Canadian Metallurgical Quarterly*, **2023**, 63, 119.
3. H.A. Al Salihi, et al. Exploring the Efficacy of Polysaccharides as Green Corrosion Inhibitors: A Comprehensive Review. *Starch - Stärke*, **2024**, 76, 2300234.
4. A. Kadhim, et al. Corrosion inhibitors. A review. *International Journal of Corrosion and Scale Inhibition*, **2021**, 10, 54.
5. B. R. Holla, et al. Plant extracts as green corrosion inhibitors for different kinds of steel: A review. *Heliyon*, **2024**, 10, e33748.
6. M. Edraki, et al. Protective Nanocomposite Coating Based on Ginger Modified Clay and Polyurethane: Preparation, Characterization and Evaluation Anti-Corrosion and Mechanical Properties. *Polymer Science, Series B*, **2022**, 64, 756.
7. K.D. Ralston and N. Birbilis. Effect of Grain Size on Corrosion: A Review. *Corrosion*, **2010**, 66, 075005.
8. M. Edraki and M. Sheydaei. Investigation of date seed powder as green corrosion inhibitor for mild steel: A study of solution and coating phases. *Hybrid Advances*, **2024**, 6, 100238.
9. N. Eliaz. Corrosion of Metallic Biomaterials: A Review. *Materials*, **2019**, 12, 407.

10. M. Zunita and V.A. Rahmi. Advancement of Plant Extract/Ionic Liquid-Based Green Corrosion Inhibitor. *Chemistry Africa*, **2023**, 7, 505.
 11. Y. Li, et al. Exploring the potential of plant extracts as corrosion inhibitors: A comprehensive review. *Progress in Organic Coatings*, **2025**, 198, 108915.
 12. P. Singh and P.N. Dave. Sustainable technology for cultural heritage preservation: The role of green corrosion inhibitors. *Science of The Total Environment*, **2025**, 975, 179301.
 13. H. Thacker and V. Ram. Green corrosion inhibitors derived from plant extracts and drugs for mild steel in acid media: A review. *Results in Surfaces and Interfaces*, **2025**, 18, 100364.
 14. M. Sheydaei, et al. An overview of the use of plants, polymers and nanoparticles as antibacterial materials. *Chemical Review and Letters*, **2022**, 5, 207.
 15. M. Edraki, et al. Enhanced Mechanical, Anticorrosion, and Antimicrobial Properties of Epoxy Coating via Pine Pollen Modified Clay Incorporation. *Iranian Journal of Chemistry and Chemical Engineering*, **2023**, 42, 2775.
 16. M. Edraki, et al. Characterization and antimicrobial properties of Matcha green tea. *Chemical Review and Letters*, **2022**, 5, 76.
 17. M.S. Butt, et al. Morus alba L. nature's functional tonic. *Trends in Food Science & Technology*, **2008**, 19, 505.
 18. S. Ercisli. A short review of the fruit germplasm resources of Turkey. *Genetic Resources and Crop Evolution*, **2004**, 51, 419.
 19. J. Zhishen, T. Mengcheng, and W. Jianming. The determination of flavonoid contents in mulberry and their scavenging effects on superoxide radicals. *Food Chemistry*, **1999**, 64, 555.
 20. A. Gryn-Rynko, G. Bazylak, and D. Olszewska-Slonina. New potential phytotherapeutics obtained from white mulberry (*Morus alba* L.) leaves. *Biomedicine & Pharmacotherapy*, **2016**, 84, 628.
 21. N.O. Eddy, et al. A Brief Review on Fruit and Vegetable Extracts as Corrosion Inhibitors in Acidic Environments. *Molecules*, **2022**, 27, 2991.
 22. T. Katsube, et al. Antioxidant flavonol glycosides in mulberry (*Morus alba* L.) leaves isolated based on LDL antioxidant activity. *Food Chemistry*, **2006**, 97, 25.
 23. I.S. Cole and D. Marney. The science of pipe corrosion: A review of the literature on the corrosion of ferrous metals in soils. *Corrosion Science*, **2012**, 56, 5.
 24. A.J. Betts and L.H. Boulton. Crevice corrosion: review of mechanisms, modelling, and mitigation. *British Corrosion Journal*, **2013**, 28, 279.
 25. L.R. Chauhan and G. Gunasekaran. Corrosion inhibition of mild steel by plant extract in dilute HCl medium. *Corrosion Science*, **2007**, 49, 1143.
 26. G. ji, et al. Inhibitive Effect of Argemone mexicana Plant Extract on Acid Corrosion of Mild Steel. *Industrial & Engineering Chemistry Research*, **2011**, 50, 11954.
 27. M. Sheydaei, M. Edraki, and S. Javanbakht. Ganoderma Lucidum-Modified Clay Epoxy Coating: Investigation of Thermal, Mechanical, Anticorrosion, and Antimicrobial Properties. *Polymer Science, Series B*, **2024**, 65, 991.
-
- © 2025 The Authors. This article is licensed under a Creative Commons Attribution 4.0 BY International License. 

Green Graphene-Based Polymer Composites: A Pathway Toward Sustainable Polymers

Kobra Yazdani *

Department of Materials Engineering, Hakim Sabzevari University, Sabzevar 9617976487, Iran

Editor's note: Green composites are becoming increasingly recognized as a sustainable alternative to the environmental problems caused by the extensive use of petroleum-based plastics. In this review paper, Yazdani provides an overview of recent advancements in graphene-based sustainable and green composites, focusing specifically on those developed using biodegradable polymers as the main matrix.

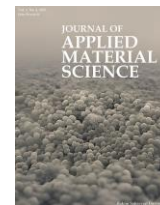
doi: 10.22034/jams.2025.210140

How to cite: K. Yazdani. *Journal of Applied Material Science*, 2025, 1, 210140.



JOURNAL OF
APPLIED
MATERIAL
SCIENCE

jams.hsu.ac.ir



Review

Green Graphene-Based Polymer Composites: A Pathway Toward Sustainable Polymers

Kobra Yazdani *

Department of Materials Engineering, Hakim Sabzevari University, Sabzevar 9617976487, Iran

Abstract

Green composites, as environmentally friendly materials, are rapidly gaining recognition as a sustainable solution to the environmental issues caused by the widespread use of petroleum-based plastics. These composites typically incorporate natural fibers and biodegradable polymers specifically designed to reduce environmental impact. This review paper aims to provide a comprehensive overview of green composites, with a particular focus on those developed from natural fibers such as cellulose, starch, and other bio-based materials. Compared to traditional plastics, these materials exhibit enhanced physical and mechanical properties, along with higher biodegradability. However, challenges such as surface compatibility and the retention of mechanical properties after moisture absorption persist, requiring further research. The paper also explores recent advancements in improving the properties of these composites through the incorporation of nanomaterials like nanocellulose and graphene. Furthermore, the paper discusses the diverse applications of green composites across industries such as packaging, biomedical, and automotive sectors.

Keywords: Green composites, Graphene oxide, Sustainable materials, Natural fiber reinforcement.

1. Introduction

In recent decades, growing environmental awareness and the increasing demand for sustainable materials have stimulated extensive interest in the use of natural and renewable resources for the development of advanced composite systems [1-3]. These materials, known as "green composites" or "biocomposites," have emerged as promising alternatives to conventional composites based on fossil resources due to their unique features, including light weight, high strength, recyclability, biodegradability, reduction of greenhouse

gas emissions, decreased reliance on non-renewable resources, and diminished environmental impact [4-6]. Green composites have established a distinct position in the field of composite materials, as they not only serve as effective solutions to environmental challenges but also promote the efficient utilization of available renewable raw materials. These materials typically consist of biodegradable or bio-based polymer matrices reinforced with natural fibers or environmentally benign nanomaterials. Their appealing features include low density, high specific strength, biodegradability, recyclability, reduced carbon footprint, and decreased dependence on non-renewable resources [7, 8].

* Corresponding author.

Email address: kobrayazdani@hsu.ac.ir (K. Yazdani)

Received 15 May 2025

Revised 26 May 2025

Accepted 26 May 2025

Available online 28 May 2025

Initial research in this field concentrated on incorporating natural fibers such as hemp, flax, and jute into biodegradable polymer matrices (Table 1). These early green composites were primarily investigated as substitutes for conventional, non-biodegradable materials in various applications. The mid 2000s to 2010s witnessed a surge in the development of biodegradable polymers, particularly polylactic acid (PLA), polyhydroxybutyrate (PHB), and thermoplastic starch (TPS). These matrices attracted significant attention due to their inherent biodegradability, mechanical performance, and low toxicity. Reinforcement with natural fibers or nanoparticles, such as cellulose nanofibers (CNFs), led to improvements in thermal stability, water resistance, and mechanical integrity. Over the past decade, research has increasingly focused on enhancing the functional performance of green composites to make them competitive with conventional materials in high-performance sectors. Strategies such as fiber surface modification, hybrid reinforcement, and nano enhancement have enabled the extension of green composites into demanding applications including aerospace, automotive, biomedical devices, cosmetics, water treatment, agriculture, and electronics [7, 9-12].

In developing green supercapacitors, materials such as graphite foil, sodium acetate, and ester-based porous membranes, which also exhibit superior performance compared to conventional materials, have been identified as more environmentally friendly

alternatives. Similarly, in brake lining materials, hybrid composites reinforced with basalt, shell, and alumina, and phenolic resin polymers have demonstrated lower wear rates and water absorption compared to traditional asbestos-based brake materials. Additionally, the use of environmentally compatible materials in additive manufacturing, such as blending polylactic acid with MoS₂ as solid lubricants, has shown potential for reducing environmental impact, despite certain challenges related to stability [13, 14].

One major area of innovation involves the integration of graphene-based materials into green composites. Graphene, graphene oxide (GO), and reduced graphene oxide (rGO) exhibit outstanding mechanical, thermal, and electrical properties and serve as highly effective multifunctional reinforcements. Their incorporation improves load transfer, reduces moisture uptake, and enhances barrier and conductive properties. Importantly, green synthesis approaches for graphene derivatives – using plant extracts, biomass, or other non-toxic reducing agents – have emerged as sustainable and cost-effective alternatives to traditional methods. Additionally, in green composites, graphene serves as a reinforcing agent that improves the adhesion between the matrix and natural fibers, leading to enhanced mechanical strength and reduced cracking [20-22].

Green graphene-based polymer composites represent a class of advanced sustainable materials that combine

Table 1. Overview of green composites: components and applications

Type of Green Composite	Bio-based Polymer Matrix	Natural Reinforcement	Key Properties	Typical Applications	Ref.
PHB + Bamboo	Polyhydroxybutyrate (PHB)	Bamboo fibers	Good thermal stability, biodegradable	Construction, furniture	[1]
Soy Resin + Hemp	Soy-based resin	Hemp fibers	Moderate mechanical performance	Coatings, building materials	[2]
Green PE + Sisal	Bio-based Polyethylene	Sisal fibers	Lightweight, moisture-resistant	Automotive, household goods	[4]
PCL + Flax	Polycaprolactone (PCL)	Flax fibers	Flexible, biocompatible	Tissue engineering, scaffolds	[5]
PLA + Hemp	Polylactic Acid (PLA)	Hemp fibers	Biodegradable, moderate strength	Packaging, automotive parts	[7]
PLA + Cellulose Nanofibers	Polylactic Acid (PLA)	Cellulose nanofibers (CNF)	High strength, improved barrier properties	Food packaging, biomedical devices	[15]
TPS + GO	Thermoplastic Starch (TPS)	Graphene Oxide (GO)	Improved mechanical and thermal stability	Biodegradable films, electronics	[15]
PLA + Vermiculite + Waste Cellulose	PLA	Waste cellulose + Vermiculite	Enhanced mechanical strength, eco-friendly	Packaging, agriculture	[16]
Chitosan + Graphene Oxide	Chitosan	Graphene Oxide (GO)	High adsorption, antimicrobial, and mechanical stability	Water treatment, biomedical	[17, 18]
PLA + PCL	PLA + PCL blend	–	Shape memory effect, tunable flexibility	Smart textiles, medical implants	[19]

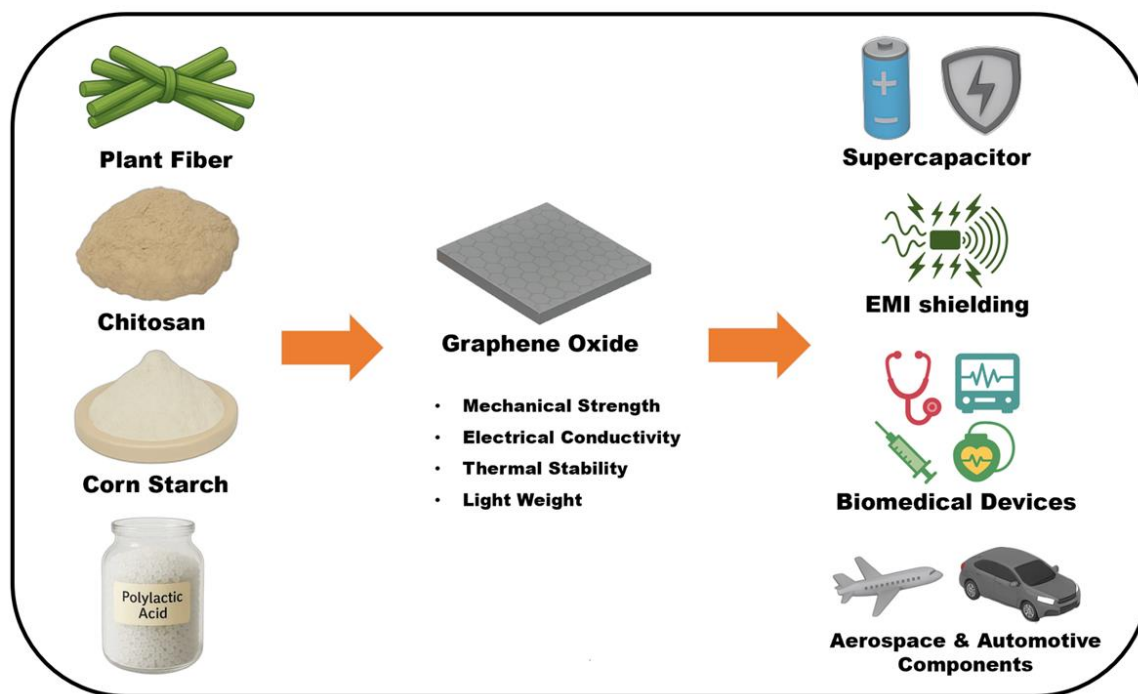


Figure 1. Schematic representation of graphene oxide bio-based polymer composites: sources, enhanced properties, and major application areas.

the desirable attributes of eco-friendly polymer matrices with the multifunctionality of graphene. These composites leverage the exceptional characteristics of graphene, such as high conductivity, strength, and thermal stability, to develop multifunctional materials suitable for diverse applications. Recent studies have highlighted their use in energy storage, electromagnetic interference shielding, aerospace, and biomedical applications. For instance, green-synthesized graphene composites show great promise in supercapacitors due to their improved charge storage capacity and durability, aligning with the demands of eco-friendly technologies [23]. Similarly, conductive polymer-graphene composites have demonstrated effective electromagnetic shielding capabilities, addressing radiation pollution with lightweight and sustainable materials [24]. Moreover, the advent of precise fabrication methods, particularly 3D printing and layer-by-layer assembly, has enabled customizable architectures suitable for next-generation electronics, optoelectronics, and sustainable packaging [25, 26]. A comprehensive schematic of the material sources, functional improvements, and industrial uses of green graphene-based polymer composites is presented in Figure 1, providing a visual summary of the concepts discussed in this review.

Despite these advances, critical challenges remain, and Further research is required to optimize their properties and scalability for commercial applications, ensuring they meet both environmental and technological demands. This comprehensive review summarizes recent progress in green polymer matrices and natural reinforcement systems, highlights the pivotal role of graphene and its derivatives in enhancing green composite performance, and explores their diverse industrial and environmental applications. Finally, it discusses the current limitations and future research opportunities towards scalable, high-performance, and environmentally friendly composite technologies.

2. Popular categories of green graphene-based nanocomposites

2.1. Green graphene-based nanocomposites on chitosan basis

Chitosan (CS), a natural biopolymer primarily derived from crustacean shells, is recognized for its exceptional biocompatibility, biodegradability, and chemical versatility [27]. These properties, combined with its

abundance and low cost, have made chitosan a valuable component in the development of green nanocomposites. When reinforced with materials such as keratin and graphene derivatives, chitosan-based composites exhibit enhanced mechanical and functional properties, making them attractive for sustainable environmental and biomedical applications [12, 28].

Due to the presence of active amino and hydroxyl functional groups, chitosan is particularly effective in adsorbing a wide range of chemical species, including heavy metals. This makes it a promising candidate for environmental remediation. To improve its adsorption capacity, solubility, and mechanical strength, chitosan has been modified with nanomaterials such as graphene oxide (GO) and metal oxide nanoparticles [17]. GO, with its high surface area and oxygen-containing groups, enhances metal ion binding, while metal oxides like MnO_2 , Al_2O_3 , and SiO_2 offer additional active sites for adsorption [17].

For example, Naicker et al. reported that incorporating metal oxides into magnetic chitosan chloride-graphene oxide (MCSCI-GO) composites significantly enhanced the removal of Cr(VI) ions from aqueous solutions through electrostatic and ionic interactions. Among these, MCSCI-GO- MnO_2 showed the highest efficiency due to its strong affinity and spontaneous interaction with Cr(VI) [17]. Similarly, Peryasamy et al. developed a hydrotalcite-modified GO-Chitosan composite (n-GO@HTCS) capable of removing chromium via a combination of electrostatic adsorption, surface complexation, and ion exchange. Notably, this composite could be regenerated and reused for up to five cycles [29]. Sherlala et al. designed chitosan-magnetic graphene oxide (CMGO) nanocomposites for arsenic adsorption, achieving a high specific surface area ($152.38 \text{ m}^2/\text{g}$) and superparamagnetic behavior (49.30 emu/g), facilitating magnetic separation and efficient chemisorption of arsenic [30].

Beyond metal ion remediation, chitosan-GO composites have been employed in wastewater treatment. Chang et al. synthesized a chitosan/polyacrylate/GO hydrogel via a semi-dissolution/acidification/sol-gel transition (SD-A-SGT) method, which effectively adsorbed both anionic and cationic dyes [31]. Zhang et al. developed a core-shell composite using modified chitosan and alginate as the shell and tungsten oxide as the core for uranium removal, enhancing chelation capacity via radical-mediated complexation [32]. In another study, Jeyaseelan et al. introduced hybrid

composites containing pectin, chitosan, and lanthanide or alkaline earth elements for fluoride removal across a wide pH range, demonstrating reusability up to six cycles [33].

Despite these advancements, chitosan's instability in aqueous environments and relatively weak mechanical properties pose challenges for industrial applications. Strategies to address these limitations include functional group modification, crosslinking, and the incorporation of reinforcing fillers. Rozova et al. fabricated elastic chitosan/GO composites with improved strength and modulus due to homogeneous dispersion and strong interfacial bonding. Additionally, GO incorporation increased the free volume of the matrix, enhancing both mechanical integrity and adsorption performance in aqueous systems, where pure chitosan films failed [34].

Hu et al. created lightweight, compressible, and hydrophobic aerogels using a chitosan matrix reinforced with reduced GO nanosheets and modified with hydrophobic silicon/polydimethylsiloxane particles. These aerogels demonstrated exceptional oil absorption ($18\text{--}45 \text{ g/g}$), chemical and thermal stability, and reusability under extreme environmental conditions, positioning them as promising candidates for oil spill cleanup [27].

Chitosan's biocompatibility and antimicrobial activity also make it a compelling material for medical uses such as wound dressings, anticoagulants, membranes, and scaffolds for tissue engineering. However, extensive hydrogen bonding among its functional groups limits solubility, stability, and mechanical strength, particularly in physiological conditions. To overcome these issues, reinforcements such as cellulose nanocrystals, carbon nanotubes, calcium phosphates, and GO have been employed. For instance, Yang et al. showed that adding 1 wt% GO to chitosan increased tensile strength by 122% and elastic modulus by 64%, while Gea et al. reported a 200% increase in modulus with 10 wt% GO. Zhou et al. demonstrated that 10 wt% GO not only improved the thermal stability and mechanical properties of chitosan but also enhanced cell adhesion, proliferation, and viability of murine mesenchymal stem cells [18, 35].

Other studies have extended these findings. Ruiz et al. examined PVA/CS/GO films, reporting enhanced mechanical strength and antibacterial activity due to GO-bacteria interactions [35]. Tavakkoli et al. optimized Cs/GO composites for orthopaedic applications,

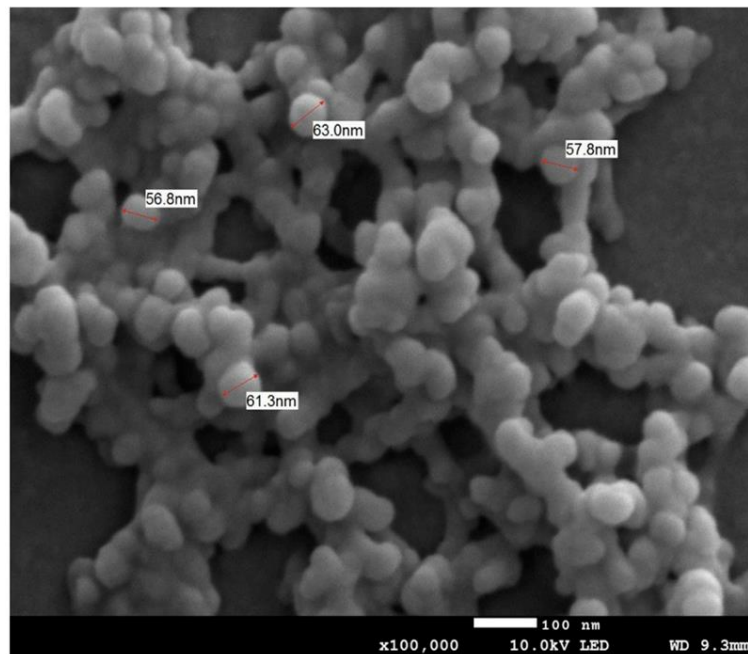


Figure 2. *B. balsamifera*-CNPs view from SEM. Reprinted with permission from [38]. 2025, MDPI.

Table 2. Summary of green chitosan–graphene nanocomposites and their key applications

Study	Composite Composition	Target/Application	Key Outcomes
Naicker et al. [17]	MCSCI-GO with MnO ₂ , Al ₂ O ₃ , SiO ₂	Cr(VI) adsorption	MnO ₂ composite showed the highest affinity and spontaneous uptake
Peryasamy et al. [29]	n-GO@HTCS (GO + hydrotalcite + CS)	Chromium removal	Spontaneous, endothermic adsorption; reusable up to 5 cycles
Sherlala et al. [30]	CMGO (Chitosan–Magnetic Graphene Oxide)	Arsenic adsorption	High surface area and magnetic separation; chemisorption confirmed
Chang et al. [31]	CS/Polyacrylate/GO hydrogel	Dye wastewater treatment	Adsorbs both anionic and cationic dyes
Zhang et al. [32]	Core-shell (CS/Alginate shell, WO ₃ core)	U(VI) removal	Enhanced complexation and mechanical flexibility
Jeyaseelan et al. [33]	PCML/PCMC (Pectin + CS + Mg + La/Ce)	Fluoride removal	Effective in a wide pH range; reusable up to 6 cycles
Rozova et al. [34]	CS/GO composite films	Mechanical enhancement in aqueous systems	Stronger films, improved adsorption, and water stability
Hu et al. [27]	CS + rGO + hydrophobic Si/PDMS	Oil spill remediation	WCA = 148°, high oil uptake, robust under harsh conditions
Yang et al., Gea et al. [18]	CS + 1–10 wt% GO	Mechanical reinforcement	Up to 200% modulus and 122% tensile strength increase
Zhou et al. [18, 35]	CS/GO scaffold	Bone tissue engineering	Enhanced thermal stability, cell adhesion, and proliferation
Tavakkoli et al. [18, 36]	CS/GO nanocomposites in PMMA bone cement	Orthopedic application	Optimal at 0.3% GO, improved bioactivity, and mechanical properties
Sivashankari et al. [37]	ACGO (Agarose/Chitosan/GO) scaffolds	Biomedical scaffold	Biocompatible, hemocompatible, enhanced water retention, and cell attachment
Villarta et al. [38]	CNPs synthesized with <i>B. balsamifera</i> extract	Antibacterial application	MIC = 25 µg/mL against <i>E. coli</i> , eco-friendly nanoparticle synthesis

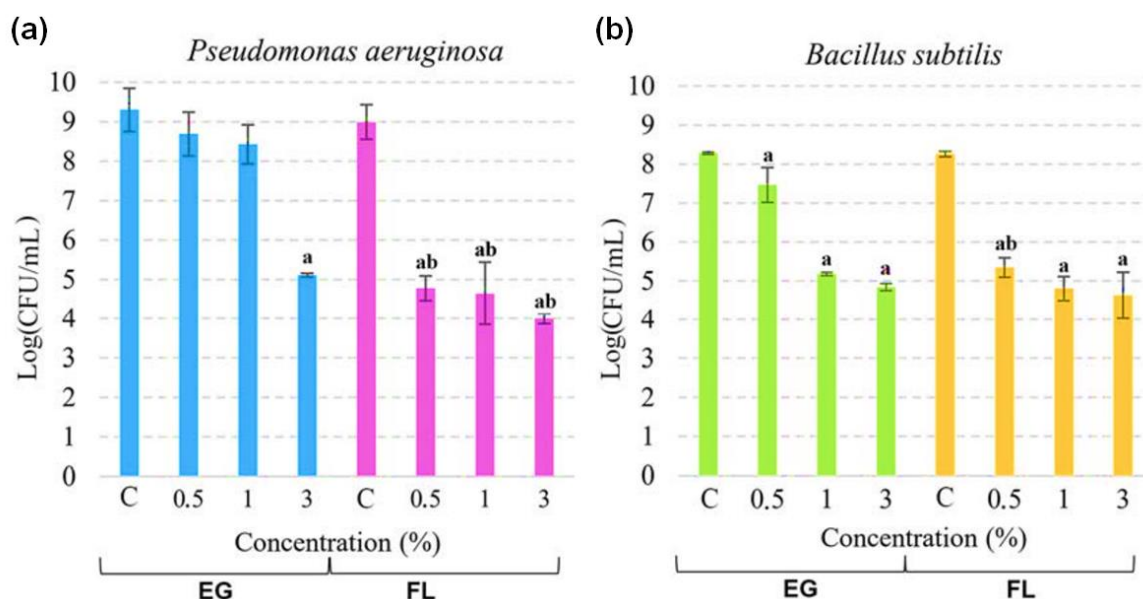


Figure 3. The viability of *P. aeruginosa* (a) and *B. subtilis* (b) under the action of EG or Flovon (FL). In the control experiment (depicted as C). Significant deviations from the control are denoted by “a” ($p < 0.05$), while values marked by “b” are significantly different from the samples of the equivalent concentration, but different additives ($p < 0.05$). Reprinted with permission from [41]. 2025, MDPI.

identifying a 2 wt% CS and 0.3 wt% GO formulation as optimal. These films exhibited notable bioactivity, strength, and degradability. When incorporated into PMMA bone cement, 25 wt% Cs/GO enhanced injectability, mechanical properties, and cellular response [18, 36]. Similarly, Sivashankari et al. developed agarose/chitosan/GO scaffolds with tunable porosity and demonstrated that GO content enhanced swelling, biodegradability, and cell proliferation while maintaining hemocompatibility [37].

Finally, Villarta et al. introduced a green synthesis route for chitosan nanoparticles using *Blumea balsamifera* leaf extract. The phenolic-rich extract acted both as a reducing and stabilizing agent, resulting in the formation of spherical nanoparticles with sizes ranging from 56.8 to 63.0 nm and effective antibacterial activity against *E. coli* at a concentration of 25 $\mu\text{g/mL}$ [38]. As illustrated in Figure 2, DLS and SEM analyses confirmed the particle morphology and size distribution, supporting the efficacy of this eco-friendly synthesis method. This sustainable approach underscores the potential of chitosan-based nanocomposites for future pharmaceutical and therapeutic applications [38]. Table 2 summarizes the chitosan-graphene green nanocomposites and their key applications investigated in this study.

2.2. Green graphene-based nanocomposites derived from starch

Starch, as a renewable, abundant, and inexpensive biopolymer, has drawn increasing interest for use in sustainable packaging. However, its native form exhibits significant limitations such as brittleness, poor water resistance, and low processability. To mitigate these shortcomings, plasticizers such as glycerol, sorbitol, ethylene glycol, and urea are commonly employed to disrupt the crystalline structure of starch through gelatinization, resulting in thermoplastic starch (TPS) with improved processability [15]. For example, the glass transition temperature of starch decreases from 87 °C to 25 °C and 35 °C upon incorporation of 30% glycerol and sorbitol, respectively. Similar to native starch, thermoplastic starch (TPS) also suffers from several drawbacks, including water sensitivity, limited thermal stability, brittleness over time due to plasticizer loss, recrystallization, and low mechanical strength. Therefore, extensive efforts have been made to improve its properties by blending with other polymers and incorporating organic nanoparticles—approaches that do not compromise its biodegradability [15].

To enhance its properties while preserving biodegradability, researchers have incorporated

Table 3. Summary of starch-based green nanocomposites and their key applications

Study	Composite Composition	Target/Application	Key Outcomes
Ramazani et al. [15]	TPS + CNF + GO	Mechanical enhancement and barrier properties	66% ↑ tensile strength, 1435% ↑ modulus, 40% ↓ light transmittance, UV blocking
Solati et al. [39]	TPS/PLA + 1–3 wt% Graphene	Compatibility, crystallinity, and biodegradability	1% graphene improved miscibility; >1% caused phase separation and TPS droplets
Rabiei et al. [40]	Starch + MIL-100 + CoFe ₂ O ₄	Photocatalytic degradation of tetracycline and dyes	Effective degradation at room temperature
Vasiliauskienė et al. [41]	Corn starch + EG/Flovan flame retardants	Antibacterial biocomposites, microbial modulation	>99.7% Proteobacteria with retardants; up to 5-log ↓ in bacterial viability

nanostructured fillers, particularly cellulose nanofibers (CNF) and graphene-based materials. Ramazani et al. examined the synergistic reinforcement of TPS with CNF and graphene oxide (GO). Their results indicated that the GO nanosheets altered the matrix morphology into a layered structure, limiting molecular mobility and reducing crystallinity through suppressed retrogradation. Mechanical testing revealed a 66% increase in tensile strength and a 527% increase in elastic modulus for TPS/CNF composites compared to neat films. With the addition of 3 wt% GO, these values rose dramatically – fracture strength increased by 440% and elastic modulus by 1435%, though elongation at break decreased by 110%. Furthermore, optical and barrier analyses showed a 40% reduction in visible light transmittance and a 30% reduction in water vapor transmission, with complete UV light blockage [15].

In another study, Solati et al. evaluated the influence of graphene nanosheets on TPS/poly(lactic acid) (PLA) blends. The inclusion of 1 wt% graphene improved interfacial compatibility, as evidenced by closer glass transition temperatures and a more uniform surface. However, at higher graphene concentrations (2–3 wt%), phase separation and TPS droplet formation occurred. Graphene addition also modified crystallization behavior, eliminating cold crystallization and raising the crystallization temperature due to graphene-induced nucleation. All graphene-containing blends exhibited greater crystallinity than their pristine counterparts [39].

Expanding beyond mechanical and thermal enhancements, Rabiei et al. synthesized a starch-based magnetic nanocomposite incorporating MIL-100 (a metal-organic framework) and cobalt ferrite. The resulting hybrid demonstrated effective photocatalytic activity for the degradation of tetracycline and dyes under ambient conditions, positioning starch as a viable platform for environmental remediation [40].

In a microbiological context, Asiliauskienė et al. explored the effects of flame retardants on the bacterial ecology of starch-based biocomposites. Their composites, composed of hemp shives, corn starch, and either expandable graphite (EG) or a Flovan compound, were analyzed after 12 months of incubation. Next Generation Sequencing (NGS) revealed that flame retardants drastically shifted microbial populations: in treated samples, Proteobacteria dominated (>99.7%), whereas untreated composites displayed higher diversity, including Bacteroidetes, Actinobacteria, and Saccharibacteria. Viability assays on *Bacillus subtilis* and *Pseudomonas aeruginosa* showed a significant antibacterial effect from both additives, with bacterial counts dropping up to five logarithmic units. As illustrated in Figure 3, statistical differences between the flame retardants further underscore their distinct microbial impacts [41].

Collectively, these studies demonstrate the multifunctionality and adaptability of starch-based nanocomposites when reinforced with graphene and related materials. These enhancements broaden starch's applicability not only in packaging and structural materials but also in biomedical, environmental, and antimicrobial domains. Table 3 summarizes the starch-based green nanocomposites and their key applications investigated in this study.

2.3. Green graphene-based nanocomposites derived from polylactic acid

Poly(lactic acid) (PLA) is a biodegradable aliphatic polyester synthesized from renewable agricultural sources such as corn and sugarcane. As a thermoplastic polymer with high strength and modulus, PLA exhibits relatively low permeability to water, oxygen, and carbon dioxide. Its biodegradability and recyclability into

organic compost, combined with its production from carbon dioxide-consuming feedstocks, make PLA an environmentally attractive material. These characteristics have facilitated its extensive applications in medicine, pharmaceuticals, packaging, and agriculture [39].

However, PLA's use is limited by several drawbacks, including low thermal resistance, poor flame retardancy, low impact strength, limited processability, high cost, and low crystallinity, which collectively diminish its mechanical properties such as stability, modulus, and strength. To address these limitations, additives such as plasticizers, lubricants, and fillers, or blending with other polymers, have been employed. For example, the glass transition temperature (T_g) and melting temperature (T_m) of PLA typically range from 50 to 70 °C and 130 to 180 °C, respectively, which are lower than those of common petroleum-based plastics like polyethylene terephthalate (PET) and polystyrene (PS), resulting in reduced energy consumption during processing [39]. Despite this advantage, the relatively slow degradation rate of PLA remains a concern, as it may require several hours or longer to decompose depending on molecular weight and morphology [39].

Blending PLA with thermoplastic starch (TPS) has been extensively studied to lower costs, improve degradability, and reduce TPS's water sensitivity. Martin et al. investigated PLA/TPS composites with varying toughness and plasticizer content, reporting a 112% increase in elongation at break for TPS with the highest plasticizer content; however, incorporation of TPS significantly reduced mechanical strength in the blends [39].

In recent years, the incorporation of graphene-based nanomaterials has gained considerable attention for enhancing PLA properties. Norazlina et al. demonstrated improved mechanical performance of PLA/graphene nanocomposites compared to neat PLA and PLA composites with conventional graphite [39].

Functionalized graphene oxide (f-GO), modified with maleic anhydride and dodecylamine, was shown by Wang et al. to improve morphology, thermal stability, crystallization behavior, weathering resistance, and protective properties of PLA-starch matrices. The addition of f-GO enhanced UV protection, surface hydrophobicity, erosion resistance, and induced heterogeneous nucleation, leading to spherical crystal growth during isothermal crystallization. Moreover, it

increased matrix thermal stability and storage modulus, making these nanocomposites promising for food and pharmaceutical packaging applications [42].

Scaffaro et al. explored the effect of graphene nanoplatelet (GNP) and pineapple fiber (PF) ratios on mechanical properties and hydrolytic degradation kinetics of PLA-based composites under acidic, neutral, and alkaline conditions. They found that hybrid fillers were well dispersed within the PLA matrix, and mechanical tests revealed increased stiffness proportional to GNP content. Degradation behavior depended on GNP loading: low GNP content accelerated degradation due to interface discontinuities, while higher GNP content created a barrier effect from hydrophobic nanocarbons, partially offsetting the hydrophilicity of lignocellulosic fillers and slowing degradation kinetics, though still faster than neat PLA [43].

Wang et al. also studied the synergistic effect of titanium dioxide (TiO_2) nanoparticles and GO nanosheets in PLA-starch composites. The combined addition significantly accelerated heterogeneous nucleation and crystal growth during isothermal crystallization more effectively than individual fillers. Strong interfacial interactions and synergism between fillers enhanced morphology, storage modulus, thermal stability, surface hydrophobicity, UV shielding, and resistance to ageing-related property changes in PLA-MST- TiO_2 -f-GO nanocomposites compared to those with single fillers [44].

In another approach, Ariturk et al. developed green PLA composites by incorporating waste cellulose fibers and vermiculite as natural reinforcements. Their results indicated that this combination improves mechanical properties and environmental compatibility, offering promising bio-based alternatives to petroleum-derived polymers [16].

Batakliiev et al. investigated biodegradable blends of PLA and polycaprolactone (PCL) at various weight ratios to achieve materials with desirable mechanical and thermal shape memory properties. Blends with higher PCL content showed increased flexibility, toughness, and elongation at break (up to ~550% for 30PLA/70PCL), while tensile strength and modulus decreased. Shape memory tests revealed excellent shape fixity (~98%) and recovery ratios improving with PLA content, with faster recovery at higher temperatures (70 °C). The co-continuous morphology and uniform

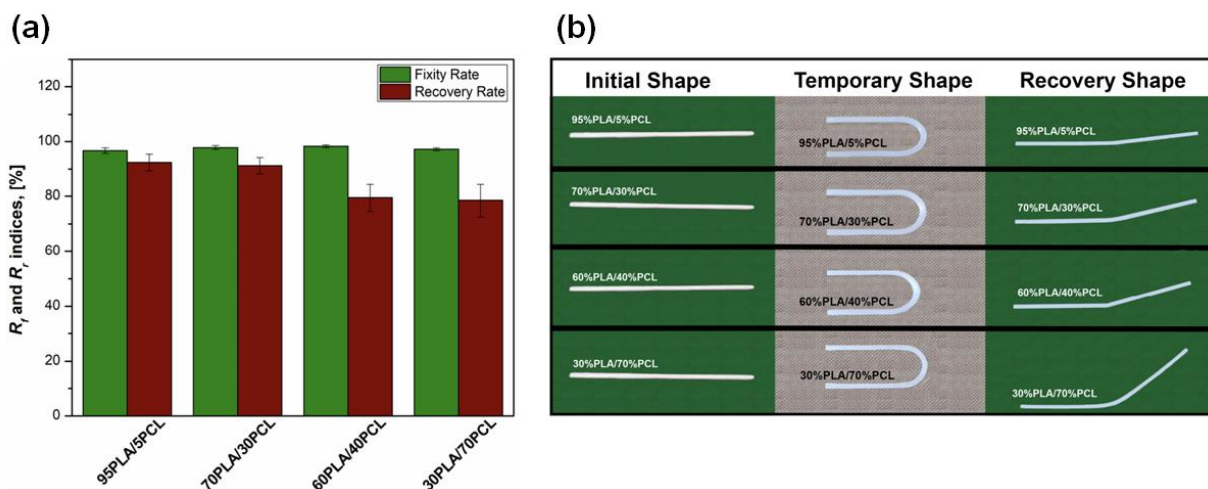


Figure 4. Optical images and comparative diagrams of shape fixation and shape recovery rate evaluation of PLA/PCL composite blend. Reprinted with permission from [19]. 2025, MDPI.

dispersion of the dispersed phase (~500 nm) without compatibilizers contributed to balanced mechanical behavior. Sample images during the shape memory cycle and comparative charts are presented in Figure 4.

Finally, Barbosa et al. examined surface treatments of 3D-printed electrodes fabricated from a PLA/carbon black filament. Among electrochemical activation, acid (HNO_3), alkaline (NaOH), and solvent (DMF) treatments, alkaline treatment notably enhanced electrochemical performance by increasing electroactive surface area and reducing charge transfer resistance through partial removal of insulating PLA. The

optimized electrode (3D-SBasic) exhibited superior sensitivity and resolution for acetaminophen detection compared to commercial and conventional electrodes, as demonstrated in Figure 5 [45]. Table 4 summarizes the Green Graphene-Based PLA and their key applications investigated in this study.

2.4. Green graphene nanocomposites based on cellulose

Cellulose is one of the most abundant natural biomolecules and serves as a primary structural component of the cell walls in most plants. It can also be sourced from marine organisms, algae, fungi,

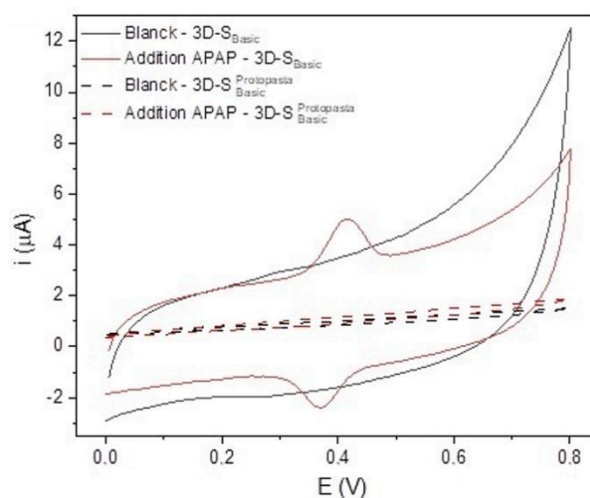


Figure 5. Cyclic voltammograms for 3D-SBasic (solid line) and 3D-SBasicProtopasta (dashed line) in the presence and absence of APAP. Reprinted with permission from [45]. 2025, MDPI.

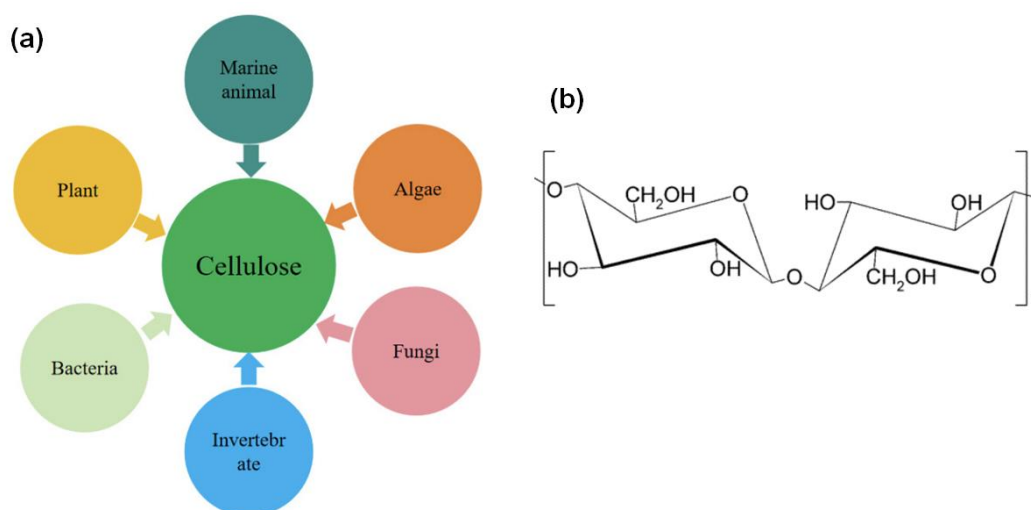
Table 4. Summary of studies on green graphene-based PLA nanocomposites and their key applications

Study	Composite Composition	Target/Application	Key Outcomes
Martin et al. [39]	PLA + Thermoplastic starch (TPS, with varying plasticizer content)	Improve degradability, reduce cost, and water sensitivity	↑ Elongation at break (112%); ↓ Mechanical properties when TPS added
Norazlina et al. [39]	PLA + Modified graphene	Mechanical reinforcement	↑ Mechanical properties vs. neat PLA or PLA/graphite composites
Wang et al. [42]	PLA + Functionalized GO (maleic anhydride + dodecylamine)	Packaging (UV protection, stability, crystallinity)	↑ UV shielding, hydrophobicity, modulus, and crystallinity
Scaffaro et al. [43]	PLA + PF + GNP (various ratios)	Mechanical enhancement and hydrolytic degradation	↑ Stiffness; degradation rate dependent on GNP loading
Wang et al. [44]	PLA + Starch + TiO ₂ + GO	Synergistic enhancement of properties	↑ Crystallinity, storage modulus, thermal stability, and aging resistance
Ariturk et al. [16]	PLA + Waste cellulose + Vermiculite	Bio-based mechanical reinforcement	↑ Mechanical properties, eco-friendliness
Bataliev et al. [19]	PLA/PCL blends (various ratios)	Mechanical tuning + Shape memory	↑ Elongation (up to ~550%), ↑ Fixity (~98%), ↑ Recovery (at 70 °C), balanced morphology (Figure 2)
Barbosa et al. [45]	PLA + Carbon black (3D-printed electrode, various surface treatments)	Electrochemical sensing (APAP detection)	NaOH treatment → ↑ Surface area, ↓ Resistance, ↑ Sensitivity (Figure 6)

invertebrates, and bacteria, as well as from wood, hemp, cotton, and bast fibers. Figure 6 illustrates the various sources and the chemical structure of cellulose. Morphologically, cellulose features a one-dimensional fibrous architecture with a high aspect ratio; however, its specific structural characteristics vary slightly depending on its origin and the applied processing techniques. Since its discovery, considerable research has focused on the chemical composition and physical structure of cellulose. It is a polydisperse polymer consisting of D-glucopyranose units connected via β -1,4-

glycosidic bonds, forming long chains of thousands of monomers. Intrachain hydrogen bonds between hydroxyl groups and ring oxygen atoms contribute to the linear configuration of cellulose chains [46].

Cellulose-based green composites have garnered increasing attention due to their environmental compatibility and stable physicochemical properties. As the most abundant natural polymer, cellulose provides a renewable matrix with desirable mechanical and functional characteristics for composite development

**Figure 6.** Major sources of cellulose & Chemical structure of cellulose. Reprinted with permission from [41]. 2025, MDPI.

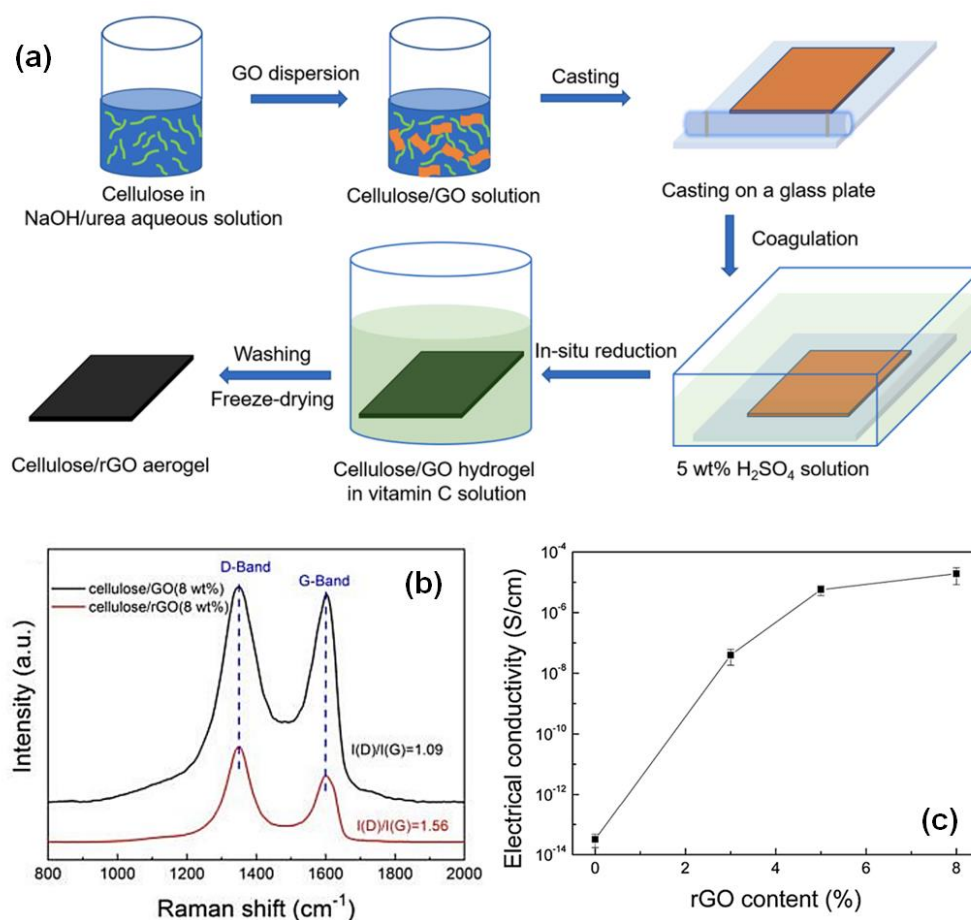


Figure 7. (a) Schematic representation of the preparation of cellulose/rGO composite aerogels. (b) Raman spectra and the D/G band intensity ratio of cellulose/GO (8 wt%) (top) and cellulose/rGO (8 wt%) composite aerogels (bottom); and (c) electrical conductivity of cellulose/rGO aerogels as a function of rGO content. Reprinted with permission from [52]. 2025, MDPI.

[47]. Its incorporation into green composites has been shown to improve mechanical strength and thermal stability [48], as well as enhance water resistance and biodegradability, offering significant advantages for sustainable material design [1]. These composites present a viable solution to mitigate plastic waste derived from petroleum sources and support environmental sustainability initiatives [49]. Moreover, the inclusion of cellulose can positively influence the structural and functional properties of polymer matrices, expanding their application potential [50].

Despite its advantages, the high hydrophilicity of cellulose fibers poses challenges for compatibility with hydrophobic polymer matrices and can lead to reduced mechanical performance due to moisture absorption. To address this issue, various surface modification strategies, such as physical treatments and chemical

grafting, have been developed to reduce fiber hydrophilicity and enhance interfacial bonding with the matrix [5].

In a notable application, Snari et al. introduced a fluorometric sensor based on cellulosic nanomaterials functionalized with Morin [2-(2,4-dihydroxyphenyl)-3,5,7-trihydroxychromen-4-one], a natural ligand capable of forming strong luminescent complexes with Al³⁺ ions. This sensor shows promise for quality control in detecting aluminium ion contamination in herbal tea production, as well as for qualitative detection of Al³⁺ in blood serum samples [51].

Cellulose also plays a role in the preparation of graphene oxide (GO)-based suspensions, where it may be added before or after GO reduction to enhance dispersion stability. When introduced prior to reduction,

cellulose facilitates GO adsorption onto its surface, effectively preventing nanosheet aggregation and promoting a homogeneous distribution. This stabilization is typically attributed to a confinement effect, in which the cellulose framework limits GO sheet mobility. However, the stabilization efficiency is highly dependent on the cellulose-to-GO ratio. Insufficient cellulose may fail to prevent agglomeration, while excessive cellulose content can diminish the functional benefits of GO, including its electrical and mechanical performance [52].

In a study by Chen et al., cellulose/reduced graphene oxide (rGO) aerogels were fabricated as chemical vapor sensors. As shown in Figure 7a, the aerogels were

prepared by dissolving cellulose and dispersing GO in a NaOH/urea aqueous solution, followed by in-situ chemical reduction and freeze-drying. Figure 7b presents the Raman spectra of the composites containing 8 wt% filler, revealing an I(D)/I(G) ratio of 1.56 for rGO and 1.09 for GO. Although this increase in I(D)/I(G) appears counterintuitive, since reduction typically decreases sp^3 -type defects, such behavior is often attributed to the formation of smaller sp^2 domains and a higher density of edge defects, enhancing the D band. Ascorbic acid, the reducing agent used in this study, enabled sufficient GO reduction to restore electrical conductivity in rGO, making the composite suitable for piezoresistive sensing applications. As illustrated in Figure 7c, conductivity increased markedly with rGO

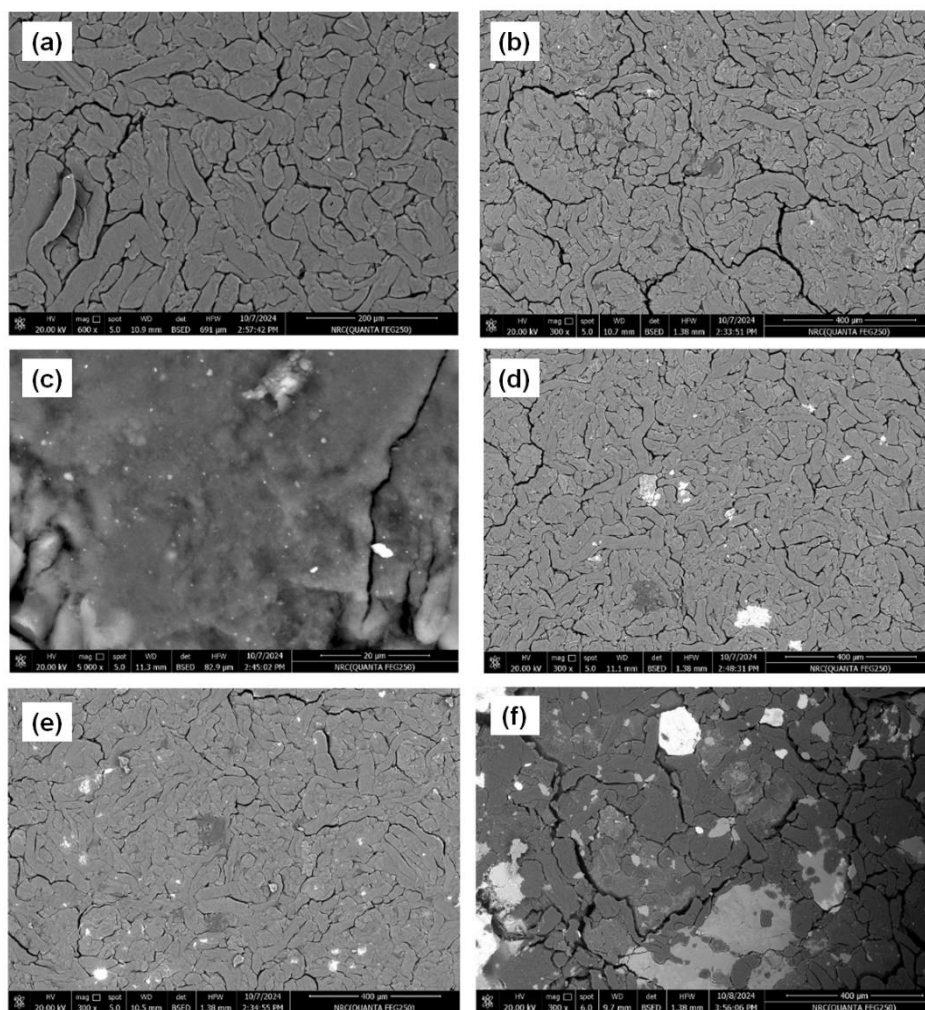


Figure 8. SEM images of (a) CMC (scale: 400 μm), (b) CMC/0.4% G (scale: 20 μm), (c) CMC/0.8% G (scale: 400 μm), (d) CMC/1% G (scale: 400 μm), (e) CMC/2% G (scale: 400 μm), and (f) CMC/3% G (scale: 400 μm). Reprinted with permission from [53]. 2025, MDPI.

Table 5. Summary of studies on green graphene-based cellulose nanocomposites and their key applications

Study	Composite Composition	Target/Application	Key Outcomes
Snari et al. [51]	Cellulose + Morin (natural ligand)	Fluorometric sensor for Al ³⁺ detection	High luminescence with Al ³⁺ ; applicable in herbal tea QC and serum analysis
Chen et al. [52]	Cellulose/rGO aerogel	Chemical vapor sensor	Conductivity up to 1.9×10^{-5} S/cm at 8 wt% rGO; I(D)/I(G) \uparrow to 1.56; good piezoresistive response
Aldaleeli et al. [53]	Sodium carboxymethyl cellulose (CMC) + 0.2–3 wt% Graphene	UV-protective biodegradable packaging	\downarrow UV transmittance, \downarrow bandgap (5.27 \rightarrow 4.81 eV), \uparrow Urbach energy (0.34 \rightarrow 0.94 eV), improved morphology

loading, reaching 1.9×10^{-5} S/cm at 8 wt%, surpassing the percolation threshold at just 3 wt% [52].

In another study, Aldaleeli et al. explored the influence of graphene loading (0.2 to 3 wt%) on the structural and optical properties of sodium carboxymethyl cellulose (CMC)-based films. Their findings showed that increasing graphene content modified surface morphology (Figure 8), reduced particle size, and enhanced optical properties. Notably, light transmittance in UV-C, UV-B, and UV-A regions decreased with higher graphene loading, while the optical bandgap narrowed from 5.27 to 4.81 eV. Conversely, Urbach energy increased from 0.34 to 0.94 eV, indicating enhanced disorder. These features render the nanocomposites promising for biodegradable, UV-protective food packaging applications [53]. Table 5 summarizes the Green Graphene-Based PLA and their key applications investigated in this study.

3. Applications of green composites

Green composites, derived from environmentally friendly materials, have emerged as viable alternatives to conventional materials across various applications, offering comparable or superior performance alongside notable environmental benefits. In energy storage, for example, supercapacitors fabricated with green composites such as graphite foil and sodium acetate have outperformed traditional systems that often rely on hazardous substances like fluorine and sulfur, enhancing both efficiency and safety [13]. In biomedical and packaging applications, bioactive films incorporating chitin nanocrystals stand out due to their excellent biocompatibility, biodegradability, and inherent antibacterial properties [3]. The automotive industry has also witnessed a shift toward sustainable alternatives, with hybrid composite materials,

comprising components such as basalt, shell powder, and alumina, being employed in brake linings. These materials demonstrate reduced wear and lower water absorption compared to conventional asbestos-based counterparts, which pose significant environmental and health risks [14]. Additionally, advancements in casting technologies, including the use of low-temperature molds and non-stick coatings, have contributed to more sustainable aluminium alloy production by minimizing harmful emissions and enhancing casting quality [54]. In additive manufacturing, polylactic acid (PLA) reinforced with molybdenum disulfide (MoS₂) shows promise as a renewable, carbon-free substitute for petroleum-based resins, although further improvement in mechanical properties is necessary. Meanwhile, the polymer industry is actively developing biopolymers such as starch, cellulose, and chitosan to replace conventional synthetic polymers, thus addressing concerns related to long-term environmental degradation [55]. Collectively, these developments highlight the significant potential of green composites to advance sustainability without compromising on functionality or performance.

4. Challenges and opportunities

The development of green composites faces several important challenges alongside promising opportunities. A primary issue lies in ensuring effective compatibility between natural fibers and polymer matrices, as inadequate interfacial bonding can compromise mechanical performance. Improving this aspect is key to advancing their structural applications. Additionally, enhancing durability and resistance to environmental factors such as moisture, UV exposure, and temperature fluctuations is essential for extending their usability in long-term and outdoor settings.

Equally important is the implementation of comprehensive life cycle assessments to evaluate and validate the environmental benefits of green composites in comparison to conventional materials. Tackling these challenges opens up opportunities for innovation, improved performance, and greater integration of sustainable materials across various industries.

5. Conclusions and future outlook

Future progress in the field of green composites is closely tied to advancements in material science and manufacturing technologies. One promising direction is the integration of nanotechnology, specifically, the use of nanomaterials such as nanocellulose and nanoclays, which can significantly improve the mechanical strength, thermal stability, and barrier properties of these composites. Additionally, the adoption of biodegradable polymer matrices derived from renewable sources, such as polylactic acid (PLA) and polyhydroxyalkanoates (PHA), enhances the environmental sustainability of the final products, making them suitable alternatives to petroleum-based plastics. To enable widespread industrial adoption, it is equally important to optimize processing techniques. Methods like extrusion, compression molding, and injection molding must be refined for better scalability, cost-efficiency, and material consistency. Moreover, research into multifunctional green composites, those combining structural performance with properties like antimicrobial activity or self-healing, could further expand their applicability in fields such as biomedical engineering, packaging, construction, and automotive manufacturing. As environmental regulations become stricter and consumer demand for sustainable products grows, the development of high-performance, eco-friendly composites is likely to become a central focus in both academia and industry.

Conflict of Interest


The authors declare no conflict of interest.

References

1. B.K. Dejene and T.M. Geletaw. Development of fully green composites utilizing thermoplastic starch and cellulosic fibers from agro-waste: a critical review. *Polymer-Plastics Technology and Materials*, 2024, 63, 540.
2. P.L. Ferrara, M. La Noce, and G. Sciuto. Sustainability of Green Building Materials: A Scientometric Review of Geopolymers from a Circular Economy Perspective. *Sustainability*, 2023, 15, 16047.
3. C. Muñoz-Núñez, M. Fernández-García, and A. Muñoz-Bonilla. Chitin Nanocrystals: Environmentally Friendly Materials for the Development of Bioactive Films. *Coatings*, 2022, 12, 144.
4. J. Ahmad and Z. Zhou. Mechanical Properties of Natural as well as Synthetic Fiber Reinforced Concrete: A Review. *Construction and Building Materials*, 2022, 333, 127353.
5. A. Ramachandran, et al. Modification of Fibers and Matrices in Natural Fiber Reinforced Polymer Composites: A Comprehensive Review. *Macromolecular Rapid Communications*, 2022, 43, 2100862.
6. G.S. Mann, et al. Green composites: A review of processing technologies and recent applications. *Journal of Thermoplastic Composite Materials*, 2018, 33, 1145.
7. P.K. Bajpai, I. Singh, and J. Madaan. Development and characterization of PLA-based green composites. *Journal of Thermoplastic Composite Materials*, 2012, 27, 52.
8. G. Janowski, et al. Effect of Coffee Grounds Content on Properties of PHBV Biocomposites Compared to Similar Composites with Other Fillers. *Polymers*, 2025, 17, 764.
9. K. Goda and Y. Cao. Research and Development of Fully Green Composites Reinforced with Natural Fibers. *Journal of Solid Mechanics and Materials Engineering*, 2007, 1, 1073.
10. M.R.M. Asyraf, et al. Potential Application of Green Composites for Cross Arm Component in Transmission Tower: A Brief Review. *International Journal of Polymer Science*, 2020, 2020, 1.
11. R. Ilyas, et al. Natural Fiber-Reinforced Polylactic Acid, Polylactic Acid Blends and Their Composites for Advanced Applications. *Polymers*, 2022, 14, 202.
12. R. Ilyas, et al. Natural-Fiber-Reinforced Chitosan, Chitosan Blends and Their Nanocomposites for Various Advanced Applications. *Polymers*, 2022, 14, 874.
13. B. Dyatkin, et al. Development of a Green Supercapacitor Composed Entirely of Environmentally Friendly Materials. *ChemSusChem*, 2013, 6, 2269.
14. K.C. Chang, et al. Development of Environmentally Friendly Brake Lining Material. *E3S Web of Conferences*, 2019, 120, 03005.
15. H. Ramezani, T. Behzad, and R. Bagheri. Synergistic effect of graphene oxide nanoplatelets and cellulose nanofibers on mechanical, thermal, and barrier properties of thermoplastic starch. *Polymers for Advanced Technologies*, 2019, 31, 553.

16. G. Ariturk, et al. Hybrid green composites of PLA incorporated with upcycled waste cellulose and vermiculite. *European Polymer Journal*, **2024**, 203, 112667.
17. C. Naicker, N. Nombona, and W.E. van Zyl. Fabrication of novel magnetic chitosan/graphene-oxide/metal oxide nanocomposite beads for Cr(VI) adsorption. *Chemical Papers*, **2019**, 74, 529.
18. M. Tavakoli, S. Karbasi, and S. Soleymani Eil Bakhtiari. Evaluation of physical, mechanical, and biodegradation of chitosan/graphene oxide composite as bone substitutes. *Polymer-Plastics Technology and Materials*, **2019**, 59, 430.
19. T. Batakliiev, et al. Tailored Polylactic Acid/Polycaprolactone Blends with Excellent Strength-Stiffness and Shape Memory Capacities. *Processes*, **2025**, 13, 1328.
20. B. Krishnasamy, et al. Optimization and multi-objective analysis of tensile, flexural and impact strength in nano-hybrid bio-composites reinforced with Helicteres isora, Holoptelea integrifolia fibers, and nanographene. *Matéria (Rio de Janeiro)*, **2025**, 30, e20240864.
21. R.S. Krishna, et al. Green Synthesis of High-performance Graphene Geopolymer Composites: A Review on Environment-friendly Extraction of Nanomaterials. *Iranian Journal of Materials Science and Engineering*, **2020**, 17, 10.
22. A. Barra, et al. Green Carbon Nanostructures for Functional Composite Materials. *International Journal of Molecular Sciences*, **2022**, 23, 1848.
23. A. Kausar, et al. Green-Synthesized Graphene for Supercapacitors – Modern Perspectives. *Journal of Composites Science*, **2023**, 7, 108.
24. S. Kumari, et al. Enhanced microwave absorption properties of conducting polymer@graphene composite to counteract electromagnetic radiation pollution: green EMI shielding. *RSC Advances*, **2024**, 14, 662.
25. Y. Wu, C. An, and Y. Guo. 3D Printed Graphene and Graphene/Polymer Composites for Multifunctional Applications. *Materials*, **2023**, 16, 5681.
26. M. Sabet. Advanced graphene-polymer composites: synthesis, properties, and applications in electronics and optoelectronics. *Journal of Materials Science*, **2025**, 60, 6807.
27. J. Hu, et al. Biocompatible, hydrophobic and resilience graphene/chitosan composite aerogel for efficient oil–water separation. *Surface and Coatings Technology*, **2020**, 385, 125361.
28. S.M. Rangappa, S. Siengchin, and H.N. Dhakal. Green-composites: Ecofriendly and Sustainability. *Applied Science and Engineering Progress*, **2020**, 13, 183.
29. S. Periyasamy, et al. Fabrication of nano-graphene oxide assisted hydrotalcite/chitosan biocomposite: An efficient adsorbent for chromium removal from water. *International Journal of Biological Macromolecules*, **2019**, 132, 1068.
30. A.I.A. Sherlala, et al. Adsorption of arsenic using chitosan magnetic graphene oxide nanocomposite. *Journal of Environmental Management*, **2019**, 246, 547.
31. Z. Chang, et al. Construction of chitosan/polyacrylate/graphene oxide composite physical hydrogel by semi-dissolution/acidification/sol-gel transition method and its simultaneous cationic and anionic dye adsorption properties. *Carbohydrate Polymers*, **2020**, 229, 115431.
32. H. Zhang, et al. Innovative free radical induced synthesis of WO₃-doped diethyl malonate grafted chitosan encapsulated with phosphorylated alginate matrix for UO₂²⁺ adsorption: Parameters optimisation through response surface methodology. *Separation and Purification Technology*, **2025**, 353, 128455.
33. A. Jeyaseelan, N. Viswanathan, and M. Naushad. Design and development of rare earth elements anchored pectin/chitosan integrated magnesia hybrid composite for effective defluoridation of water. *Separation and Purification Technology*, **2025**, 352, 128137.
34. E.Y. Rozova, et al. Sorption and Mechanical Properties of Chitosan/Graphene Oxide Composite Systems. *Russian Journal of Applied Chemistry*, **2019**, 92, 415.
35. S. Ruiz, et al. Antimicrobial Films Based on Nanocomposites of Chitosan/Poly(vinyl alcohol)/Graphene Oxide for Biomedical Applications. *Biomolecules*, **2019**, 9, 109.
36. M. Tavakoli, S.S.E. Bakhtiari, and S. Karbasi. Incorporation of chitosan/graphene oxide nanocomposite in to the PMMA bone cement: Physical, mechanical and biological evaluation. *International Journal of Biological Macromolecules*, **2020**, 149, 783.
37. P.R. Sivashankari and M. Prabakaran. Three-dimensional porous scaffolds based on agarose/chitosan/graphene oxide composite for tissue engineering. *International Journal of Biological Macromolecules*, **2020**, 146, 222.
38. J.D.A. Villarta, et al. Green Synthesis, Characterization, and Optimization of Chitosan Nanoparticles Using Blumea balsamifera Extract. *Processes*, **2025**, 13, 804.
39. M. Solati, A. Saeidi, and I. Ghasemi. The effect of graphene nanoplatelets on dynamic properties, crystallization, and morphology of a biodegradable blend of poly(lactic acid)/thermoplastic starch. *Iranian Polymer Journal*, **2019**, 28, 649.
40. B. Rabeie and N.M. Mahmoodi. Green and environmentally friendly architecture of starch-based ternary magnetic biocomposite (Starch/MIL100/CoFe₂O₄): Synthesis and photocatalytic degradation of tetracycline and dye. *International Journal of Biological Macromolecules*, **2024**, 274, 133318.

41. D. Vasiliauskiene, et al. Changes in the Bacterial Communities of Biocomposites with Different Flame Retardants. *Life*, **2023**, 13, 2306.
42. P. Wang, et al. Crystallization, thermal stability, barrier property, and aging resistance application of multi-functionalized graphene oxide/poly(lactide)/starch nanocomposites. *International Journal of Biological Macromolecules*, **2019**, 132, 1208.
43. R. Scaffaro, et al. Lignocellulosic fillers and graphene nanoplatelets as hybrid reinforcement for polylactic acid: Effect on mechanical properties and degradability. *Composites Science and Technology*, **2020**, 190, 108008.
44. P. Wang, et al. Synergistic effects of modified TiO₂/multifunctionalized graphene oxide nanosheets as functional hybrid nanofiller in enhancing the interface compatibility of PLA/starch nanocomposites. *Journal of Applied Polymer Science*, **2020**, 137, 49094.
45. T.G. Barbosa, et al. Influence of Surface Treatments on the Electrochemical Performance of Lab-Made 3D-Printed Electrodes. *Analytica*, **2025**, 6, 9.
46. Q. Yuan, et al. Advances in the Study of Flame-Retardant Cellulose and Its Application in Polymers: A Review. *Polymers*, **2025**, 17, 1249.
47. D. Paukszta and S. Borysiak. The Influence of Processing and the Polymorphism of Lignocellulosic Fillers on the Structure and Properties of Composite Materials – A Review. *Materials*, **2013**, 6, 2747.
48. T. Senthil Muthu Kumar, et al. Preparation and Properties of Cellulose/Tamarind Nut Powder Green Composites. *Journal of Natural Fibers*, **2017**, 15, 11.
49. A. Wattanakornsiri and S. Tongnunui. Sustainable green composites of thermoplastic starch and cellulose fibers. *Songklanakarin Journal of Science and Technology*, **2014**, 36, 149.
50. V.K. Thakur, A.S. Singha, and M.K. Thakur. Ecofriendly Biocomposites from Natural fibers: Mechanical and Weathering study. *International Journal of Polymer Analysis and Characterization*, **2013**, 18, 64.
51. R.M. Snari, et al. Green composite colorimetric and “Turn-on” fluorescent material for the detection of Al³⁺ ion in blood serum and herbal tea. *Journal of Photochemistry and Photobiology A: Chemistry*, **2024**, 451, 115539.
52. G. Ramezani, T.G.M. van de Ven, and I. Stiharu. Novel In-Situ Synthesis Techniques for Cellulose-Graphene Hybrids: Enhancing Electrical Conductivity for Energy Storage Applications. *Recent Progress in Materials*, **2025**, 07, 1.
53. N.Y. Aldaleeli, et al. Evaluation of Different Concentrations of Graphene on the Structural and Optical Properties of Carboxymethyl Cellulose Sodium. *Polymers*, **2025**, 17, 391.
54. T. Lysenko, et al. Environmentally Friendly Materials and Technologies for the Production of Castings from Aluminum Alloys. *Odes'kyi Politechnichnyi Universytet Pratsi*, **2022**, 2, 5.
55. R. Rendón-Villalobos, et al., *The Role of Biopolymers in Obtaining Environmentally Friendly Materials*, in *Composites from Renewable and Sustainable Materials*, M. Poletto, Editor. **2016**, InTech.

© 2025 The Authors. This article is licensed under a Creative Commons Attribution 4.0 BY International License. 

Author Biography



Kobra Yazdani is a Ph.D. candidate in Materials Engineering at Hakim Sabzevari University. Her research interests focus on advanced materials, eco-friendly porous materials, biomaterials, metal-organic frameworks (MOFs), and hydrogels.

Rational Design and Development of Metal-Organic Frameworks

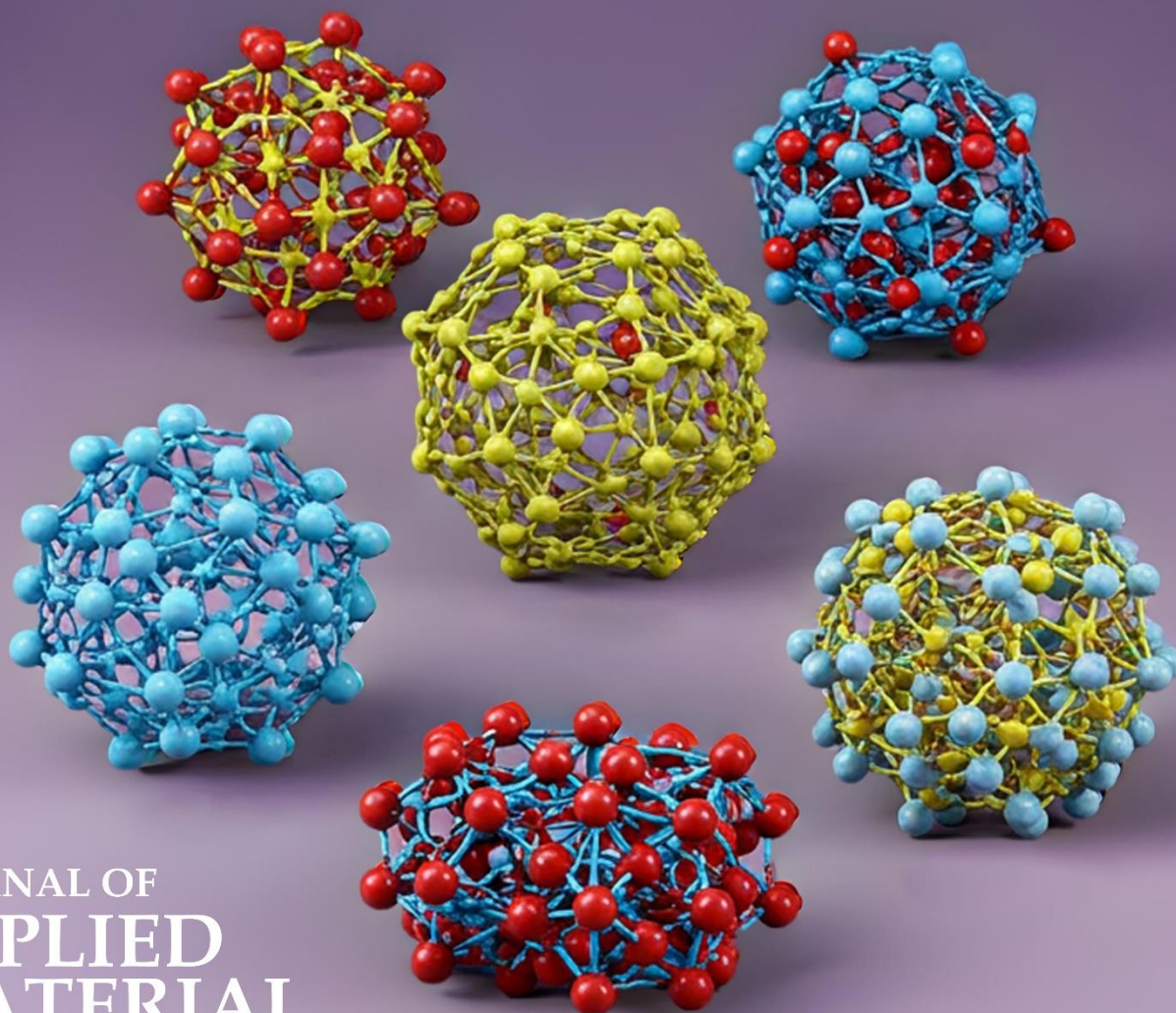
Hosein Ghasempour *

Department of Chemistry, Faculty of Sciences, Tarbiat Modares University, Tehran, Iran

Editor's note: Metal-organic frameworks (MOFs) are an innovative class of hybrid materials that hold great promise for tackling energy and environmental challenges. This invited mini-review provides an overview of recent developments by Ghasempour regarding the rational design of MOF topology. These advancements have significantly improved the catalytic, sensing, and sorption capabilities of these advanced porous materials.

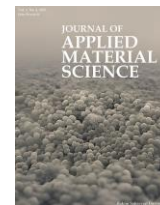
doi: 10.22034/jams.2025.210141

How to cite: H. Ghasempour. *Journal of Applied Material Science*, **2025**, 1, 210141.



JOURNAL OF
APPLIED
MATERIAL
SCIENCE

jams.hsu.ac.ir



Invited Review

Rational Design and Development of Metal-Organic Frameworks

Hosein Ghasempour *

Department of Chemistry, Faculty of Sciences, Tarbiat Modares University, Tehran, Iran

Abstract

Metal-organic frameworks (MOFs) represent a revolutionary class of hybrid materials with immense potential to address energy and environmental challenges, such as gas sorption and separation, as well as the detection and degradation of toxic chemicals. Recently, several commercial technologies utilizing MOFs have been developed for applications in the food safety industry, as well as for the storage and transportation of toxic gases like Arsine (AsH_3) and Boron trifluoride (BF_3). Despite these significant advancements, one of the most important and unresolved challenges in the synthesis of MOFs is controlling their network topology, which refers to the geometric arrangement of building blocks within the 3D architecture of the framework. Effective topology control is crucial for predicting the final structure and its properties, which depend on that structure. By carefully selecting the size, geometry, and connectivity of the building blocks, we can create a variety of network topologies that contribute to the design of MOFs with both high stability and permanent porosity. In this minireview, our recent studies on how controlling the topology affects the structural variations and enhances the catalytic, sensing, and sorption capabilities of MOFs are discussed.

Keywords: Metal-organic frameworks; Topology; Secondary building units.

1. Introduction

Metal-Organic Frameworks (MOFs) are an emerging class of crystalline porous materials, formed through coordination bonds between metal ions or clusters and multi-donating organic linkers, which are often referred to as molecular building blocks [1-3]. These structures can be developed in two or three dimensions, creating a periodically ordered porous network. One of the most notable features of MOFs is their exceptionally high porosity, with reported surface areas reaching up to $7,800 \text{ m}^2/\text{g}$. This makes them the leaders in surface area

among all traditional porous materials, such as zeolites and activated carbons [4, 5].

The structural diversity of MOFs is remarkable [6], as these highly porous materials consist of a wide variety of organic (linkers) and inorganic (metal nodes) secondary building units (SBUs) [7]. Metal nodes can take the form of single metal ions or clusters consisting of two, three, four, six, eight, or even twelve nuclei, or even infinite chains [8]. Organic ligands can also connect to two, three, four, six, eight, or twelve metal nodes, resulting in three-dimensional frameworks of MOFs with diverse underlying network topologies [9].

* Corresponding author.

Email addresses: h.ghasempour@modares.ac.ir, h.ghasempoor92@gmail.com (H. Ghasempour)

Received 17 May 2025

Revised 26 May 2025

Accepted 26 May 2025

Available online 28 May 2025

For over two decades, MOFs have been at the forefront of scientific research, especially in applications that address various energy and environmental challenges [10-13]. The performance of any MOF in a particular application is largely determined by its building units, namely the metal clusters and organic ligands [14, 15]. As such, porosity and stability are considered the most critical properties of MOFs [16].

Despite these impressive characteristics, controlling the geometric arrangement of SBUs within the overall MOF network, referred to as the underlying network topology, presents one of the most significant challenges in the design and development of these materials [17]. Consequently, understanding, predicting, and classifying network topologies are essential for designing novel MOFs with specific properties. This focus on topological exploration has become increasingly important for chemists working with MOFs in recent years [18, 19].

Designing the network topology in MOFs can be approached through two main methods: modifying the connectivity of metal clusters [20] or altering the topological geometry of linkers [21]. Metal clusters

typically adopt established geometries that are difficult to modify for changing connectivity. Therefore, logically designing linker geometry is crucial for discovering specific topologies that serve as ideal platforms for MOF design [9]. For instance, the first MOF was reported in 1995, featuring a framework composed of zinc acetate ($\text{Zn}_4\text{O}(\text{COO})_6$) clusters and a well-known ditopic benzene dicarboxylate linker [22]. This design has been expanded upon to create a series of isorecticular MOFs (IRMOFs) by substituting the original linker with various ditopic linkers in a process known as reticular synthesis [23].

Despite their potential, the susceptibility of zinc acetate clusters to hydrolysis limits their applicability in gas adsorption and separation, as these processes often occur in humid environments [24]. This limitation prompted the design of MOFs that incorporate binuclear M_2 -paddlewheel clusters (where $\text{M} = \text{Zn}$ or Cu), which exhibit improved water stability. However, combining these clusters with ditopic linkers typically results in a 2D layered coordination polymer instead of a 3D framework. In contrast, the combination of a tricarboxylate linker, benzene tricarboxylate, and a

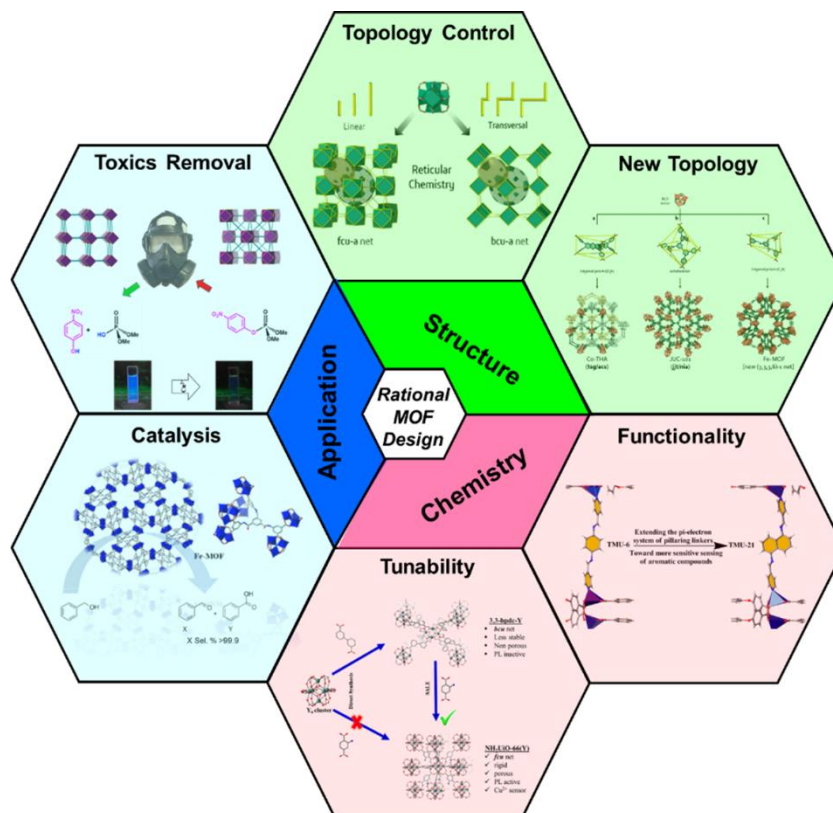


Figure 1. Rational design and intelligent development of MOFs.

copper paddlewheel cluster has led to the creation of the highly porous and stable 3D framework HKUST-1 ($[\text{Cu}_3(\text{BTC})_2 \cdot 3\text{H}_2\text{O}]_n$) [25], which has served as a benchmark in adsorption studies for many years [23]. Choosing linkers with flexible branches, desired dihedral angles, and specific topological shapes offers several advantages, particularly when using multitopic linkers [26].

Today, the application of topology, a branch of mathematics, to molecular building blocks or secondary building units (SBUs) has enabled the synthesis of a myriad of MOFs based on predicted topologies [27-29]. In conjunction with these methods, researchers have recently developed new design strategies to further enhance the rational design of MOFs. These include supermolecular building blocks (SBBs) [30], supermolecular building layers (SBLs) [31], and the merged-net approach, which combines two highly ordered topologies into one net. This strategy is particularly useful for rational MOF design [32].

This minireview focuses on the role of rational design in MOFs, considering their structure, chemistry, and applications (Figure 1). It emphasizes how intelligent control over MOF growth can lead to various outcomes, including: 1. Predictability of final MOF topology, 2.

Enhanced detection and degradation of nerve agents, 3. Discovery of new topologies, 4. Conversion of undesired structures into desired structures, 5. Selective oxidation of alcohols, 6. Adsorptive removal of organic dyes.

3. Topology control

Knowledge, prediction, and classification of network topology are important for designing novel MOFs with specific characteristics, and, as such, topological exploration in MOFs has become an important focus of MOF chemists in recent years [33]. The geometric arrangement of the secondary building units (SBUs), which include linkers and metal ions, in MOFs is very similar to children's toy building blocks. The logical selection of the type, size, shape, and arrangement of these SBUs is crucial in determining the final geometry of the structure, as well as its physical and chemical properties geometry misgeometry ge. Consequently, discovering novel methods to control and even predict the network topology has become one of the most exciting research areas in MOF chemistry. One such strategy introduced is called "net-clipping". According to the proposed hypothesis, changing the geometry of

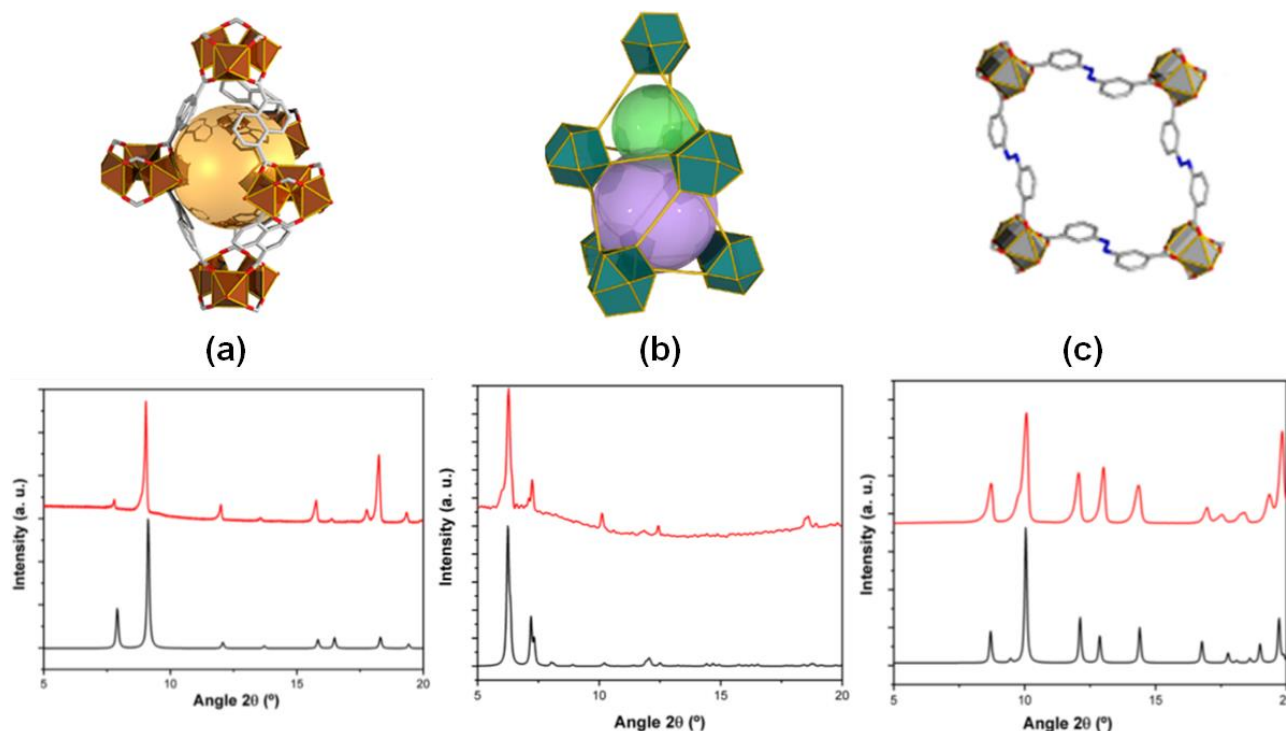


Figure 2. Crystallographic structure and XRD of Cu-3,3'-ABDC (a), Tb-3,3'-BPDC (b), and Fe-1,5-NDC (c). The black and red lines are related to simulated and experimental patterns, respectively. Reprinted with permission from [34]. Copyright 2020 American Chemical Society.

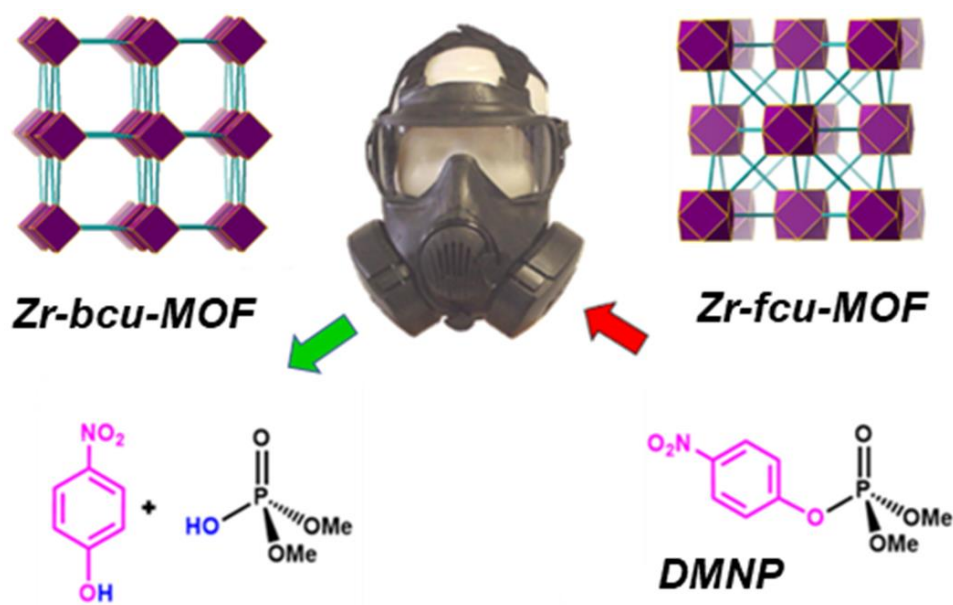


Figure 3. Function–topology relationship in the catalytic hydrolysis of DMNP in two Zr-MOFs.

the ligands from linear to zigzag allows for the prediction of the final MOF topology [34].

Computational data indicate that applying this method to 17 reported MOFs results in 10 structures exhibiting unique underlying topologies. Additionally, investigations of some existing structures in the literature have experimentally validated the results derived from this method. To further demonstrate this approach as a valuable strategy for topology control, three new MOFs, Cu-sql-3,3'-ABDC, Tb-fcu-3,3'-BPDC, and Fe-acs-1,5-NDC, were synthesized as single crystals and identified using X-ray diffraction. Interestingly, even though these three synthesized MOFs consist of different building blocks in terms of type, number, and geometry of the metal clusters, all three frameworks exhibit the same topology predicted by the net-clipping method. We reasoned that MOF structures made of zigzag ligands could be anticipated via rational clipping of the connecting groups of more symmetric SBUs in nets. Figure 2 represents the determined structure through single X-ray crystallography analysis and the compared XRD pattern of prepared MOFs by net-clipping.

3. Topology-function relationship

Among different types of MOFs synthesized to date, highly chemically, mechanically, and thermally stable

zirconium (VI)-based MOFs (Zr-MOFs, containing Zr_6 cluster, $[Zr_6O_4(OH)_4]^{12+}$) show amazing hydrolysis rates toward organophosphate nerve agents (OPNs) [35]. In addition to various parameters such as morphology [36], defect [37], and functionality [38], network topology can positively affect the hydrolysis rate of OPNs. The importance of controlling network topology in enhancing the catalytic rate of MOFs for the removal of organophosphates, particularly as nerve agent simulants, has been emphasized [39]. A comparative study was conducted on the catalytic capabilities of two Zr-MOFs that were constructed from identical SBUs but exhibited different topologies: Zr-bcu-tmuc and Zr-fcu-tmuc [40]. This study focused on the hydrolytic degradation of DMNP, which serves as a nerve agent simulant [40].

Despite being made up of the same molecular building blocks, the distinct differences in catalytic ability between these two Zr-MOFs can be attributed solely to their differing network topologies. The findings indicate that the 8-connected Zr-bcu-tmuc network offers greater accessibility to the active Zr(VI) sites compared to the 12-connected Zr-fcu-tmuc network, resulting in a several-fold increase in the hydrolysis rate. Furthermore, fluorescence sensing experiments revealed that Zr-bcu-tmuc exhibits significantly higher sensitivity to DMNP than Zr-fcu-tmuc, corroborating the catalytic results (Figure 3). This study paves the way for scientists

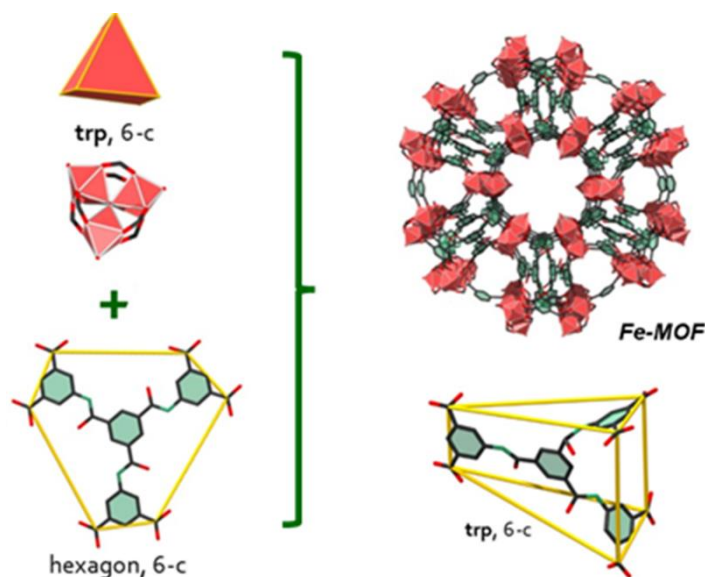


Figure 4. Schematic representation of flexible linker-based Fe-MOF structure.

to design more effective MOFs for countering chemical threats by manipulating topology.

4. Topology discoveries

Among the various rational design strategies that have emerged over time, selecting suitable SBUs with the appropriate connectivity and directionality can facilitate the assembly of MOFs with highly regular, predictable topologies [20]. The majority of studies in the field of MOFs focus on combinations of octahedral Zn_4O clusters [41], square-like paddlewheel Zn_2/Cu_2 clusters [25], and Zr_6 clusters [42] with various carboxylate ligands. One exciting study was the discovery of the gea net as an ideal blueprint net by Guillerm et al. Their geometrical analysis of the gea-a net revealed that transposition of pre-known copper paddlewheels to MOP into the anticipated gea-MOF platform required the employment of a multicarboxylate ligand with two branches that contain 120° angle dicarboxylic acid extremities and a third branch with a 90° angle dicarboxylic acid extremity [43].

Despite the numerous reported structures, MOFs composed of MIII triangular prismatic metal clusters, such as iron, chromium, and aluminum, are less studied. This limited focus is likely due to a relative lack of understanding regarding their formation conditions [44]. In this work, we present a geometry mismatch

strategy for assembling a non-interpenetrated, porous iron-based MOF, identified as Fe-MOF. By combining trigonal prismatic (trp, 6-c) metal clusters with a 6-connected hexagonal linker, components that initially appear incompatible due to the absence of a net for their assembly, we successfully discovered a new topology (Figure 4). The Fe-MOF structure is formed through the pillaring of a new type of supramolecular building layer, characterized by a rare 4-nodal, 3,3,3,6-connected topology. This structure demonstrates high water stability and significant porosity, featuring functionalized one-dimensional hexagonal channels. The findings highlight the potential for discovering new topologies, even when utilizing a common building block such as a basic Fe acetate cluster [45].

5. Converting the undesired structure to the favorite network

The main method for synthesizing metal-organic frameworks (MOFs) is through a self-assembly process that occurs under solvothermal conditions. However, this method can be difficult to control, resulting in the formation of undesirable networks [46]. To address this issue, post-synthesis techniques can effectively modify these undesirable networks into more desirable structures. Consequently, research has concentrated on controlling the topology of MOFs.

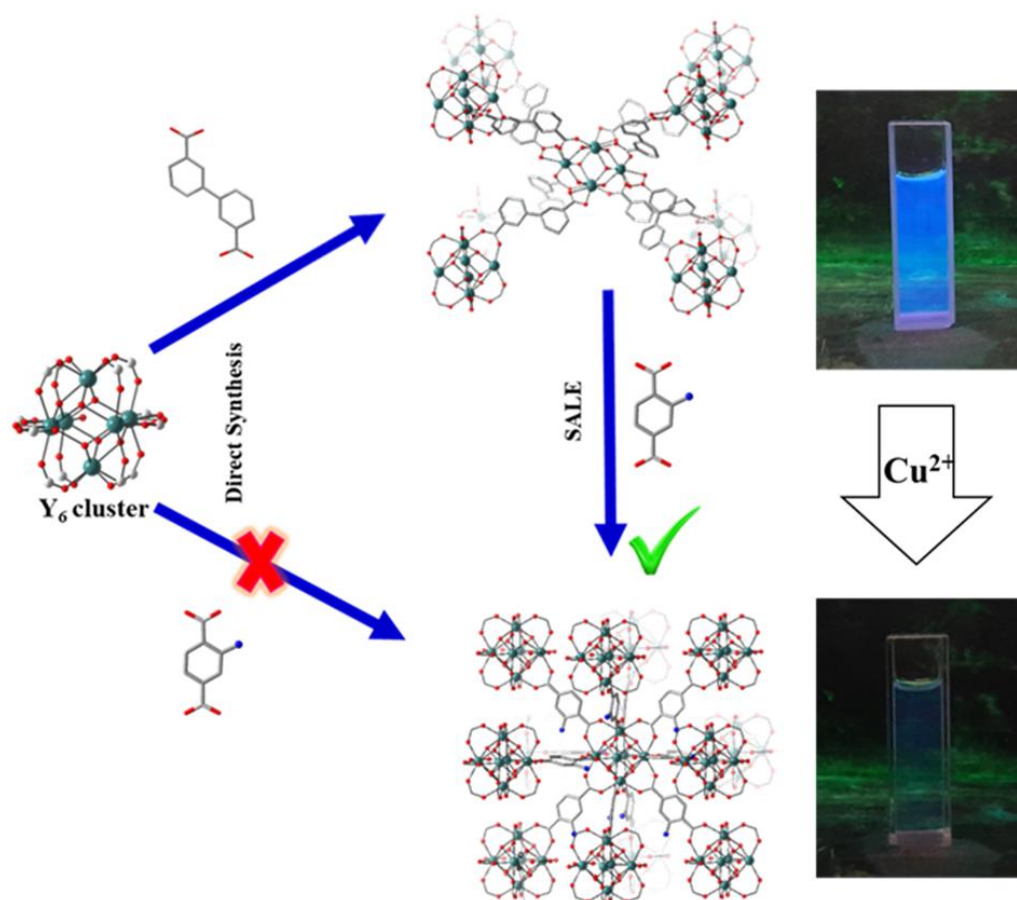


Figure 5. Representation of solvent-assisted linker exchange synthesis of $\text{NH}_2\text{UiO-66(Y)}$. Reprinted with permission from [47]. Copyright 2022 American Chemical Society.

One such method employed was solvent-assisted ligand exchange (SALE), which was utilized to prepare an yttrium-based aminated UiO-66 framework—this framework cannot be created through direct synthesis. Notably, SALE successfully transformed a completely non-porous initial structure, 3,3-bpdc-Y, into a porous framework. Additionally, it altered the topology from an unstable 8-connected bcu network to a much more stable 12-connected fcu topology (Figure 5). Importantly, SALE not only resulted in the creation of the relatively highly porous $\text{NH}_2\text{UiO-66(Y)}$ from the completely non-porous 3,3-bpdc-Y but also changed its network topology from an 8-connected bcu structure to a 12-connected fcu framework. To the best of our knowledge, this is one of the rare instances where SALE has successfully modified the entire network topology of the final MOF. Furthermore, $\text{NH}_2\text{UiO-66(Y)}$ demonstrated a promising ability to selectively detect Cu^{2+} ions at low concentrations [47].

6. Catalytic oxidation of alcohols

Iron-based metal-organic frameworks have garnered significant attention as heterogeneous catalysts for oxidation reactions [48]. Despite several reports on MOF-based catalysts for the selective oxidation of benzyl alcohol, preventing overoxidation to benzoic acid remains a challenge [49]. Therefore, the catalytic activity of Iron-based MOF was evaluated in the aerobic oxidation of benzyl alcohol in air. Due to its iron-containing clusters, high porosity, large channel dimensions, functionality, and especially high stability, Fe-MOF is an excellent candidate for the selective oxidation of benzyl alcohols. Interestingly, Fe-based MOF exhibited enhanced activity compared to the neat Fe_3O_4 cluster, achieving a yield of benzyl alcohol oxidation that increased from 31.7% to 91.9% toward benzaldehyde.

This improvement can be attributed to the high surface area and the suitable aperture size of its 1D channels, which provide an optimal environment for the oxidation process. Additionally, host-guest interactions, such as hydrogen bonding between benzyl alcohol and the amide functions in the Fe-MOF channels, can enhance the accessibility of reagents to active sites, resulting in excellent catalytic activity. In comparison to previously reported MOF-based catalysts, Fe-MOF demonstrates remarkable selectivity and activity for the catalytic oxidation of benzyl alcohol within a relatively short reaction time, achieving a yield of 91.9% in just 3 hours. This work illustrates that it is still possible to identify promising MOF-based heterogeneous catalysts, even when utilizing one of the most common building blocks, the basic Fe acetate type Fe_3O cluster [45].

7. Adsorptive removal of dyes

The structural properties of Fe-MOF, including its water-resistant nature, the presence of two types of large channels measuring 1.2 and 0.6 nanometers, a high BET surface area of 1740 m^2/g , and acyl amide functional groups, were assessed for their effectiveness in adsorbing organic dyes from aqueous environments. A range of anionic and cationic dyes was tested, including methyl orange (MO), methyl red (MR), congo red (CR), rose-bengal B (Ros B), rhodamine B (Rhod B), and methylene blue (MB), to evaluate the efficiency of Fe-MOF. The presence of acyl amide groups enhances the interaction between the framework and anionic dyes, particularly with MO, which exhibited an adsorption capacity of 232.5 mg/g .

Interestingly, Fe-MOF demonstrated one of the fastest adsorption rates for MO, with a kinetic constant of 0.013 $\text{g}/\text{mg}\cdot\text{min}$. This rate surpasses that of several well-known metal-organic frameworks (MOFs) such as UiO-66, MIL-53, UiO-66- NO_2 , and ZIF-67. The study also explored the adsorption mechanism, uptake kinetics, and selectivity of the framework regarding different dyes. Overall, the water-stable Fe-MOF, characterized by significant permanent porosity and functionalized pores, enhanced the size and charge-selective removal of dyes through preferred hydrogen bonding and π - π interactions. The experimental results indicated that Fe-MOF has a greater affinity for anionic dyes over cationic dyes, achieving substantial adsorption capacities of 232 mg/g for the toxic MO dye and 120 mg/g for the MB dye, indicating its high efficiency in this application [50].

8. Conclusions

In summary, this study highlighted how the rational design and intelligent control of MOFs network topology affects their structure-dependent properties and consequently their capability toward divers application area including; (1) detection and catalytic destruction of the organophosphorus nerve agents, (2) precise identification of copper ions in aquatic environments, (3) investigation of selective catalytic properties, and (4) correlation between structure and the adsorption of organic dyes. An innovative, creative, and efficient technique for deducing the network topology of MOFs built up from zigzag linkers, called net-clipping, was introduced. Designing MOFs with unique topology results in structures with excellent applicability in detecting and hydrolysis of organophosphorus nerve agents, adsorptive removal of dyes, and copper (II) ion sensing, which are significant environmental hazards in today's industries. Additionally, the study shows that it is possible to discover a novel porous iron-based MOF named Fe-MOF even using incompatible SBUs, which acts as a heterogeneous catalyst for the selective oxidation of benzyl alcohol to benzaldehyde under mild conditions. The compilation of these exceptional applications highlights the effectiveness of this design approach and the extraordinary capabilities of the porous MOF materials across a wide range of chemical industry sectors.

Conflict of Interest


The authors declare no conflict of interest.

References

1. H.-C. Zhou, J.R. Long, and O.M. Yaghi. Introduction to metal-organic frameworks. *Chemical Reviews*, 2012, 112, 673.
2. J. Xu, Y. Xu, and X.-H. Bu. Advances in emerging crystalline porous materials. *Small*, 2021, 17, e2102331.
3. H. Furukawa, et al. The chemistry and applications of metal-organic frameworks. *Science*, 2013, 341, 1230444.
4. O.K. Farha, et al. Metal-organic framework materials with ultrahigh surface areas: is the sky the limit? *Journal of the American Chemical Society*, 2012, 134, 15016.
5. I.M. Höncke, et al. Balancing mechanical stability and ultrahigh porosity in crystalline framework materials. *Angewandte Chemie International Edition*, 2018, 57, 13780.

6. S.M. Moosavi, et al. Understanding the diversity of the metal-organic framework ecosystem. *Nature communications*, **2020**, *11*, 4068.
7. M. Eddaoudi, et al. Modular chemistry: secondary building units as a basis for the design of highly porous and robust metal-organic carboxylate frameworks. *Accounts of chemical research*, **2001**, *34*, 319.
8. M.J. Kalmutzki, N. Hanikel, and O.M. Yaghi. Secondary building units as the turning point in the development of the reticular chemistry of MOFs. *Science advances*, **2018**, *4*, eaat9180.
9. H. Ghasempour, et al. Metal-organic frameworks based on multicarboxylate linkers. *Coordination Chemistry Reviews*, **2021**, *426*, 213542.
10. M. Shanmugam, et al. Metal-organic frameworks (MOFs) for energy production and gaseous fuel and electrochemical energy storage applications. *Physical Chemistry Chemical Physics*, **2023**, *25*, 30116.
11. M.A. Abdelkareem, et al. Recent advances on metal-organic frameworks (MOFs) and their applications in energy conversion devices: Comprehensive review. *Energy*, **2024**, *299*, 131127.
12. S. Bhayana, R. Nandal, and S. Khatri, *Metal Organic Frameworks as Energy Storage Material: Their Contributions and Challenges*, in *Materials for Boosting Energy Storage. Volume 1: Advances in Sustainable Energy Technologies*, S.S. Kumar, et al., Editors. **2024**, ACS Publications: USA. 125.
13. Z.A. Sandhu, et al. Metal-organic frameworks for next-generation energy storage devices; a systematic review. *Materials Advances*, **2024**, *5*, 30.
14. V.F. Yusuf, N.I. Malek, and S.K. Kailasa. Review on metal-organic framework classification, synthetic approaches, and influencing factors: applications in energy, drug delivery, and wastewater treatment. *ACS omega*, **2022**, *7*, 44507.
15. R.U. Rajesh, et al. Metal-organic frameworks: Recent advances in synthesis strategies and applications. *Inorganic Chemistry Communications*, **2024**, *162*, 112223.
16. V. Aggarwal, S. Solanki, and B.D. Malhotra. Applications of metal-organic framework-based bioelectrodes. *Chemical Science*, **2022**, *13*, 8727.
17. M. Li, et al. Topological analysis of metal-organic frameworks with polytopic linkers and/or multiple building units and the minimal transitivity principle. *Chemical Reviews*, **2014**, *114*, 1343.
18. L.T. Glasby, et al. Topological characterization of metal-organic frameworks: a perspective. *Chemistry of Materials*, **2024**, *36*, 9013.
19. V. Guillerm and D. Maspoch. Geometry mismatch and reticular chemistry: strategies to assemble metal-organic frameworks with non-default topologies. *Journal of the American Chemical Society*, **2019**, *141*, 16517.
20. V. Guillerm and M. Eddaoudi. The importance of highly connected building units in reticular chemistry: thoughtful design of metal-organic frameworks. *Accounts of Chemical Research*, **2021**, *54*, 3298.
21. D. Zhao, et al. Tuning the topology and functionality of metal-organic frameworks by ligand design. *Accounts of Chemical Research*, **2011**, *44*, 123.
22. H. Li, et al. Design and synthesis of an exceptionally stable and highly porous metal-organic framework. *Nature*, **1999**, *402*, 276.
23. M. Eddaoudi, et al. Systematic design of pore size and functionality in isorecticular MOFs and their application in methane storage. *Science*, **2002**, *295*, 469.
24. N.C. Burtch, H. Jasuja, and K.S. Walton. Water stability and adsorption in metal-organic frameworks. *Chemical Reviews*, **2014**, *114*, 10575.
25. S.S.-Y. Chui, et al. A chemically functionalizable nanoporous material [Cu₃ (TMA) ₂ (H₂O) ₃] n. *Science*, **1999**, *283*, 1148.
26. Z.-J. Lin, et al. Metal-organic frameworks based on flexible ligands (FL-MOFs): structures and applications. *Chemical Society Reviews*, **2014**, *43*, 5867.
27. O.M. Yaghi, et al. Reticular synthesis and the design of new materials. *Nature*, **2003**, *423*, 705.
28. A. Stein, S.W. Keller, and T.E. Mallouk. Turning down the heat: Design and mechanism in solid-state synthesis. *Science*, **1993**, *259*, 1558.
29. M. O'Keeffe and O.M. Yaghi. Deconstructing the crystal structures of metal-organic frameworks and related materials into their underlying nets. *Chemical Reviews*, **2012**, *112*, 675.
30. J.J. Perry Iv, J.A. Perman, and M.J. Zaworotko. Design and synthesis of metal-organic frameworks using metal-organic polyhedra as supermolecular building blocks. *Chemical Society Reviews*, **2009**, *38*, 1400.
31. V. Guillerm, et al. A supermolecular building approach for the design and construction of metal-organic frameworks. *Chemical Society Reviews*, **2014**, *43*, 6141.
32. H. Jiang, et al. Enriching the reticular chemistry repertoire: merged nets approach for the rational design of intricate mixed-linker metal-organic framework platforms. *Journal of the American Chemical Society*, **2018**, *140*, 8858.
33. A. Divya and A. Karunyan. Topological analysis of metal-organic frameworks: A regression approach to enhance molecular modeling. *Computational and Theoretical Chemistry*, **2025**, *1248*, 115156.
34. B. Ortín-Rubio, et al. Net-clipping: an approach to deduce the topology of metal-organic frameworks built with zigzag ligands. *Journal of the American Chemical Society*, **2020**, *142*, 9135.

35. S. Daliran, et al. Defect-enabling zirconium-based metal-organic frameworks for energy and environmental remediation applications. *Chemical Society Reviews*, **2024**, 53, 6244.
36. G. Wu, et al. Morphology Regulation of UiO-66-2I Supporting Systematic Investigations of Shape-Dependent Catalytic Activity for Degradation of an Organophosphate Nerve Agent Simulant. *Inorganic Chemistry*, **2024**, 63, 12658.
37. M. Bakhtiyari-Ramezani, N.R. Jalal, and H. Ghasempour. Plasma-Assisted Solid Phase Modification of UiO-66 Metal-Organic Framework for Enhanced Hydrolysis of Nerve Agent Simulant. *Colloids and Surfaces A*, **2025**, 721, 137244.
38. M. Ran, et al. Amino-Functionalized Nano-UiO-66 for the Detection of Nerve Agent Analogs. *ACS Applied Nano Materials*, **2025**, 8, 8231.
39. H. Ghasempour, B. Habibi, and P. Soleimani Abhari. Mechanically Synthesized Zirconium-based MOFs for Adsorptive Removal of Nerve Agent Simulants. *Journal of Applied Material Science*, **2025**, 1, 210132.
40. H. Ghasempour and A. Morsali. Function-Topology Relationship in the Catalytic Hydrolysis of a Chemical Warfare Simulant in Two Zr-MOFs. *Chemistry-A European Journal*, **2020**, 26, 17437.
41. M. Eddaoudi, H. Li, and O. Yaghi. Highly porous and stable metal- organic frameworks: structure design and sorption properties. *Journal of the American Chemical Society*, **2000**, 122, 1391.
42. Z. Chen, et al. Reticular chemistry in the rational synthesis of functional zirconium cluster-based MOFs. *Coordination Chemistry Reviews*, **2019**, 386, 32.
43. V. Guillermin, et al. Discovery and introduction of a (3, 18)-connected net as an ideal blueprint for the design of metal-organic frameworks. *Nature Chemistry*, **2014**, 6, 673.
44. D. Feng, et al. Kinetically tuned dimensional augmentation as a versatile synthetic route towards robust metal-organic frameworks. *Nature Communications*, **2014**, 5, 5723.
45. H. Ghasempour, et al. Development of a highly porous Fe-based MOF using symmetrically incompatible building blocks: Selective oxidation of benzyl alcohols. *Applied Materials Today*, **2021**, 24, 101157.
46. M. Bosch, et al. Stepwise synthesis of metal-organic frameworks. *Accounts of Chemical Research*, **2017**, 50, 857.
47. H. Ghasempour, et al. Converting a Non-Porous Rare-Earth Metal-Organic Framework into a Porous Yttrium-Based NH₂UiO-66 Network via a Linker Exchange Approach. *Inorganic Chemistry*, **2022**, 61, 16221.
48. X. Liu, et al. Iron containing metal-organic frameworks: structure, synthesis, and applications in environmental remediation. *ACS Applied Materials & Interfaces*, **2017**, 9, 20255.
49. A. Dhakshinamoorthy, M. Alvaro, and H. Garcia. Aerobic oxidation of benzylic alcohols catalyzed by metal- organic frameworks assisted by TEMPO. *ACS Catalysis*, **2011**, 1, 48.
50. H. Ghasempour, F. Zarekarizi, and A.J.C. Morsali. Acyl amide-functionalized and water-stable iron-based MOF for rapid and selective dye removal. *CrystEngComm*, **2022**, 24, 4074.

© 2025 The Authors. This article is licensed under a Creative Commons Attribution 4.0 BY International License. 

Author Biography



Hosein Ghasempour was born in Tabriz, Iran, in 1990. He earned his MS degree in Inorganic Chemistry from Tarbiat Modares University (TMU) in Iran. He was subsequently accepted into the Ph.D. program at TMU and defended his thesis under the supervision of Prof. Ali Morsali in 2021. Additionally, he spent eight months as a visiting researcher in Prof. Daniel MasPOCH's group at the Catalan Institute of Nanoscience and Nanotechnology (ICN2) in Barcelona, Spain. His research interests primarily focus on coordination chemistry and Metal-Organic Frameworks.